UNIVERSITÀ DEGLI STUDI DI TRIESTE

XXX CICLO DEL DOTTORATO DI RICERCA IN

SCIENZE DELLA TERRA E MECCANICA DEI FLUIDI

Integrated analysis of glacial sediment input and ocean circulation in NW Barents Sea

Settore scientifico-disciplinare: **GEO/02**
GEOLOGIA STRATIGRAFICA E SEDIMENTOLOGICA

DOTTORANDO / A
Leonardo Rui

COORDINATORE
Prof. Pierpaolo Omari

SUPERVISORE DI TESI
Dr. Michele Rebesco

CO-SUPERVISORE DI TESI
Dr. Manuel Bensi

ANNO ACCADEMICO 2016/2017

Index

Abstract

The Arctic Ocean is one of the most climatically sensitive areas, being the crossway of global ocean circulation (*Charles et al., 1994; Thiede and Myhre, 1996; Knies et al., 1999; Hald et al., 2004*). The West Spitsbergen continental margin is characterized by the presence of the West Spitsbergen Current, a warm Atlantic Water that flows northwards along the continental margin. This Atlantic Water is the major heat advection toward the Arctic, mixing with the cold and partially sea-ice covered Polar Water; thanks to the West Spitsbergen Current, the Atlantic Water is driven into the northern hemisphere circulation system. Studies on the natural variability of the Arctic Ocean circulation are vital for understanding the future of the Arctic climate system and specifically its feedback mechanisms related to global warming (*Spielhagen et al., 2011*). Moreover, the investigation of past climate variations in the Arctic Ocean is essential to predict future scenarios. During the Last Glacial Maximum (LGM), around 20.000 years ago, the Arctic was mainly covered by a large ice sheet (*Hughes et al., 2016*) and the glacial sedimentary processes controlled erosion, transport and deposition along the entire margin. The following deglaciation can be considered to a certain extent as an analog to the climatic period we are facing towards the end of the present century. The sedimentary processes were affected by the ocean circulation to an extent that was also varying according to cyclicity at glacial-interglacial and shorter scales. In this Ph.D. project I focus on the interactions between glacial sedimentary input and ocean circulation in the area of NW Barents Sea, during LGM and deglaciations. The available geophysical data were acquired during several research cruises in the study area. From the analysis of this dataset I was able to identify a number of sedimentary bodies related both to a glacial sediment input and current circulation, responsible for downslope and along-slope sedimentary processes, respectively.

The downslope processes affected by the presence of ice sheet and ice streams generated structures like the INBIS Channel System situated between the Bear Island and the Storfjorden Trough Mouth Fans (TMFs). This channel system starts at the shelf edge with a series of gullies that merge and grow in dimensions becoming channels and eventually a 15 km large and 60 km long channel. I infer that the formation of this channel system was possible thanks to its protected location: the glacial debris flows responsible for the formation of the adjacent TMFs could not reach directly the area where the gullies are situated, due to the presence of the Bear Island to the East, acting as a barrier or watershed for the ice. I infer that this part of the INBIS Channel System is the product of melt-water flows during ice retreat. The major evidence of this phenomenon is the exceptional dimension and development of the gullies dissecting the shelf edge in this area compared to those found along the rest of the West Spitsbergen margin.

The structures mainly controlled by along-slope processes include Isfjorden and Bellsund drifts, sedimentary deposits produced by bottom currents driven by thermohaline circulation,

geostrophic currents and also by the effect of the local topography and climate (*Hanebuth et al., 2014*). To investigate the mechanism responsible for the formation of these drifts, the present circulation has been investigated by mean of oceanographic data. The oceanographic investigation included the analysis of the datasets recorded for few years in two moorings on top of the Isfjorden and Bellsund drifts. From this analysis I infer that dense and salty waters formed at the shelf edge, through shelf convection and brine rejection processes, and during the descent down the slope mix through entrainment with the surrounding cold water. During the descent these waters also entrain sediments and the transport of sediments results in an overall high density and in a high kinetic energy. Thanks to these characteristics, these waters may reach larger depths than their equilibrium point in the water column (*Fohramnn et al., 1998*)**.**

1 Introduction

In this chapter I will present the research carried out in this Ph.D. project. I will start by providing a brief excursus on the scientific importance of the research topic. Consecutively, I will introduce the scientific question motivating my study and define the aim of this project.

Scientific Importance: The interest of the scientific community in Polar Regions is increasing recently, in particular due to their importance in climate changes. Both the Arctic and the Antarctic regions are in fact the areas on our planets that react more rapidly and drastically to global warming. In particular climate studies conducted recently predicted that the global warming will have its largest impact in high northern latitudes (*Hal der al., 2004*). The Arctic Ocean, in particular, is one of the most climatically sensitive areas, being the crossway of global ocean circulation (*Charles et al., 1994; Thiede and Myhre, 1996; Knies et al., 1999; Hald et al., 2004*). Climate changes in the Arctic Ocean and resulting changes in its circulation may impose large adaptations, primarily in the North Atlantic Ocean and more generally in the whole northern hemisphere. Therefore the studies on the natural variability of the Arctic Ocean circulation are vital for understanding the future of the Arctic climate system and specifically its feedback mechanisms related to global warming (*Spielhagen et al., 2011*).

Moreover, the investigation of past climate variations in the Arctic Ocean is essential to predict future scenarios. In fact, during the Last Glacial Maximum (LGM), between 23,000 and 20,000 years ago (*Jessen et al., 2010*), the Arctic was mainly covered by a large ice sheet (*Hughes et al., 2016*) and the glacial processes controlled sedimentary erosion, transport and deposition along the entire margin. The deglaciation following the LGM can be considered to a certain extent as an analog to the climatic period we are facing towards the end of the present century, with the atmospheric concentration of CO2 forecasted to reach levels even higher than past interglacial periods (*Charles et al., 1994*). The sedimentary processes were affected by the ocean circulation to an extent that was also varying according to cyclicity at glacial-interglacial and shorter scales. The continental margin morphology we can observe today has been molded by processes imposed by these paleo-ice sheets and by their interaction with the ocean circulation. The study of these margins may shed some light on past ice sheets and their growth and decay cycles, which is a key point for better understanding and predicting the effects of climate change on ice sheets in the present.

Lastly, the deposits we can observe today along glaciated continental margin are also of importance for natural resources assessment such as hydrocarbons exploration and deep sea mining. Studying the genesis of these margins may lead to the detection of hydrocarbons and raw materials.

Scientific Question: This PhD study focuses on the interactions between the glacial system and ocean circulation in the area of NW Barents Sea. To study how the glacial and ocean systems interacted in the past is ambitious and challenging, due the quite different spatial/time scales of the many phenomena involved. I strive for studying the relationship between ocean currents and sediment input in this area in the past, during LGM and deglaciation, to eventually relate my observations with present conditions.

This study, produced by the integration of a geophysical dataset with the body of knowledge in oceanography, may be useful for other environments such as other Arctic areas, as well as for all glaciated continental margins. In particular, similar studies may be conducted in the Antarctic region where ice sheets and ice streams are presently reaching the continental margin. Moreover present day ice sheets (in particular those covering Antarctic Peninsula and Greenland) are melting due to global warming. The study of last deglaciation may help in understanding what is happening in the present and/or what will happen in the future.

The Aim: The aim of this PhD project is to present the evolution of the west Spitsbergen margin in the area NW Barents from the LGM through the combined analysis of geophysical and oceanographic datasets, in order to decipher the relationship between glacial sediment input and ocean circulation.

1.1 Background

In the first part of this chapter a synthesis of the geological background of the Arctic Ocean is presented, focusing in particular on the area of NW Barents Sea. In this synthesis specific attention to the Last Glacial Maximum is payed, occurred in Late Quaternary around 21,000 years ago and the subsequent deglaciation up to present days. In the second part of this chapter a synthesis on the oceanographic background is provided, summarizing the state of the art and offering a concise introduction to the main processes taken into account for this Ph.D. research.

1.1.1 Geological background

The Arctic Ocean extends in a roughly circular area of about 14,055,000 km^2 (see Figure 1).

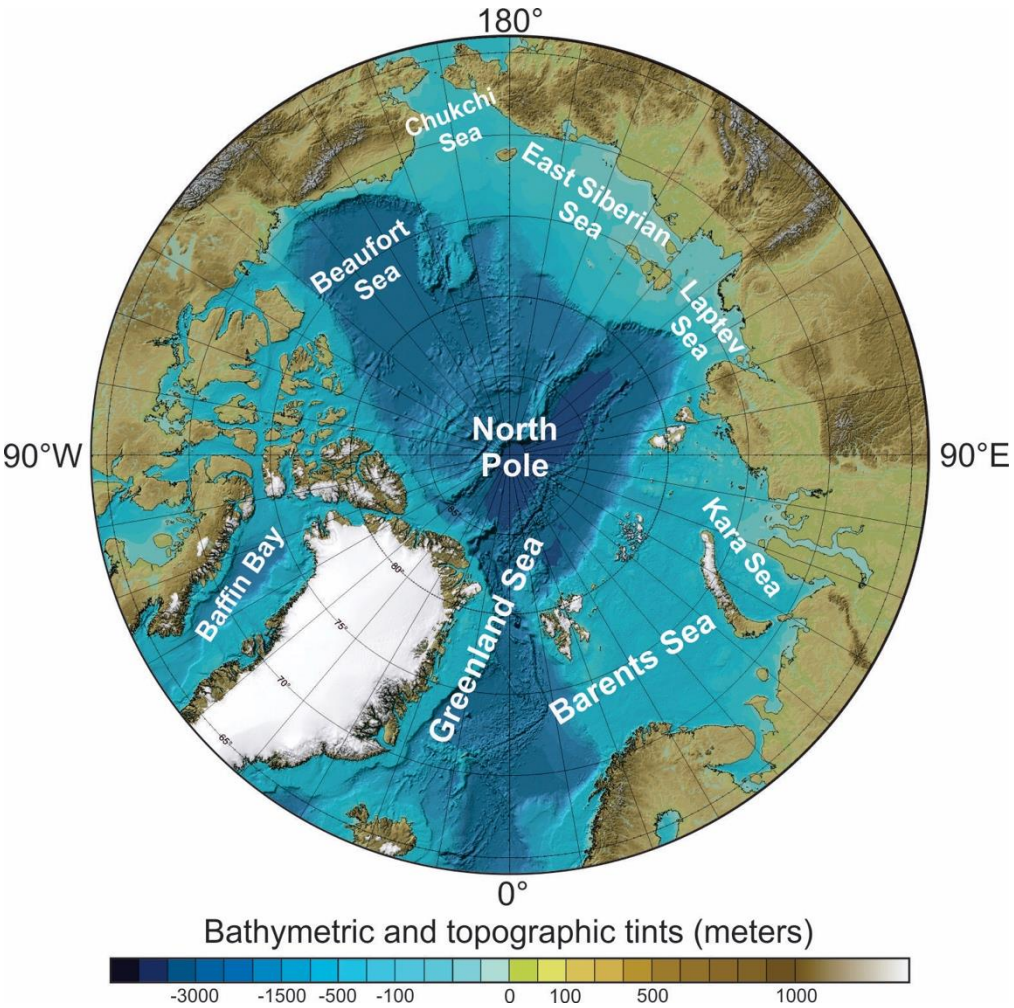

Figure 1: Bathymetric map of the Arctic Ocean modified from the International Bathymetric Chart of the Arctic Ocean (IBCAO), *Jakobsson et al., 2012*.

It is composed of the Greenland Sea, White Sea, Barents Sea, Kara Sea, Laptev Sea, East Siberian Sea, Chukchi Sea, Beaufort Sea and Baffin Bay. The reconstruction of the tectonic evolution of the Arctic region since the breakup of Pangea is still a matter of debate due to the meagre amount of data (*Shepard et al., 2013*) as well as to the complexity of the Phanerozoic history of this area, characterized by several periods of compression and extension, changes in geometry and location of plate boundaries as well as multiple reactivation events. Despite its complex history, it is possible to divide the Arctic Ocean into two major bathymetric features: the Amerasia Basin and the Eurasia Basin. The dividing line between these two basins is the Lomonosov Ridge, an underwater ridge of continental crust that spans for about 1,800 km, extending from the New Siberian Islands (Russia) to Ellesmere Island (Canada). The sub-triangular Amerasia Basin is further divided into two smaller basins by the Mendeleev Ridge and the Alpha Ridge: these are the Makarov Basin (between Lomonosov Ridge and Mendeleev-Alpha Ridges) and the Canada Basin (between the Mendeleev-Alpha Ridges and Alaska/Canada). The elongate Eurasia Basin is also divided into two smaller basins by the Gakkel Ridge: the Amundsen Basin, which extends from the Lomonosov Ridge to the Gakkel Ridge, and the Nansen Basin, delimited by the Gakkel Ridge and the Franz Josef Land (see Figure 2).

The Arctic Ocean (Eurasia Basin) opens towards the Norwegian – Greenland Sea through the Fram Strait. The Fram Strait extends for about 450 km, between 77° N and 81° N latitudes and it is centered on the prime meridian. The Fram Strait plays a major oceanographic role for the Arctic Ocean, being the only deep-water gateway between the latter and other oceans. The deep oceanic part of this gateway, called Lena Trough, a segment of the Eurasia – North America plate boundary, is about 150 km wide, 3 km deep and spreading at a half rate of 7 mm yr^{-1} (*Engen et al., 2008*). Due to its oceanographic importance, the opening of the Lena Trough is a major tectonic as well as paleoceanographic event (*Thiede et al., 1998; Jakobsson et al., 2007; Engen et al., 2008*). The opening of the Lena Trough and formation of the Fram Strait gateway is dated either in early or middle Miocene times, around 20 – 15 Ma (*Lawver et al., 1990, Engen et al., 2008*), after a seafloor spreading phase in the Eurasia Basin and the Norwegian – Greenland Sea that started in early Eocene times, during the separation of Eurasia from Greenland and North America (*Vogt et al., 1979*).

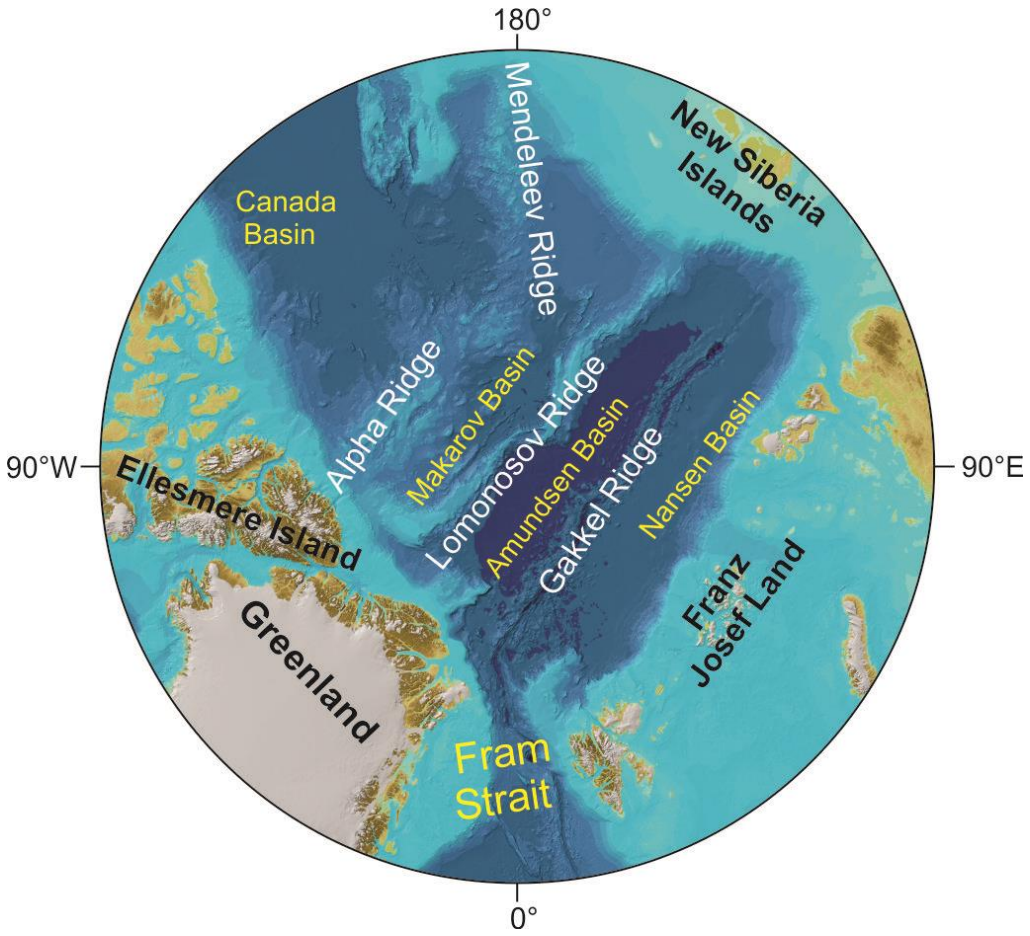

Figure 2: Map of the Arctic Ocean providing the location of the main tectonic structures cited, modified from the International Bathymetric Chart of the Arctic Ocean (IBCAO), *Jakobsson et al., 2012*.

South of the Fram Strait there is the northernmost member of the mid-ocean ridge system of the Norwegian-Greenland basin, called Knipovich Ridge. The latter is located adjacent to the west Spitsbergen margin, since Miocene time (*Gusev, 2001*) and it has the morphology of a rift valley, with an active center of spreading characterized by numerous active submarine volcanoes, faults and hydrothermal activity. These structures originate with both a northern-eastern as well as northern-western orientation, creating a rhombus structure, proof of the Knipovich Ridge complicated tectonic position as a transition zone between the Atlantic Mid-ocean Ridge and the Arctic Gakkel Ridge (*Talwani & Eldholm, 1977; Crane et al., 1995; Gusev, 2001*).

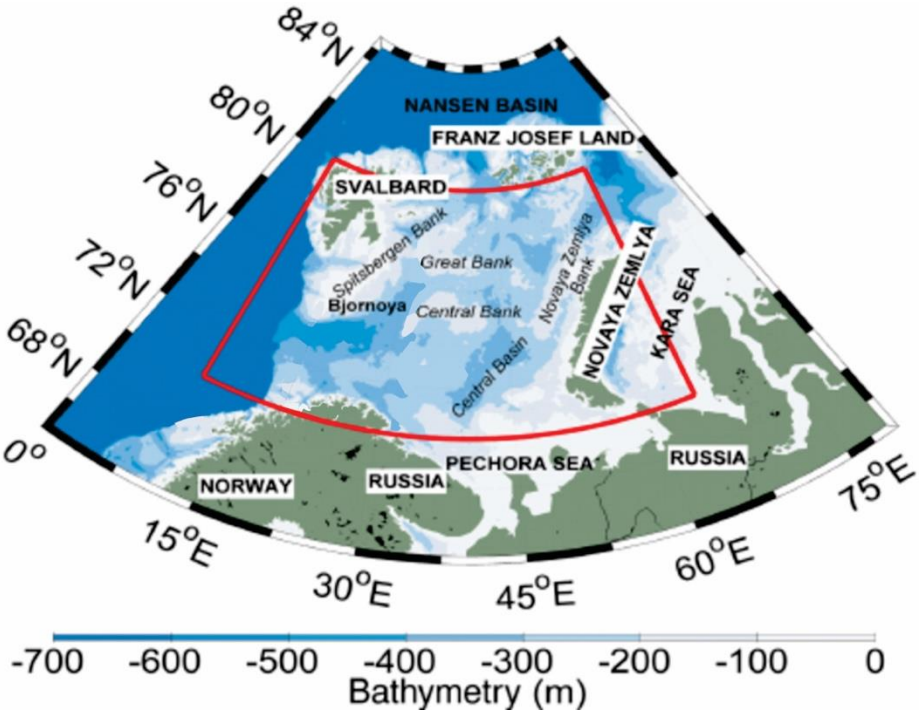

Figure 3: Bathymetric map, modified from *Harris et al., 1998*, showing the location of the NW Barents Sea (red sector in figure).

The Barents Sea, extending for about 1,400,000 km^2 is bordered by the Norwegian Sea and Greenland Sea to the west, Norway and Kola Peninsula to the south, Novaya Zemlya to the east, Svalbard archipelago to the northwest and Franz Josef Land at North (see Figure 3). Analysis of Ice-Rafted Debris and mineralogical data suggest that the ice growth phase in the Barents Sea began in the Late Plio-Pleistocene, around 3.6 and 2.4 Ma (*Knies et al., 1999, 2009*). The glaciation started on the exposed lands, i.e. the mountains and coast of Svalbard, Franz Josef Land and Novaya Zemlya. During a subsequent growth phase, around 2.4 Ma, the ice started to expand beyond the coastline in the north-western Barents Sea. In this phase, between 2.4 and 1.0 Ma the ice expanded far beyond the coastline, forming an interconnected mass of ice called Svalbard-Barents-Kara Ice Sheet (SBKIS) (*Hughes et al., 2016*). The SBKIS continued its expansion, reaching the continental shelf edge of Bjørnøyrenna around 1.5 Ma and later on, around 1.2 – 1.0 Ma, Storfjorden/southern Spitsbergen continental shelf (*Rebesco et al., 2013*). Around 1.0 Ma a large-scale intensification of glaciation took place in the Barents Sea, coinciding with glacial expansion in the circum-Atlantic region (*Knies et al., 2009*) (see Figure 4). Afterwards, the SBKIS reached the shelf edge in the Barents Sea at least five or six times during glacial maxima, in a series of repeated advances over the past 800 ka (*Knies et al., 2009*).

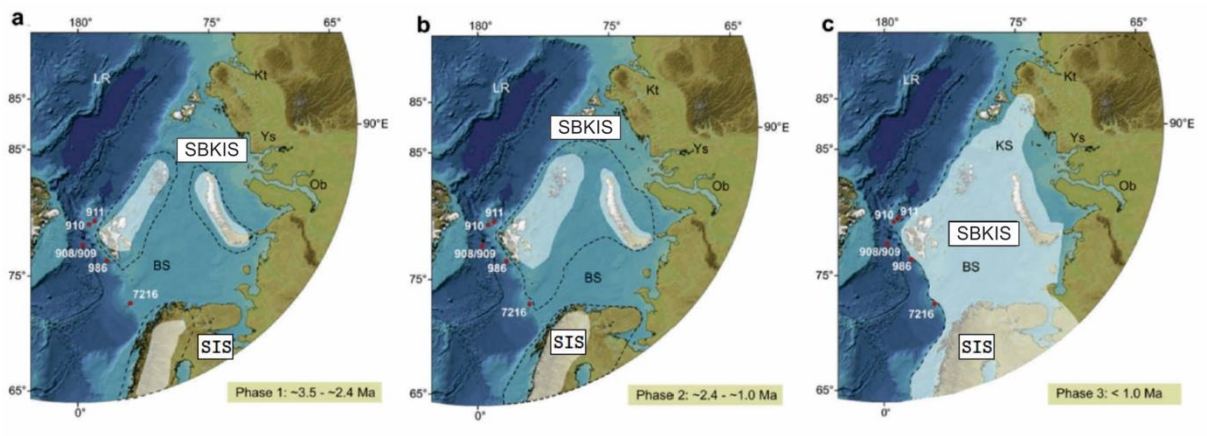

Figure 4: From *Knies et al. 2009*; Scheme of ice extension in the Barents Sea region during the Late Plio-Pleistocene time period (black dotted lines = maximum; white transparent polygons = minimum).

Phase 1 (⇠3.5–2.4 Ma) (a), Phase 2 (⇠2.4–1.0 Ma) (b), Phase 3 (<1.0 Ma) (c) is represented by the reconstructed Saalian (maximum) and LGM (minimum) glaciations, from *Svendsen et al. 2004*.

Several studies have been conducted in order to decipher the deglaciation of the northwestern Barents Sea continental margin (including western Svalbard): *Hyvärinen, 1968; Elverhøi et al., 1995; Salvigsen & Slettemark, 1995; Wohlfarth et al., 1995; Svendsen et al., 2004; Rasmussen et al., 2007; Rebesco et al., 2011, 2013; Rüther et al., 2011*. The dynamics and exact timing of the deglaciation is still a matter of debate, but there is agreement that the glacial retreat started in the deeper troughs, under the influence of ocean warming and sea-level rise *(Jones & Keigwin, 1988; Landvik et al., 1998; Winsborrow et al., 2010; Rüther et al., 2012)*. The Last Glacial Maximum (LGM) in the area of the NW Barents Sea occurred around 21.5 ka when the SBKIS extended to the shelf edge of the western Barents Sea margin *(Vorren & Laberg, 1996)*. At the time of the LGM, the SBKIS extended for about $2x10^6$ km^2, covering the entire Svalbard area (up to the Taimyr and Yamal peninsulas) (see Figure 5).

The onset of the deglaciation in the outermost portion of the Spitsbergen Bank is inferred to have begun around 20-19 ka *(Elverhoi et al., 1995; Rasmussen et al., 2007)* but was probably not synchronous. In the Kveithola Trough the onset of deglaciation is dated between 20 and 19 ka. In this area the ice retreated through an alternation of rapid retreats and stillstand periods *(Rasmussen et al., 2007; Pedrosa et al., 2011; Rebesco et al., 2011, 2016; Lucchi et al., 2013)*. In the Bear Island trough, the ice is inferred to have re-advanced hundreds of kilometers toward the shelf break around 17.1 ka bp *(Rüther et al., 2011)* before starting its final retreat. The small island of Bjørnøya (Bear Island), located between the Storfjorden and Bear Island troughs was ice-free at 11.2 ka bp *(Hyvärinen 1968; Wohlfarth et al., 1995)*.

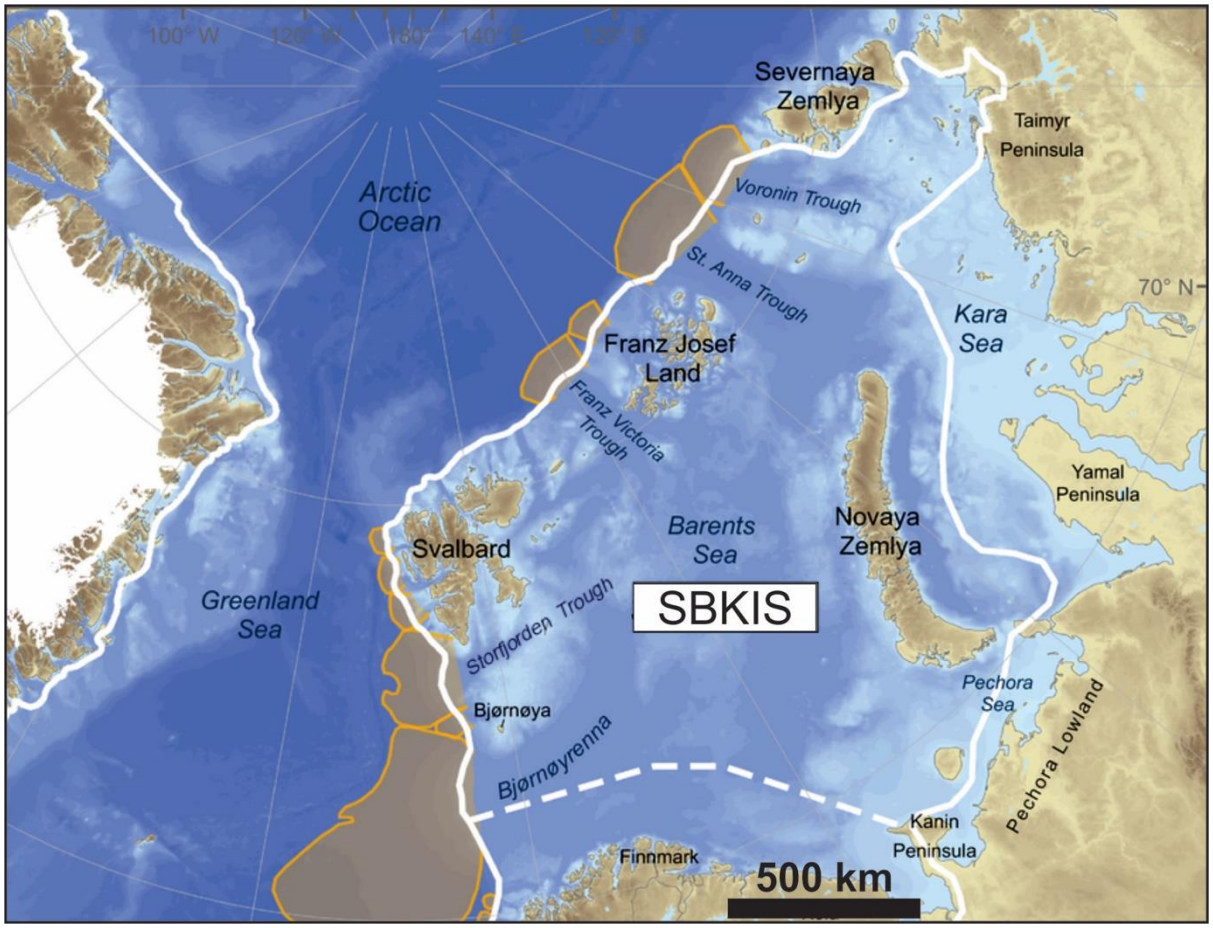

Figure 5: From *Hughes et al. 2016*; map of Barents Sea, illustrating maximum SBKIS extent during the last glacial period according to *Svendsen et al. 2004*. SBKIS = Svalbard-Barents-Kara Ice Sheet. Orange areas represent they extension of main Trough Mouth Fans. Topography and bathymetry from the GEBCO Digital Atlas, published by the British Oceanographic Data Centre on behalf of IOC and IHO (2003).

In an attempt to characterize such diversified ice sheet retreats, it is necessary to focus on ice streams, fast-moving region of an ice sheet (compared to the surrounding ice) that are acknowledged to fulfill a primary role in the ice sheet decay (*Margold et al., 2015*). Present-day ice streams are located in Greenland and Antarctica, where they are responsible for the majority of ice discharge, possibly affecting the entire ice sheet stability (*Weertman, 1974*). Present day ice streams, measured in the Antarctic region can move up to 1.5 km/year, generating shear stress at their bottom and producing a vast amount of geological structures. Anyhow, the study of present-day ice streams is restricted temporally, limited to a time window of decades at most, therefore excluding observations related to entire ice sheet decay cycles. In order to study ice streams and ice sheet retreat it is necessary to focus the attention on paleo-ice streams, reconstructing location and timing of advance/retreat cycles. Reconstruction of paleo-ice stream behavior on a high-latitude glaciated continental margin is possible through the analysis of the associated characteristic features in the sedimentological and geomorphological record (*Stokes & Clark, 2001*). The most prominent of these features

is probably the development of Trough Mouth Fans (TMFs), prograding fan-shaped sediment wedges (see Figure 6). The study of TMFs is the key to deciphering paleo ice streams, as the latter leave geological evidences on the whole margin structure, from the bottom of the slope of the TMFs to inner part of the shelf.

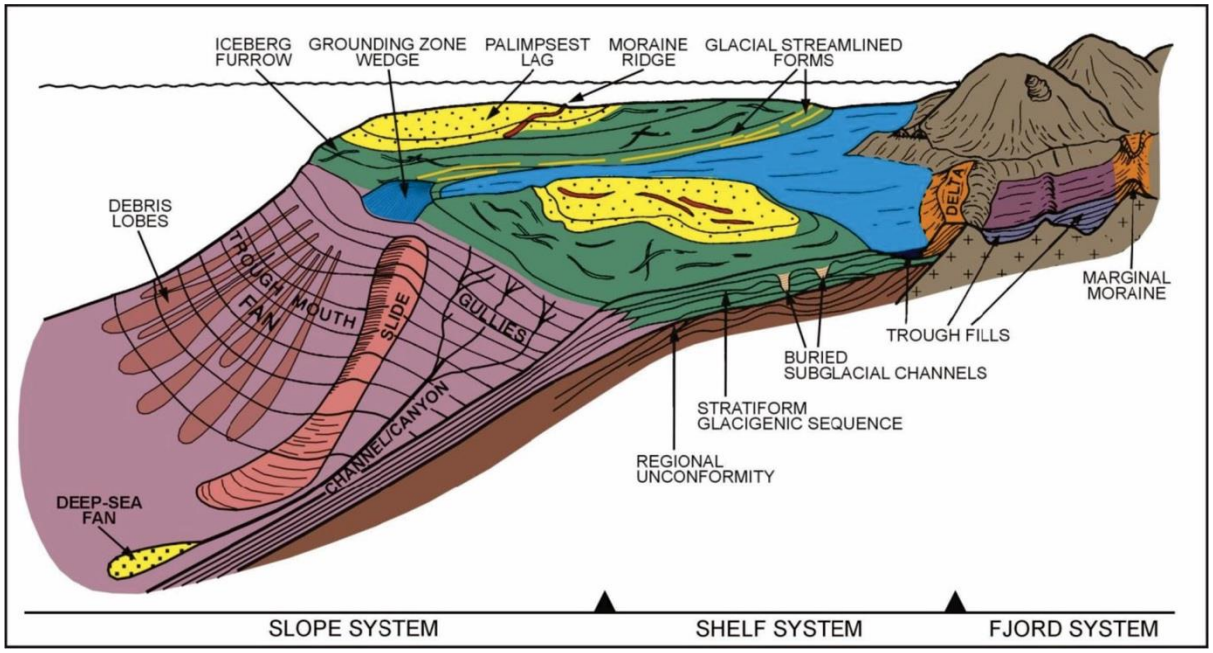

Figure 6: From *Vorren et al., 2003*: Scheme of the possible evidences (sedimentological and geomorphological structures) related to the presence of a paleo ice-sheet and/or a paleo ice-stream on a high-latitude glaciated continental margin.

On the west Spitsbergen margin and in particular in the NW Barents Sea, four main TMFs have been identified (*Vorren & Laberg, 1996, 1998; Rebesco et al., 2013*): Isfjorden TMF, Bellsund TMF, Storfjorden TMF and Bear Island TMF. TMFs can be studied both with a sedimentological approach, to reconstruct paleoclimate and paleoenvironment during glacial maxima and deglaciation periods (*Lucchi et al., 2013*), and with a geophysical approach, reconstructing past ice sheet dynamics of advance and retreat. TMF wedges are composed by a series of debris flows discharged at the mouth of cross-shelf troughs by the flow of ice streams. Starting from the shelf, clear markers of the presence of paleo-ice streams are Mega Scale Glacial Lineations (MSGLs), elongated landforms associated with fast-flowing ice found on the shelf. MGSLs are up to 10 km wide and can extend for more than 100 km, providing information regarding ice flow path and directions (*Clark, 1993*). Other evidence observable on the shelf are: moraine ridges, accumulation of unconsolidated glacial debris carried along by the ice stream marking the advances of the glacier; grounding zone wedges, sedimentary depocentres, 5 to 20 km long, tens of kilometers wide and up to 100 m thick, formed in a stillstand period during the retreat of an ice stream through the rapid

accumulation of glacigenic debris at the terminal part (grounding zone) of an ice stream (*Batchelor & Dowdeswell, 2015*) (see Figure 6 and 7).

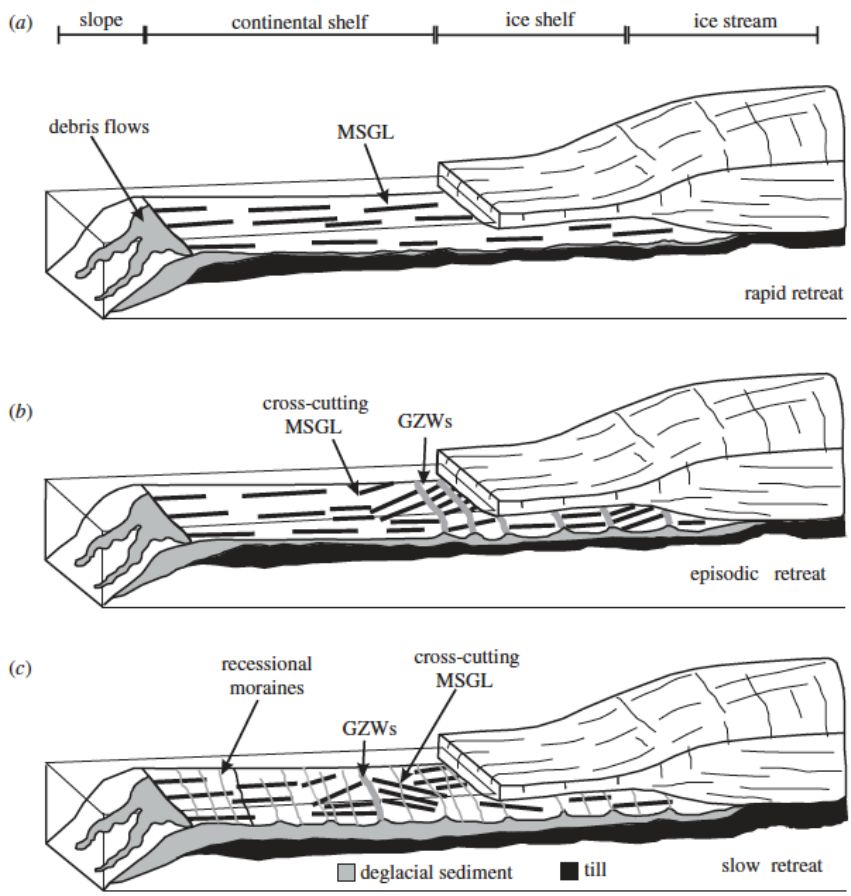

Figure 7: From *O'Cofaigh et al., 2012*: Scheme of the geological evidences produced during the retreat of an ice stream in the case of (a) a fast retreat, (b) an episodic retreat and (c) a slow retreat.

Meltwaters produced by the bottom friction of the ice stream are expelled into the surrounding waters, where, depending on their thermohaline characteristics, they can produce rising or descending turbulent meltwater plumes. At the shelf edge the ice in the distal part of the ice streams detaches from the bottom surface, eventually breaking and forming drifting icebergs which in turn can leave scours on the bottom surface known as ploughmarks (*Dowdeswell & Ottesen, 2013*) as well as producing ice rafted debris.

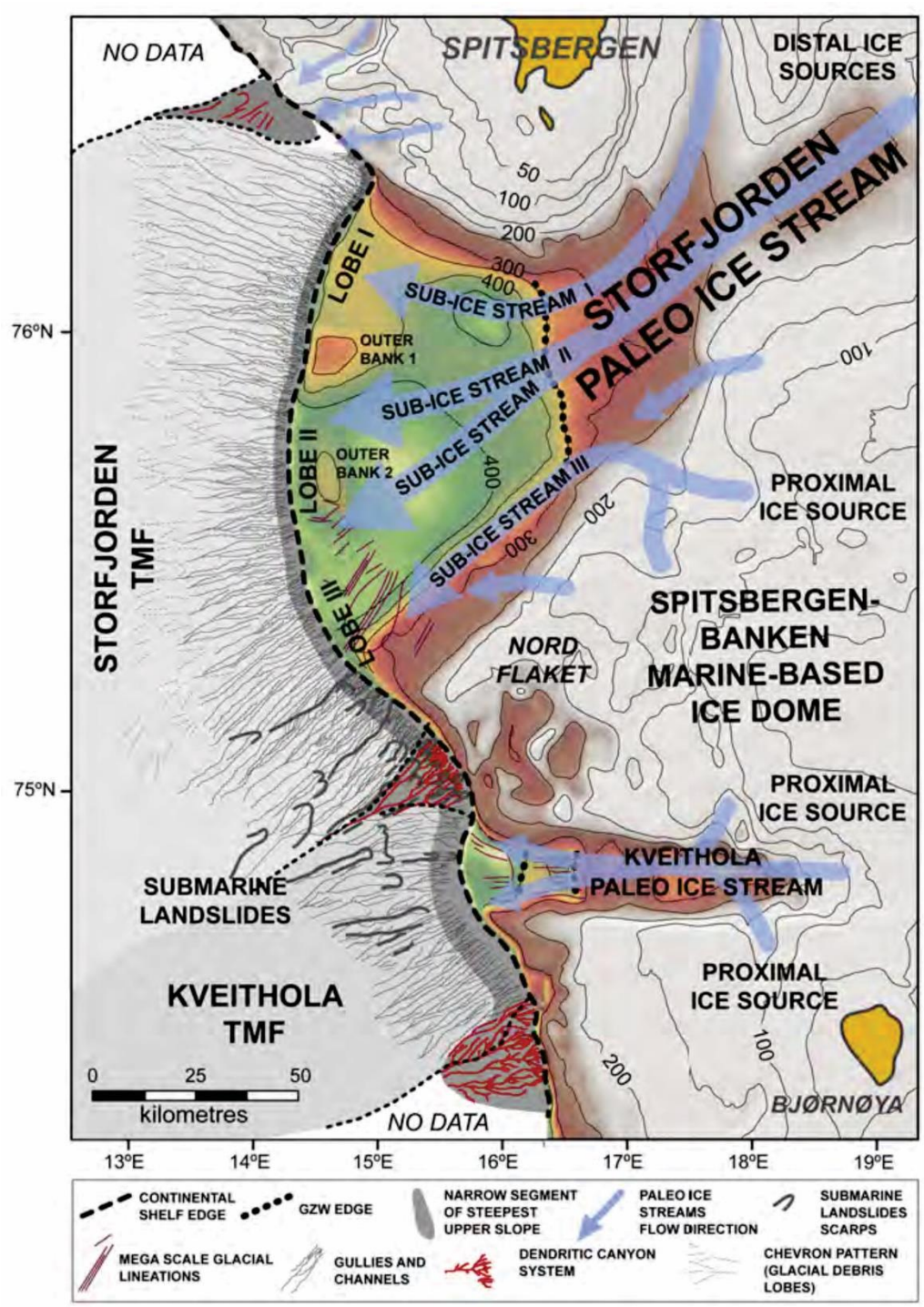

Figure 8: From *Pedrosa et al., 2011*: Scheme of the Storfjorden and Kveithola TMFs, with all geological evidences found in the bathymetric dataset and an interpretation of the dynamics of paleo-ice streams.

On the slope of TMFs it is possible to identify several features related to ice stream transport mechanics: some of these features are related to a transport and deposition process, generating debris lobes or even deep-sea fans produced by debris flows (see Figure 6). Debris flows are gravity flow involving the movement of inhomogeneous, unconsolidated material down a slope as slurry; in the case of a glacigenic debris flow, the movement of the material

is directly sourced from an ice margin or ice stream reaching the shelf edge (*Wilken & Mienert, 2006*). Another slope process (later discussed in this project) that may occur along a glaciated margin is a turbidite. The last is large mass of relatively fine grained sediments transported in suspension by a usually turbulent density-based flow (*Dowdeswell et al., 1998*). The initial density of turbidites, higher than the one of surrounding water, is preserved and/or even increased by the entrain of sediments, increasing the kinetic energy of the flux (*Fohrmann et al., 1998*).

Lastly, on the slopes of TMFs as well as in close proximity of the latter, it is possible to identify gullies/canyons/channels systems, carved into the slope by bypass-processes, i.e. involving transport and erosion rather than deposition. Gullies are small V-shaped erosional features dissecting the shelf edge and upper continental slope (*Gales et al., 2013*). If the processes responsible for the formation of gullies are persistent in time and/or increase in intensity they can lead to the formation of canyons, larger erosional features that can dissect the shelf edge and can extend across the seafloor from continental shelves into the deepest reaches of the oceans (*Normark & Carlson, 2003; Canals et al., 2004; Harris & Whiteway, 2011*), where they can eventually transition into U-shaped, lower-relief channels across the lower continental slope and beyond (*Shepard and Emery, 1941; Normark et al., 1993*). Canyon-channel systems can be effectively carved by sediment-gravity flows, delivering material from the shelf edge into deep water from rivers and/or ocean currents preferentially at sea-level lowstand periods (*Harris & Whiteway, 2011*). The majority of our knowledge on deep-sea canyon-channel systems is based on the study of those systems situated at low latitudes. These structures are quite frequent at low latitude, while they become rare in high-latitude continental margins. The development of canyon–channel systems aside from TMFs is attributed primarily to the sediment input from major ice streams, the main sediment source during glacial maxima. Sediment delivery from ice streams and ice sheets varies in fact both over time, through glacial-interglacial cycles and over space, with largest occurrences outside transverse troughs (*Dowdeswell et al., 2004*).

In the Norwegian – Greenland Sea the oldest channel system is located on the East Greenland continental margin (see Figure 9), in front of the Kaiser Franz Joseph Fjord and dated around 2.5 Ma (*Mienert et al., 1993; Dowdeswell et al., 2002; Evans et al., 2002; Ó Cofaigh et al., 2004; Wilken & Mienert, 2006; García et al., 2012, 2016; Peakall et al., 2012*; *Forwick et al., 2015*). This channel system originates at a water depth of about 1500 m on the continental slope in front of the Kaiser Franz Joseph Fjord, crossing the glacigenic debris flow deposits located on the final portion of the slope (*Wilken & Mienert, 2006*); it extends north-east for 500 kilometers, reaching the Greenland Basin at a water depth of 3700 m. The formation of this channel system is mainly attributed to sediment-laden meltwater produced by the ice sheet of East Greenland (*Wilken & Mienert, 2006*).

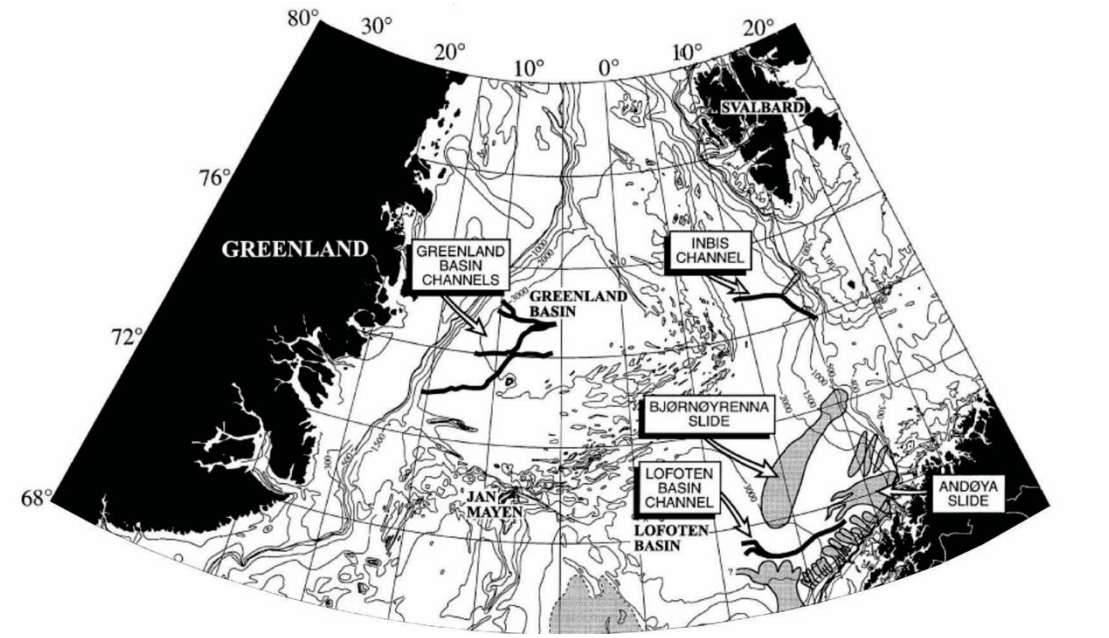

Figure 9: Modified from *Vorren et al., 1998*: Map of the Norwegian – Greenland Sea with the location of the Greenland Basin Channels, Lofoten Basin Channel and INBIS Channel.

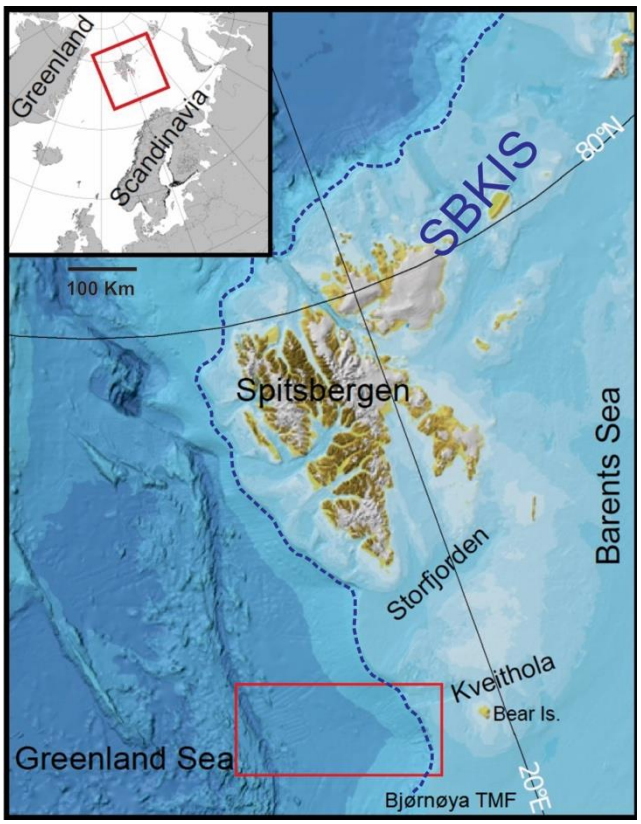

Figure 10: Bathymetric map (IBCAO) (*Jakobsson et al., 2012*), with the location of the INBIS Channel System (red rectangle), presented in Figure 33. The dotted blue line represents the extent of the SBKIS, after Hughes et al., 2006. See Figure 5 for further details.

Along the Norwegian continental margin, channel systems are far less frequent and less developed than those on the East Greenland continental margin (*Wilken & Mienert, 2006*). In fact only two large deep-sea channel have been observed: the Lofoten Basin Channel and the INBIS Channel (*Vorren and Laberg, 2001; Taylor et al., 2003; Rydningen et al., 2015; Forwick et al.,2015*) (see Figure 9 and Figure 10). The INBIS (Interfan Bear Island and Storfjorden) Channel System, one of the rare high-latitude channel systems on a glaciated margin, is located on the continental slope west of Bear Island (Bjørnøya) (NW Barents Sea) and it was detected for the first time by *Vorren et al*. (*1998*). The INBIS Channel is a 60 km long and 5-15 km wide nearly flat bottomed east-west oriented channel. The upslope part of the channel was at first described as buried under debris flows (*Vorren et al., 1998*).

The analysis of geological structures in the NW Barents Sea was not constrained only to those related to glacial systems, but it also extended on an equally developed group of structures, related to bottom-water circulation and known as contourites. The latter were first discovered nearly 53 years ago through deep-sea bottom photographs by *Heezen and Hollister* in *1964* in the Northern and Southern Atlantic Ocean. Since then, contourites has been the topic of many researches (*Hollister & Heezen, 1972; Rebesco et al., 2001, 2005, 2008, 2014*) and the even if at present day some uncertainties still remain, such as an undisputed identifying criteria. The definition of contourites is "sediments deposited or substantially reworked by the persistent action of bottom currents" (e.g. *Stow et al., 2002; Rebesco et al., 2005, 2014*). Among the considerable amount of contourites, those identified in the NW Barents Sea and analyzed in this project are contourite drifts. The latter are thick extended accumulations characterized usually by a mounded geometry. Dimensions, shape and sedimentary structure vary greatly, depending on many factors, such as the geological setting in which they develop and the characteristics of the currents system and water masses associated with them (velocity, direction, depth) (*Faugères & Stow, 2008*) (Figure 11). Contourite drifts usually develop in an elongated mounded geometry, growing up to 2 km thick, hundreds of kilometers long and more than 100 km wide (*Rebesco et al., 2014*). On the slope of the Western Spitsbergen margin, in the NW Barents, two of these giant elongated mounded drifts have been identified (*Rebesco et al., 2013*), located in front of the Isfjorden TMF and Bellsund TMF.

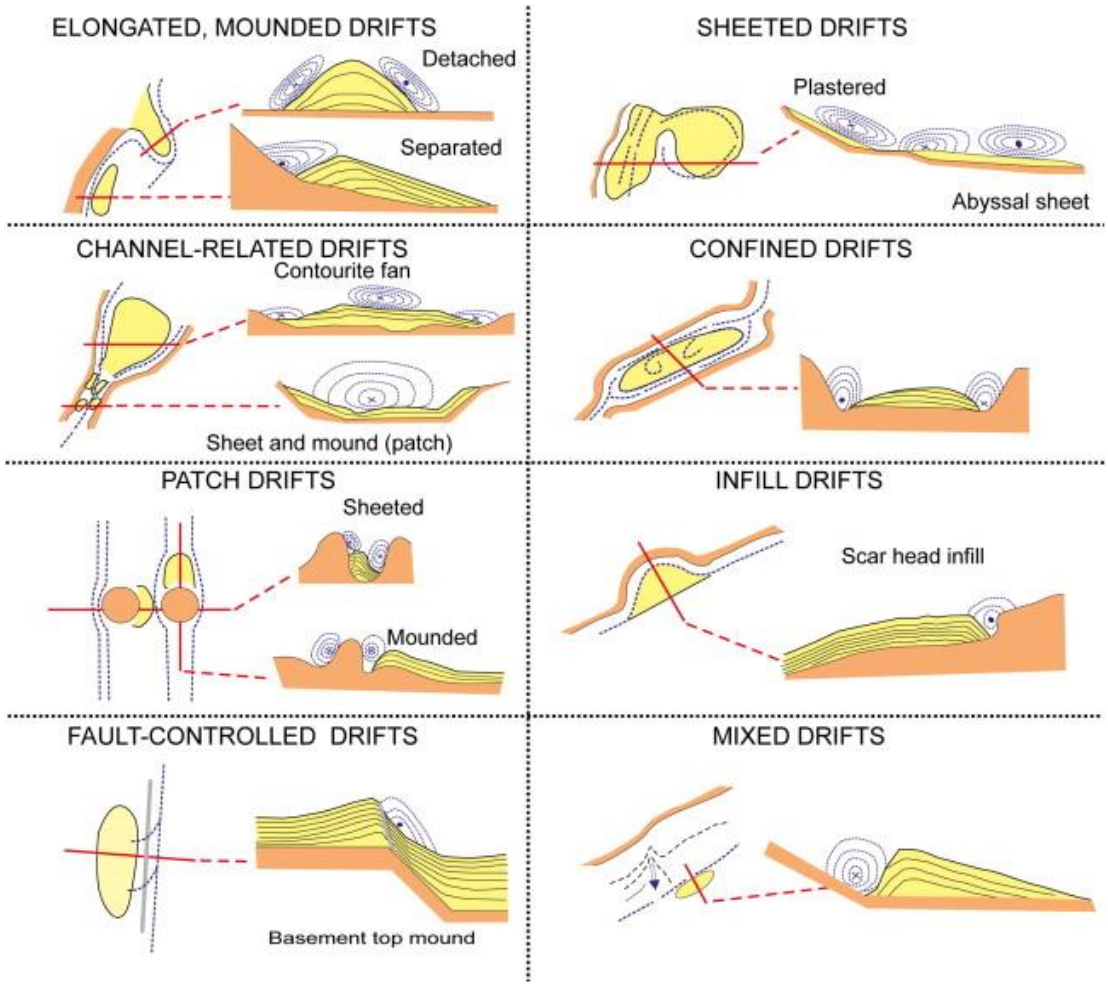

Figure 11: From *Rebesco et al., 2014*: Scheme of the possible shapes and dimensions of countourite drifts (yellow). Currents are represented by the dotted concentric lines.

1.1.2 Oceanographic background

In this section, the main circulation system of the NW Barents Sea and the main oceanographic processes that have a large impact on the ocean dynamics around Svalbard, linked with the geological features described in section 1.1.1, are presented.

The Arctic Ocean is of great interest for the scientific community, being the crossway of oceanic currents as well as the core for the exchange of heat and salt in the northern hemisphere of our planet. The study of circulation in the Arctic Ocean is however challenging due to a climate characterized by a strong arctic intrinsic variability, with long-term climate trends, multi-decadal fluctuations and high sub-annual variations (*Polyakov et al., 2013*). The Arctic Ocean circulation is dominated, at present conditions, by a continuation of the North Atlantic Current, called West Spitsbergen Current (WSC). The WSC is the biggest water inflow from the Nordic Seas and Atlantic Ocean. At around 69° N it splits into two major branches: one is the WSC (described further below) while the other is the North Cape Current, flowing eastward along the northern continental slope of Scandinavia. The WSC is the strongest and most persistent flow in this area, situated on the west Spitsbergen margin (*Aagaard et al., 1985; Aagaard et al., 1987; Rudels et al., 2000; Langehaug and Falck, 2012; Rebesco et al., 2013*) and it is considered the main source of the Atlantic warm and saline water to the Arctic (*Aagaard & Greisman, 1975*). In the northward flow, WSC is influenced by topography and tidal forces (*Rudels, 1987; Pfirman et al., 1994; Slubowska et al., 2005*). The lower part of the slope is instead crossed by the deepest reach of the WSC which carries a cold and saline water mass called Norwegian Sea Deep Water (NSDW) (see e.g. *Rebesco et al., 2013*). The WSC transports the Atlantic water into the Arctic Ocean through the Fram Strait (see Figure 12), where it dives at about 78° N and forms the Atlantic Layer that extends into the Arctic Ocean along the northern continental slope of Svalbard (*Aagaard & Carmack, 1989; Slubowska et al., 2005*) (see Figure 13). Around 79.5° N the WSC splits into two branches: one branch flows toward the Yermak Plateau while the other proceeds along the northern continental slope of Svalbard (*Manley, 1995*). The counterpart of the WSC in the Fram Strait is the southward East Greenland Current, a southward current which is the largest export path of sea ice from the Arctic Ocean (*Saloranta & Haugan, 2001*).

A study by *Slubowska et al.* (*2005*) reconstructed the paleoceanographic evolution of the Arctic Ocean after the LGM, from about 15 ka through the Holocene, with the analysis of foraminifera, oxygen isotopes and IRD in sediment cores. The study focuses on the role of the Atlantic water, since even small variations of the current system may produce distinct signals in the paleoceanographic record. It is stated that under polar conditions, sea ice cover prevailed through the Younger Dryas, during which the influx of Atlantic water was reduced. With the early Holocene, around 11.7 ka, the flow of Atlantic water became stronger, introducing more saline but still cold water. During the mid-Holocene the inflow of Atlantic

water began to gradually lower, reaching the lowest intensity between 4.5 and 1.1 ka. Eventually, in the last 1100 years, the Atlantic water inflow increased, due to improved climatic conditions.

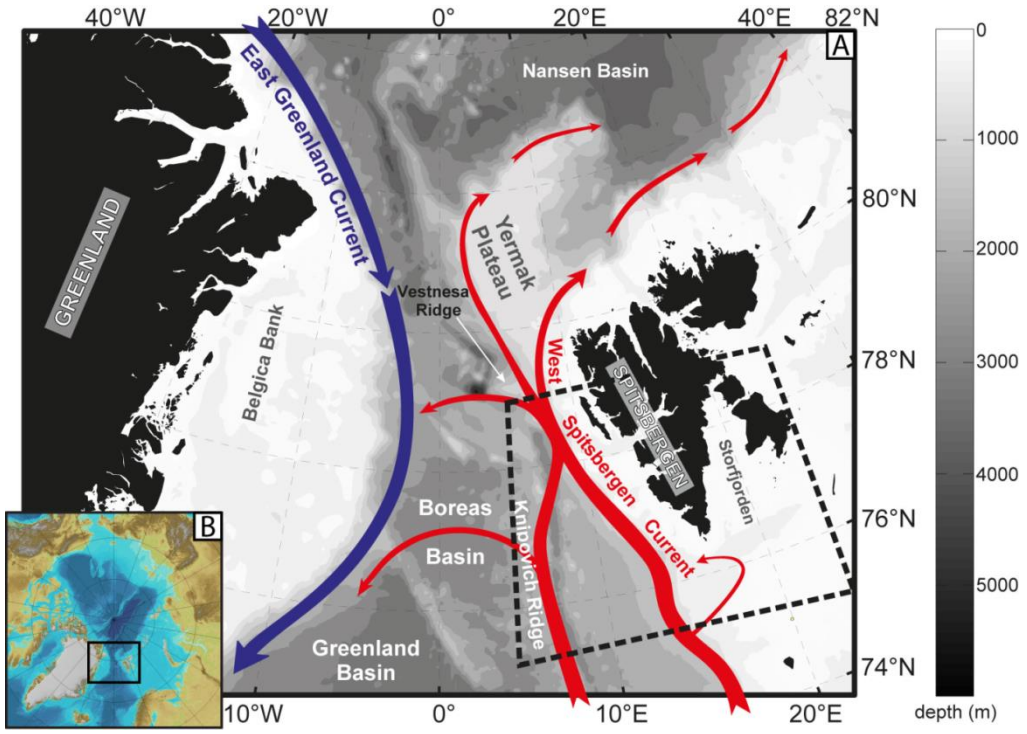

Figure 12: From *Rebesco et al., 2013*: Bathymetric map with a scheme of the ocean circulation through the Fram Strait, based on the bathymetric map ETOPO1. In red the West Spitsbergen Current, in blue the East Greenland Current.

The west Spitsbergen circulation is characterized by the presence of the WSC, flowing northward along slope west of the Spitsbergen archipelago (see Figure 12 and Figure 13). The thermohaline properties of the WSC are characterized by a variable temperature and salinity, accordingly with variable atmospheric conditions and large scale circulation processes, with high fluctuations on a sub-annual time scale (*Jonsson et al., 1992; Teigen et al., 2011; Rebesco et al., 2013; Polyakov et al., 2004, 2013*). Its Atlantic core, at around 300-400 m depth, has a temperature ranging between 2° and 4°C and a salinity ranging between 35.1 and 35.3 (*Aagaard et al., 1987*). The WSC has a relative strong barotropic velocity structure (*Teigen et al., 2010*), meaning that its density is a function of pressure only. The eastern branch of the WSC slope current develops into a slope/break confined barotropic component and a more baroclinic component over the deeper slope (*Gascard et al., 1995; Schauer et al., 2004*). The barotropic component occupies the upper 750 meters of the water column between the 1000 meters isobath and the West Spitsbergen shelf break; this structure is influenced by the wind field, as proved by a 13 year long time series of moorings array

data (velocity, temperature and salinity) analyzed by *Beszczynska-Möller et al*. (*2012*). The barotropic structure of the WSC shows instability in those areas characterized by horizontal shear between two masses of waters and by wind stress (*Teigen et al*., *2010*). The deeper baroclinic component occupies the part of the water column between the 1000 meter and 2400 meter isobaths and it exhibits instability in those areas characterized by vertical shear, i.e. bottom friction, eddies and cascading of dense water (*Teigen et al*., *2010*). The WSC flow is characterized by velocities of more than 20 cm/s registered near the surface due to a baroclinic shear associated with the Atlantic layer temperature maximum. High velocities are also registered at a near bottom (10 m above seabed) baroclinic core at 7°E, with the average value of 8.5 ± 0.2 cm/s; this value can increase up to 30 cm/s during winter and early spring, possibly due to the injection of dense water plumes (*Skogseth et al*., *2003, 2013; Rebesco et al*., *2013*). A further increase in velocity is registered around the depth of 1420 m (*Teigen et al*., *2011*), due to baroclinic pressure gradients from dense waters. Outside of this baroclinic core at 7°E, the velocities range between 4.2 and 5.6 ± 0.2 cm/s. The lowest part of the WSC, located below 1000 m depth, carries the Norwegian Sea Deep Water (NSDW). The NSDW is a water mass colder than the WSC, with a temperature <-0.9°C and a salinity >34.91.

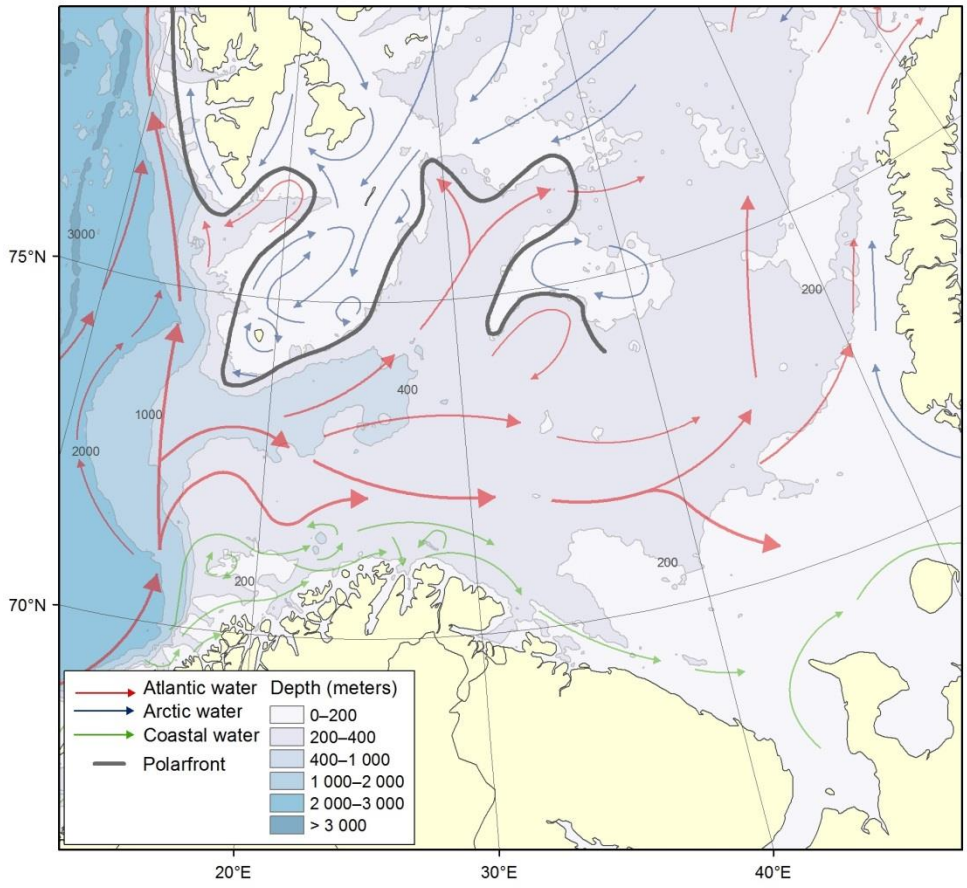

Figure 13: From *Stiansen and Filin, 2007*. Scheme of the circulation of the WSC in the NW Barents Sea.

In addition to the annual variability of the WSC, several other phenomena contribute to the complexity of the circulation in the NW Barents Sea. Among them, the ones I will address, of key importance for my study, are three: convection (open and shelf), brine rejection and entrainment

- **Convection**

  Normally, the vertical movement of water in the ocean is inhibited by strong vertical density gradients (i.e. pycnoclines). This stratification "protects" the deep ocean from variations linked to surface meteorology. However, in few special regions of the oceans, where the stratification is weaker, violent phenomena of open ocean convection reach the deeper portions of the water column during winter periods, producing mixing between surface waters with deep ones. Major known sites of open convection are the center of the Greenland Sea (*Schott et al., 1993; Visbeck et al., 1995*), Labrador Sea (*LabSea Group, 1998*) and small regions in the north-western Mediterranean Sea (*Gulf of Lions, see e.g. Schott et al., 1996*) and in the Eastern Mediterranean sub-basins (Adriatic, Aegean, and Levantine seas, see e.g. *Gacic et al., 2001*; *Manca et al., 2006*; *Bensi et al., 2013*; *Theocaris et al. 1993, 1998*; *Vilibic et al. 2003, 2004*). Accurately described by *Marshall and Schott* (*1999*), open convection is an intermittent phenomenon, happening on an annual time scale, in a cycle of convection and re-stratification. Open ocean convection involves a hierarchy of scales and develops through three phases known as preconditioning, deep convection and lateral exchange.

  - The initial phase, preconditioning, is a large scale phenomenon that could extend to an area of up to 100 km of diameter: in this phase the presence of gyre-scale cyclonic circulation shifts the weakly stratified waters of the interior portion of the water column closer to the surface. During winter, meteorological events with strong cold and dry winds may cause large buoyancy losses, due to the sea surface cooling. It erodes the near-surface stratification and triggers the deep convection.
  - The deep convection is the phase subsequent to the preconditioning, involving smaller areas (compared to the preconditioning) of about 1 km. During this phase a substantial part of the fluid column is inverted into numerous plumes, upwelling fluxes of water that rapidly mixes the dense surface water in the vertical. Deep convection and the "next" phase (lateral exchange) may be either subsequent or they may happen at the same time.
  - The third phase, called lateral exchange, in fact consists of returning to the equilibrium state after perturbation through the spreading and interchange of fluid between the mixed patch created by the plumes with the surrounding waters. Gravity and rotation disperse the mixed waters, forcing them slowly (i.e. on a time scale ranging from weeks to months) into their neutral buoyancy levels,

dissipating the mixed patch and re-establishing a stratified water column. An important fact regarding the convective process is that its timescale is sufficiently long that it may be modified by the Earth's rotation.

The cooling of surface water induced by winter heat loss and evaporation happens also on the shelf areas affected by cold and dry winds, such as the Arctic Ocean shelves (*Gawarkiewicz et al., 1997*), the Gulf of Lions (*Schoot et al., 1996*), the north Adriatic Sea (e.g. *Vilibic et al., 2003, 2004*) and the Aegean Sea (e.g. *Theocharis et al., 1993, 1998; Nittis et al., 2003*), where convection can easily reach the seafloor producing a layer of well-mixed dense water (see Figure 14). This dense water cascades through the shelf and down the slope via descending plumes (e.g. *Durrieu de Madron et al., 2012; Rubino et al., 2012*). Shelf convection is however more difficult to represent in climate models due to the fact that it is heavily influenced by the bathymetry, coastal fronts, mesoscale eddies (*Gawarkiewicz & Chapman, 1995*) and entrainment of ambient water (*Baringer & Price, 1997*).

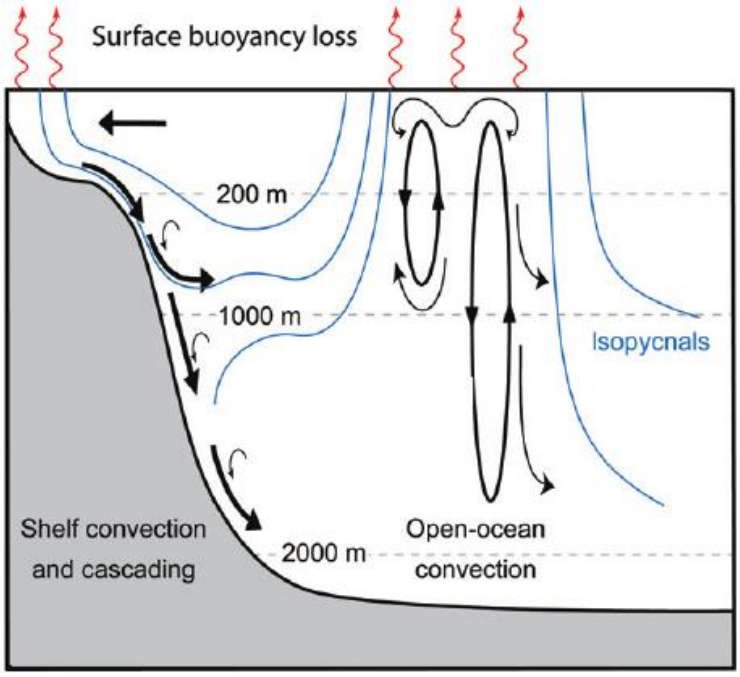

Figure 14: From *Pusceddu et al., 2010*: Scheme of the shelf convection and open-ocean convection processes.

- **Brine rejection**

Brine rejection is the process of expulsion of the salt from the ice pack into the surrounding water, generating a very salty and dense fluid (compared to the average sea water) called brine (*Cox & Weeks, 1974; Wettlaufer et al., 1997; Shcherbina et al., 2004; Vrbka & Jungwirth, 2005, 2007*). During sea ice formation, when the temperature of the water reaches the crystallization point, salt ions are rejected from the ice molecules and are either pushed into the seawater or enveloped by ice crystals into brine cells. The amount of brine expelled and/or brine cells formed is directly proportional to the velocity of the freezing processes (*Cox & Weeks, 1974*).

Brine rejection is a continuous process that starts during ice formation and proceeds with the ice grow. As sea ice becomes thicker with the passing of time, the initial salinity decreases thanks to the rejection of the brines trapped in the brine cells in three different ways:

- Solute diffusion: the brines begin to migrate from the brine cells toward the warmer end of the ice block that is the ice-water interface.
- Gravity drainage: the brines are denser than the surrounding ice, so they will naturally move toward the bottom of the ice pack due to the effect of gravity.
- Expulsion: thermal expansion of the ice together with the pressure produced by the increased volume of newly formed ice causes cracking; brines can move easily through these cracks.

The brine draining from the ice is partially replaced by fresh water, flowing from the liquid region below it. This fresh fluid partially freezes within the ice crystals, increasing the solidity of the ice.

In Storfjorden the production of these brine-enriched waters is often associated to coastal polynyas, areas of open water surrounded by sea ice. Brine-enriched shelf waters (BSW) fill sea-floor depressions, in particular inside fjords, accumulating and eventually spilling out of these depressions. The overflow of these BSW show a strong interannual variability, associated to both local factors as well as large-scale ones (e.g. North Atlantic – Barents Sea circulation) (*Skogseth et al., 2005*). When BSW spills out of a depression, if its density exceeds the surrounding water due to a lower temperature and/or a higher salinity, it sinks down the continental slope while entraining ambient waters. The ultimate depth reached by BSW overflows, as well the path of the overflow, strongly depends on its salinity (more than temperature), which shows strong inter-annual variability governed by many factors such as rate of ice formation, initial salinity, stability of the water column, location of the polynya, winter ice coverage and large-scale circulation (*Skogseth et al., 2003, 2005*).

- **Entrainment**

The term "entrainment" is intended to cover the transport of a fluid across an interface by a shear induced turbulent flux, between two volumes of fluid with distinctive properties: a relatively dense turbulent fluid and a non-turbulent lighter fluid at a higher virtual temperature (*Breidennthal et al., 1985*). Entrainment is fundamental in currents research, being involved in turbulent jets, plumes and gravity currents (*Scase et al., 2006*). Entrainment is observed in descending or upwelling plumes in particular, where the mixing of the plume water with surrounding water can increase the overall volume of about 500% (*Quadfasel et al., 1988; Jungclaus et al., 1995*).

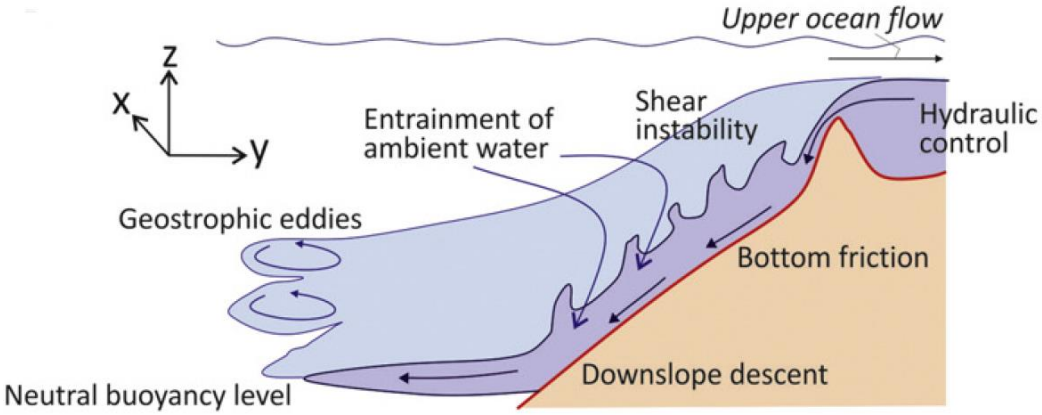

Figure 15: From *Rebesco et al., 2014*: Scheme of the entrainment process during the cascade of a dense water (for example, a BSW). The relatively dense turbulent fluid is represented in violet; the non-turbulent lighter fluid at a higher virtual temperature is represented in light blue.

In the case of BSW, the latter changes its temperature and salinity characteristics through the entrainment of ambient waters. BSW overflows are turbulent fluxes, much saltier and generally colder compared to surrounding waters, resulting in the entrainment of the latter. This process reduces the density, lowering salinity and raising temperature, up to a thermohaline equilibrium point in the water column (see Figure 15).

However, combined results from long-term time-series observations in the Storfjorden area (*Fohrmann et al., 1998; Sternberg et al., 2001; Skogseth et al., 2003*) suggests that these BSW propagate more rapidly than a plume driven only by a thermohaline anomaly. During fall and winter in fact, surface cooling and winds can induce near-bed currents or bottom stress (such as the transition of a turbulent fluid), resulting in the re-suspension of sediments. BSW overflows can pick up and transport this sediment as bedload or in suspension, resulting in even higher density fluxes that reach deeper portions of the water column compared to a sediment-free fluid with same thermohaline characteristics. Eventually, upon reaching

equilibrium density, suspended sediment starts to deposit, considerably reducing the density, and initiating upward convection in the water column (*Skogseth et al., 2005*).

2 Methods

In this chapter the methods adopted in my study are illustrated. In the first section the approach followed in this research to address the main scientific question is presented. The geophysical approach, i.e. swath bathymetry, sub-bottom and seismic data, will be addressed in the second part, describing how the data were acquired and providing a brief summary on the data processing. The last section will identify what kind of data is taken into account for the integration of results hailing from the geophysical dataset in a larger oceanographic setting.

2.1 Approach of the study

To address the scientific question motivating this research (see 1 Introduction), a geophysical dataset was acquired, analyzed and compared to the body of knowledge in ocean circulation of the NW Barents Sea. I therefore organized my research into three steps:

- the re-organization of the existing dataset into a single Kingdom Suite project (on a server located at OGS) of all the available pre-existing geophysical data, with the insertion of new ones in selected areas requiring additional data and/or further information (see subsection 2.2);

- the analysis and interpretation of the dataset, with the objectives to identify and describe the geological structures present on the West Spitsbergen continental margin (see section 3 and subsection 4.1);

- the comparison of results and interpretations hailing from the geophysical dataset with ocean circulation of the NW Barents Sea to depict the relationship at present conditions (and envisaged past conditions) between glacial depositional mechanisms and ocean circulation. To achieve this goal I also analyzed and discussed results hailing from *Bensi et al*., *in prep*., a paper of which I am co-author.

The geophysical dataset used in this Ph.D. study consists in three different data types: swath bathymetry data, sub-bottom data and seismic data. Kingdom Suite (provided by IHS, http://www.ihs.com/products/oil-gas-information/analysis-software/kingdom-seismic-interpretation/index.aspx) is the software that I used for the imaging and interpretation of geophysical data. It allows the loading and storing of point data ("*wells*"), line data ("*surveys*"), static (i.e. non-interactive) images ("*cultures*") and surfaces or volumes ("*polygons*"). In this research, it was used to store the swath bathymetry map of the NW

Barents Sea, covering an area of about 15.000 km^2, 38 sub-bottom profiles and 39 seismic profiles. The last two types of data required the linking of the SEGY files, final product of the processing phase, with the NAV file, i.e. *surveys* formed by list of geographical coordinates hailing from the GPS system on board research vessels (see subsection 3.2 for further details). The analysis of the swath bathymetry dataset was carried out using Global Mapper, a geographic information system (GIS) software useful for store, manipulate and analyze spatial/geographic data.

2.2 Geophysical dataset

I acquired a considerable part of the geophysical dataset used in this study during the development of the Ph.D., in a multidisciplinary EDIPO/DEGLABAR research cruise conducted in the NW Barents Sea in the summer of 2015, from the 19th of September to the 5th of October, on board the research vessel OGS Explora. The main objective of this research cruise was the acquisition of swath bathymetry, sub-bottom and seismic data along the west Spitsbergen continental margin, focusing in the area of the Isfjorden TMF, Bellsund TMF and the slope of an inter-fan area located directly West of Bear Island (Bjørnøya). The remaining portion of the geophysical dataset hail from several other research cruises conducted in the NW Barents Sea:

- SVAIS, conducted on board the R/V Hesperides, in 2007;
- EGLACOM, conducted on board the R/V OGS Explora, in 2008;
- GLACIBAR, conducted on board the R/V Jan Mayen, in 2009;
- CORIBAR, conducted on board the R/V Maria S. Merian, in 2013;
- PREPARED, conducted on board the R/V G.O. Sars, in 2014;
- High North 17, conducted on board the R/V Alliance, in 2017.

The first type of data, swath bathymetry, was acquired through the use of Multibeam echo sounders (MBES). Echo sounders are devices for remote detection and localization of objects in water producing a short pulse of sound called “ping”; this pulse travels into the water in a compressional wave, i.e. a moving series of pressure fronts propagating in water at the speed of sound (~1500 m/s).

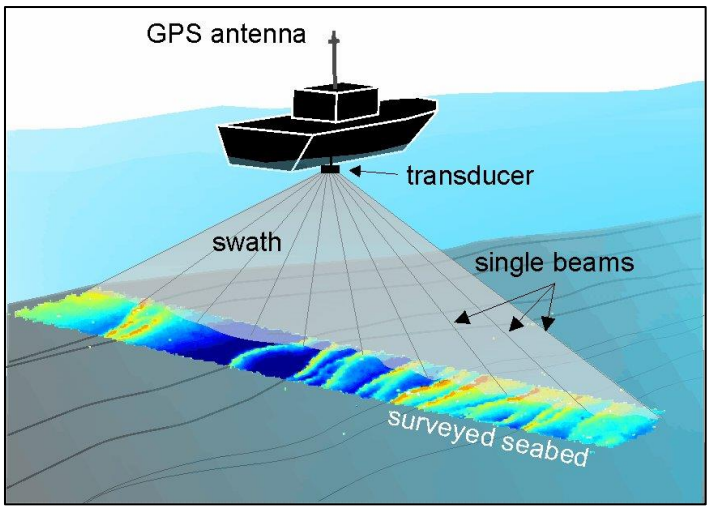

Figure 16: Scheme of the Multibeam functioning.

Sound speed in water needs to be acquired with high precision to properly calibrate several instruments, among which the MBES; therefore, immediately before calibration, a sound velocity vertical profile needs to be acquired through the use of a sound probe. The frequency (i.e. in this case, the number of pressure fronts that pass a stationary point in the water per unit time, *Yilmaz Ö., 2001*) of the pulse emitted by the MBES can be regulated, consequently modifying the wavelength, which is the physical distance between pressure fronts. After reaching the bottom surface, a portion of the pulse is reflected: echo sounders "listen" to this echo through hydrophones, instruments that convert into voltages the physical oscillations that they experience when sound waves infringe upon them. The time between transmission of a pulse and the return of its echo is the time the sound takes to travel to the bottom and back; therefore the distance from the echo sounder to the bottom is: *Distance* = *Velocity* x *Echo Time* x *(1/2)*.

Single-beam echo sounders however are not a time-efficient survey instrument because of several limitations, among which the main one is that they can only measure one depth point at a time. The area of the bottom effectively measured by the beam is the only part of the sea floor that can be considered "mapped" in a ping. A MBES is an instrument that can map more than one location on the ocean floor with a single ping and with higher resolution than those of conventional echo sounders. MBES electronically form a series of beams in a swath (a ribbon-shaped surface of depth measurement) perpendicular to the ship track; simultaneously the MBES receives beams in the transducer hardware, measuring the depth to the sea floor in discrete angular increments or sectors across the swath (*Hughes-Clarke et al., 1996*). Transmit frequencies varies depending on different MBES systems and on the sea floor depth. Low frequency (12 kHz) systems are utilized to collect swath soundings at full ocean depths, up to 10 km. In contrast, high frequency systems (300+ kHz) are utilized for collecting swath bathymetry shallower water depths, up to 20 meters or less. Fundamental

instruments for acquisition paired with the MBES are the GPS (Global Positioning System) and MRU (Motion Reference Unit). GPS and MRU provide precise and essential information for all the data collected during a research cruise.

The swath bathymetry data collected during the EGLACOM and DEGLABAR cruises were acquired using keel mounted MBES, Reson MB8111 – MB8150 and Reson MB8111 – MB7150, respectively. The SVAIS cruise used the MBES Kongsberg Simrad EM 120. The MBES Kongsberg Simrad EM 300 was used for the GLACIBAR cruise. For the CORIBAR cruise the swath bathymetry data were collected with the shallow-water Kongsberg EM1002 MBES and the moderate-deep water Kongsberg EM122 MBES. The MBES Kongsberg EM120 was used during the PREPARED cruise. The keel mounted MBES Kongsberg EM 302 was the instrument used during the High North 17 cruise. All systems used have an angular coverage of 150°.

Name	Cruise(s)	Optimal depth range	Operating Frequency	Beams number
MB8111	EGLACOM & EDIPO/DEGLABAR	<500 m	100 kHz	101
MB8150	EGLACOM	500-1500 m	12 kHz	234
MB7150	EDIPO/DEGLABAR	500-1500 m	12 kHz	880
EM300	GLACIBAR	<5000 m	30 kHz	135
EM120	SVAIS/PREPARED	<1100 m	12 kHz	191
EM1002	CORIBAR	<400 m	95 kHz	111
EM122	CORIBAR	>400 m	12 kHz	432
EM302	High North 17	10-7000 m	30 kHz	864

Table 1: Table summing up all the Multibeam systems used for the acquisition of the joint dataset presented in this paper.

The data collected underwent a processing phase using two software: PDS2000 and CARIS. The elaboration of swath bathymetry data collected with a MBES is needed to:

- Estimate and correct for roll/pitch/heave effects;
- Remove noise effects;
- Sound velocity calibration;
- Correction of tide effects;
- Editing of a grid and interpolation of data.

Eventually all the data collected were merged into a single dataset, with a data gridding of 30 meters. Total horizontal uncertainty (THU) is related to the multibeam instrument used, while to obtain the total vertical uncertainty (TVU) it was necessary to combine the uncertainties from both GPS and multibeam instruments. TVU was calculated as follow:

$$TVU = \pm\sqrt{a^2 + (b * d)^2}$$

a = instrument precision

b = uncertainty varying with depth (coefficient)

d = depth

d < 200 m	Max. allowable THU 95% Confidence level	5 metres + 5% of depth
	Max. allowable TVU 95% Confidence level	a = 0.5 metre b = 0.013
d > 200 m	Max. allowable THU 95% Confidence level	20 metres + 10% of depth
	Max. allowable TVU 95% Confidence level	a = 1.0 metre b = 0.023

Table 2: Total vertical (TVU) and horizontal (THU) uncertainties, based on IHO STANDARDS FOR HYDROGRAPHIC SURVEYS (S-44) (5th Edition February 2008).

Through the use of the software GlobalMapper, I was also able to create slope maps (visible in figures30, 33 and 38). Setting up a proper range for the gradient scale (0.0° < x <15.0°), slope maps helped in the detection of smaller geological features otherwise hard to detect and/or not appreciable in the large bathymetric dataset.

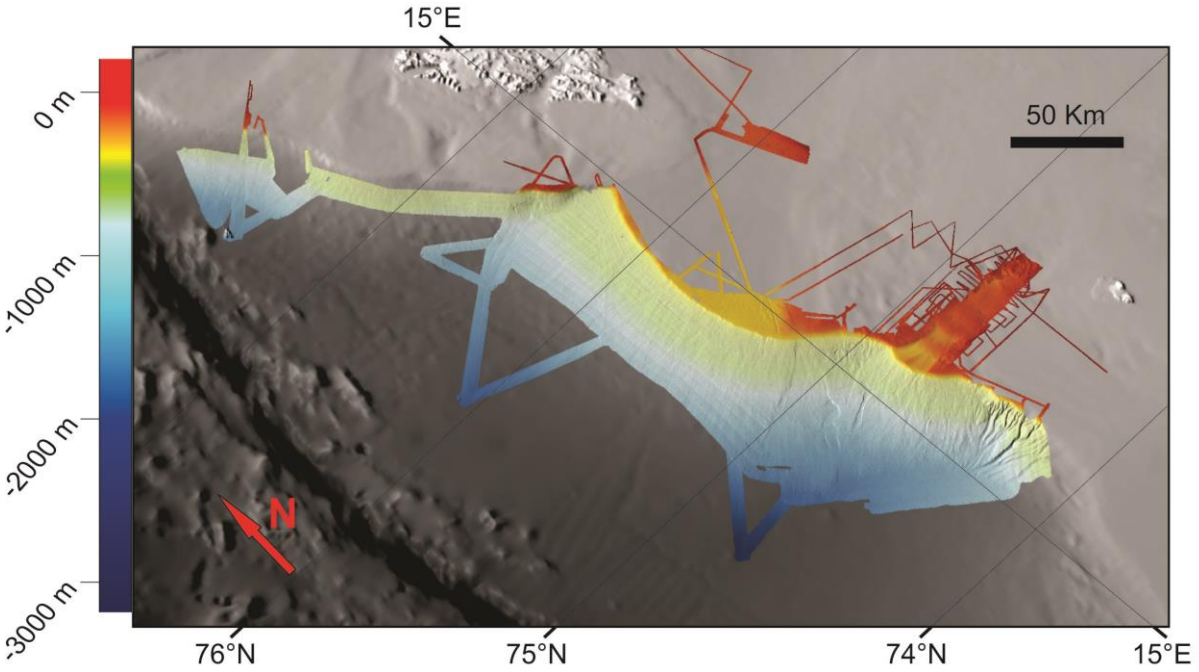

Figure 17: A 3D view of the joint multibeam dataset from SVAIS (P.I. Camerlenghi), EGLACOM (P.I. Rebesco), GLACIBAR (P.I. Andreassen), CORIBAR (P.I. Hanebuth), EDIPO (P.I. Caburlotto) and DEGLABAR (P.I. Casamor).

In addition to swath bathymetry data, during the High North 17 cruise, Backscatter data were also collected in order to describe the seabed morphology. Multibeam backscatter was previously considered a by-product of multibeam bathymetry acquisition; with advances in instrumentation and new methods of analysis, backscatter data potential was increased and became useful for seabed characterization (*Lockhart et al., 2001*). While bathymetry gives depth information, multibeam backscatter data provides information regarding the intensity of the reflected waves. A preliminary sediment classification based on both backscatter data and morphology were produced with software CARIS "Hips & Sips".

The second group of data, i.e. information regarding the first tens of meters below the sea bottom, was acquired through the use of sub-bottom profilers. The latter is a sound source that directs a pulse, consisting of a frequencies sweep, toward the seafloor. Parts of this sound pulse reflect off of the seafloor, while other parts penetrate the seafloor, involving a trade-off between penetration into the seafloor and resolution. The parts of the sound pulse that penetrate the seafloor are both reflected and refracted as they pass into different layers of sediment; eventually hydrophones mounted on the research vessel detect these signals when they return toward the surface. Lower frequency pulses achieve greater penetration at the cost a lower-resolution image, while higher frequency pulses penetrates a shallower part of the seafloor, yet producing a high resolution image. The penetration-resolution relationship is not linear but it is fairly constant, allowing real-time adaptation of the frequency pulse to obtain optimal results. The SBP data presented in this study were collected during the EGLACOM

and EDIPO/DEGLABAR cruises using a hull mounted 16 transducers Chirp Benthos system; the ping rate was set to 0.25 sec (with a speed of about 4 Knots, that is 2 m/s, this corresponds to two trace/m). The data were stored in SEGY format with the positioning from GPS automatically incorporated within the data headers. During the final portion of the EDIPO/DEGLABAR cruise, rough weather conditions highly affected the acquisition of both bathymetric and sub-bottom data. This resulted in a considerably lower quality of the data (both bathymetric and sub-bottom) in the southernmost portion of the INBIS Channel System. The vessel, when moving, may be subjected to different and simultaneously motion as roll, pitch, yaw, and heave. The last is the major error component of the four listed motions. In case of bad weather conditions, such as those encountered during the final portion of the EDIPO/DEGLABAR cruise, these motions can increase dramatically: this affect the quality of the sub-bottom data, causing sideward reflections of the emitted signal. Furthermore bad weather conditions might produce synchronization problems between the sub-bottom acquisition system and PDS2000 device, or problems due to different acquisition time annotation. In an attempt to compensate the decrease in data quality, a post-processing procedure was applied to the sub-bottom data. The latter has been performed after a general Quality Control during the acquisition. This procedure is divided in three scripts: the first one converts the format of the heave data file, extracted manually from the ship motion sensor through PDS2000, making it compatible with sub-bottom data format.

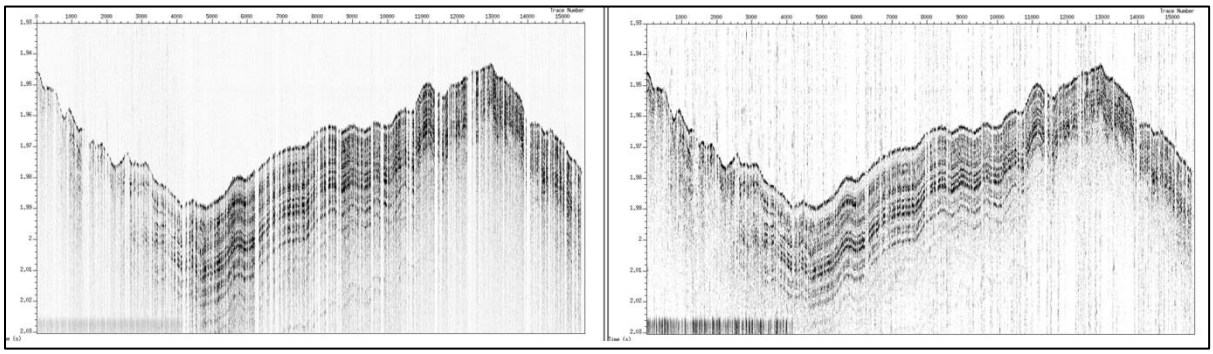

Figure 18: Image of the same sub-bottom profile (SV15_SBP03) before (left) and after (right) the wave motion correction procedure. After the correction, reflectors appear more clearly and the noise produced by vessel movement is partially reduced.

The second one is the most consistent, performing time correction for each single trace using the heave data files extracted and as consequence removing the vertical component of the wave motion (see Figure 18). The third script performs a further adjustment of the sub-bottom data headers, so that it can be properly displayed as a “sub-bottom profile”.

The third data type, seismic data, was acquired during the SVAIS, EGLACOM and EDIPO/DEGLABAR cruises. The purpose of seismic surveys is to accurately record the

ground motion caused by a known *source* in a known location; the record of ground motion with time is the basic information used for interpretation (through modelling or imaging) and it is called seismogram (*Kearey et al., 2013*). The essential instruments for seismic acquisition are:

- *Source* (or sources): The source must be able to produce sufficient energy concentrated in the type of wave energy required for a specific survey, generating a seismic pulse. The seismic pulse must have a repeatable waveform; when it is possible (depending on time/costs factors) to run field tests on the seismic source, source waveform is known, dramatically increasing both the product of the acquisition and the quality of the processing phase as well. In the case of marine acquisition, the ideal seismic source is the air gun, thanks to their mechanical simplicity and the ability to operate with great reliability and repeatability. This is a pneumatic source, compressing air (fed through a shipboard compressor) into a chamber. Different chamber volumes lead to different energy outputs and frequency characteristics, therefore the choice of the correct air gun is a fundamental step during the planning phase of a seismic survey. When this high-pressured air is released into the water it forms a primary high-pressure bubble, generating a seismic pulse. Depending on the available seismic sources, it is also possible to use arrays of seismic sources, to increase penetration. The propagation of this pulse is similar to the one described previously in the case of the MBES (and of the sub-bottom profiler as well) in the sense that when this pulse reaches the sea bottom a part is reflected and a part penetrates (refracted) into the ground, depending on values of *acoustic impedance* (*Z*). Such impedance is an intrinsic propriety of the medium(s), defined as the product of its *density* (ρ) and acoustic velocity (*V*). The distribution of how the pulse splits and further propagates into the ground, as well as the description of how the pulse energy is redistributed are complex and too long to be exhaustively taken into account and explained in this work (for further details see *Yilmaz Ö., 2001* and *Kearey et al., 2013*). Summarizing, the pulse propagates into the ground, repeating the splitting process every time a contrast (i.e. a change of the value) of acoustic impedance is met, i.e. whenever it meets a geological variation (lithology, facies, porosity, fluid content…) generating a reflection. These reflections travel back into the ground and into the water through the surface, to eventually intercept one (or multiple) receiver.

- *Transducers* (*streamer*): Special receivers, called transducers, are needed to convert the ground motion into electrical signal. Transducers are sensitive to some component of the ground motion and can record frequency and amplitudes without distortion. Many different types of transducer exist and can be selected, depending on the case. In marine acquisition, the ideal transducers are *hydrophones*, devices made of ceramic

piezoelectric elements able to detect transient pressure changes in the water produced by the passage of a compressional seismic wave and to produce an output voltage proportional to it. Therefore, with the use of hydrophones it is possible to register the reflections traveling back from the sea-bottom and the ground beneath it (up to the maximum penetration reached). Marine multichannel seismic entails a large number of hydrophones distributed along a plastic tube called *streamer*. Streamers are made of material with acoustic impedance similar to the one of the water and they have neutral buoyancy, controlled by special instrument attached to it called "fish". Hydrophones may also be arranged into arrays (*groups*), linear or areal, to enhance the signal and suppress certain types of noise.

Both the source and the streamer are towed from the stern of the research vessel, with specific distances between them and the ship. Positioning of source and streamer is a key feature to be accurately considered during the planning phase of a seismic survey, as it influences the geometry of acquisition and results in different types of data elaboration.

A scheme of the acquisition configuration adopted during the EDIPO/DEGLABAR cruise is presented in Table 3 and Figure 19.

ACQUISTION PARAMETERS					
SOURCE		STREAMER		RECORDING	
Model	Mini GI-GUN Sercel GI-GUN Sercel	Model	Geometrics Geoeel	Model	Geometrics CNT-1
Array	1 x 60 cu.in (1l) 1x210 cu.in (3.44l)	Length	300 m	Sampling rate	0.5 ms
Gun Mode	30G+30I Harmonic 105G+105I Harmonic	Ch. No.	96	Record length	4.5 sec
Shot Interval	15.625 m	Ch. Dist.	3.125 m	LC filters	3 Hz (LC);
Depth	3 m ± 0.5 m	Depth	3 m ± 0.5 m	HC filters	Antialias
Pressure	140 atm.	Min off.	40 m	Aux channels	Ch.2
SYNCHRONIZATION		Max off.	340 m		
Controller	RTS Big Shot	Max fold	9.6		
Aim Point	50 ms delay				

Table 3: From EDIPO/DEGLABAR Cruise Report, *Facchin et al., 2017*. Table with the acquisition parameters adopted during the EDIPO/DEGLABAR cruise.

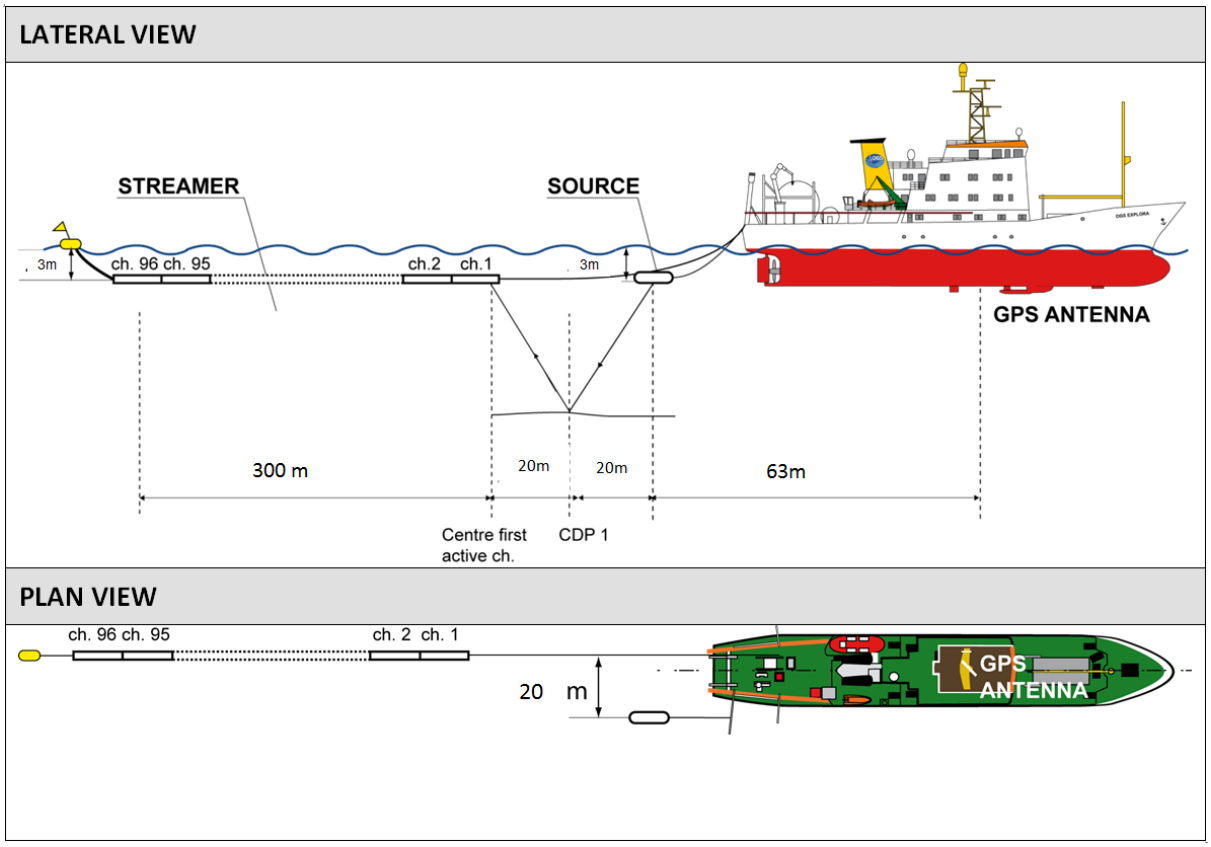

Figure 19: From EDIPO/DEGLABAR Cruise Report, *Facchin et al., 2017*. A scheme of the acquisition configuration adopted during the EDIPO/DEGLABAR cruise.

Subsequently, seismic data requires processing (to enhance the signal, remove noise and produce a seismic section) in a post-acquisition phase called *processing*. The latter is a procedure that, even following some mandatory steps, is highly influenced by the type of data acquired, the quality of the data acquired, the geometry of acquisition, the type of product to be obtained and so on. To describe every possible step of seismic processing is a task that far exceeds the aims of this work (for further information see *Kearey et al., 2013*), therefore only the processing procedure related to the EDIPO/DEGLABAR cruise is briefly addressed. I processed these data through the use of FOCUS.

The first step was a pre-processing operation to match *shot points* (when the source effectively releases a pulse) and *field records* (when a pulse release is actually registered by the acquisition system). After a subsequent format change, a header of the raw trace is created and reordered in a specific sequence (called *marine*). The next step is the creation of the *geometry*, i.e. the reconstruction of the acquisition geometry, based on position and dimensions of every instrument (source, streamer and distance from boat) and on the rate of the acquisition (shot interval, in time and space). All these information were accurately registered during the cruise. Further in the processing procedure, the *near trace* (trace registered from the first hydrophone of the streamer) is analyzed, to allow a series of

operations (*deconvolution*, *sea bed muting* and *filters*). The next step is *velocity analysis*, to determine the correct velocity from every layer crossed by the seismic pulse. This analysis must be done many times on a selected interval of traces to ensure a high quality data. Successively, the data goes through a *normal move out* correction, low band *filtering* and *muting*, in preparation of the final step (for these data): the *stack*. The latter is the sum of all the shots illuminating (i.e. acquiring a pulse reflection from) the same point in the ground. With this sum it was possible to increase the signal of true reflections and to decrease noise.

39 seismic profiles were acquired, processed and/or analyzed for this Ph.D. project; in particular, in the area of the Isfjorden TMF (see subsection 3.1), I also correlated the available seismic profiles with data by *Forsberg et al*. (*1999*), *Knies et al*. (*2009*) and *Rebesco et al*. (*2013*) hailing from the ODP (Ocean Drilling Project) Site 986, located in a distal offshore position southwest of the Isfjorden TMF (*Raymo et al*., *1999*). I also extended the same type of correlation further south along the slope, on the seismic profiles acquired in the Bellsund area (see subsection 3.2).

2.3 Overview of the oceanographic data

In this section, an overview of the oceanographic data that I used in support of the geophysical data is presented. In section 4, the results that I obtained from the geophysical dataset will be discussed and compared with oceanographic data. The latter hails from a paper in preparation (*Bensi et al., in preparation*) based on data recently collected along the west Spitsbergen margin through the use of two deep moorings (Figure 20). I discuss the results obtained from the geophysical and oceanorgraphic data with those presented in several studies focused on the NW Barents Sea and Fram Strait areas (*Aagaard et al., 1987; Rudels et al., 1987, 2000; Quadfasel et al., 1988; Pfirman et al., 1994; Gascard et al., 1995; Jungclaus et al., 1995; Sternberg et al., 2001; Ślubowska et al., 2005; Rasmussen et al., 2007; Teigen et al., 2010, 2011; Akimova et al., 2011; Beszczynska-Möller et al., 2012; Langehaug & Falck, 2012; Skogseth et al., 2003, 2013*).

I wish to specify that I had no part in the processing of the oceanographic data. The following methodologic part is needed to provide a clear description of acquisition and processing procedures carried on by *Bensi et al*. (*in preparation*). I collaborated in the discussion and contextualization of the oceanographic results in the geophysical and geological setting.

An oceanographic mooring is a fixed underwater autonomous platform deployed for a certain period of time to collect high temporal resolution (e.g. minutes to hours) time-series (i.e. thermohaline properties, ocean currents, etc.). Moorings are exceptional tools for obtaining data in areas that are difficult to be reached by oceanographic vessels, such as the polar ones. The presence of a research team is needed during the deployment and recovery phases and during the maintenance operations. Mooring design varies accordingly with scientific objectives and it can host different instruments throughout its rope line. A large amount of instruments can be attached to a mooring and a complete description would exceed the objective of my project; therefore only the instruments related to the oceanographic data taken into account for this study are addressed. All the following information comes from the cruise reports of two research cruises: the first one being the EUROFLEETS2 - PREPARED (PREsent and PAst flow REgime On contourite Drifts west of Spitsbergen) (*Lucchi et al., 2014*) cruise on board the R/V G.O. Sars (5th - 15th June 2014); the second one being the PNRA-DEFROST (DEep Flow Regime Off SpiTsbergen) (*Bensi et al., 2016*) on board the R/V Polarstern (13th - 23rd June 2016).

EUROFLEETS2 was a 48 months European programme started in March 2013 with the aims of consolidating a cooperation strategy for optimizing the sharing and use of research vessels, including those sailing in Polar Regions. PNRA is the Italian National Antarctic Program, recently expanding its area of interest also in the Arctic Ocean.

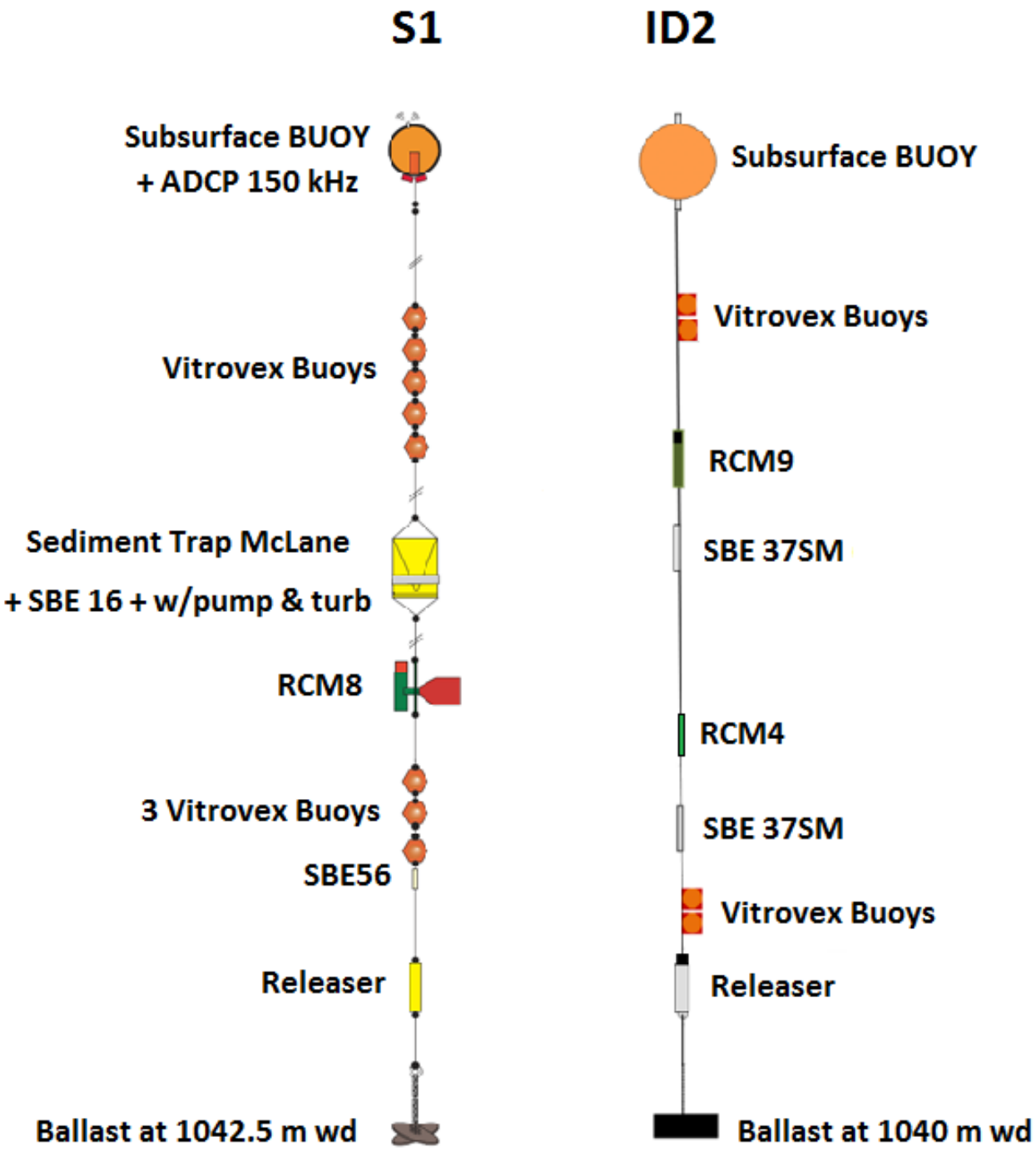

Figure 20: Modified from EUROFLEETS2 - PREPARED cruise report (*Lucchi et al., 2014*). Scheme of moorings S1 and ID2. For further information see Table 4.

Mooring Information	Type of Instrument	Instrument depth (m)	Sample time (min)
Mooring ID2 From 10/06/2014 to 22/06/2016 Depth 1040 m Latitude: 77° 38.760' N Longitude: 10° 16.890'E (Isfjorden drift)	RCM9 SBE37SM(1st year)/SBE56 (2st year) RCM4 SBE37SM(1st year)/SBE56 (2st year)	~ 921 ~ 922 ~ 1024 ~ 1025	120 (1st year) - 60 (2st year) 15 60 15
Mooring S1 From 09/06/2014 to 21/06/2016 Depth 1042 m Latitude: 76° 26.288' N Longitude: 13° 56.907' E (Bellsund drift)	ADCP 150 KHz Sediment Trap McLane SBE 16 + turbidity RCM8	~ 906 ~ 1017 ~ 1017 ~ 1022	30 from 15 to 30 days 30 60

Table 4: Information regarding moorings S1 and ID2 with relative location, water depth, instruments and sample times.

RCM4 and **RCM8** are single point **current meters** by Aanderaa, designed for depths down to 2000m and 6000m respectively. The current meter consists of a recording unit and vane assembly which is equipped with a rod that shackled into the mooring line, allowing the instrument to swing freely and align with the current. These instruments contain:

- Savonius rotor magnetically coupled to an electronic counter: starting speed of 2 cm/s, range from 2.5cm/s to >250cm/s, accuracy greater of 1 cm/s or 2%;
- Vane, which aligns instrument with current flow and ensures static and dynamic balance in flows up to 250cm/s;
- Magnetic compass, direction recorded with 0.35° resolution, 5° accuracy for speeds from 5 cm/s to 100 cm/s, 7.5° accuracy for remaining speeds within 2.5 cm/s to 200 cm/s;
- Quartz clock, accuracy better than 2 sec/day within temperature range 0°C to 20°C;
- Thermistor, range from -2.46°C to 21.48°C, accuracy of 0.15°C and 0.05°for RCM4 and RCM8 respectively, resolution of 0.1% of range.

RCM9 and **RCM11**: they are single point **current-meters** by Aanderaa, designed for depths down to 1000 m and 6000 m respectively. With respect to the RCM4 these instruments have an acoustic sensor to determine current velocity. This Acoustic Doppler sensor sends out 600 pings during each recording interval, with an accuracy of 0.15 cm/s. During PREPARED cruise, the hull-mounted Teledyne **RDI ADCP BB150** was used to acquire current velocity using the Doppler Effect. Specifics are the following:

- Single ping accuracy of 1 cm/s at 16 m depth cell;

- Maximum profiling range of 230 m (300 m at high power mode);
- Minimum range to start of first depth cell at 4 m;
- From 1 to 12; depth cells, size from 5 cm to 3200 cm;
- Heading accuracy of 5 deg; Tilt accuracy of 1 deg; Temperature accuracy of 0.5 deg.

Seabird SBE 37-SM: this instrument is a high-accuracy moored **conductivity and temperature recorder**. It is equipped with an internal-field conductivity cell and a pressure protected thermistor. Specifics are the following:

	Measurement Range	**Initial Accuracy**	**Typical Stability**	**Resolution**
Conductivity	0 to 7 S/m (0 to 70 mS/cm)	± 0.0003 S/m (0.003 mS/cm)	0.0003 S/m (0.003 mS/cm) per month	0.00001 S/m (0.0001 mS/cm)
Temperature (°C)	-5 to 45	± 0.002 (-5 to 35 °C); ± 0.01 (35 to 45 °C)	0.0002 per month	0.0001

Table 5: SBE37-SM parameters.

SBE 16plus V2: this instrument is a **conductivity and temperature recorder** is self-powered and self-contained, for depths up to 10,500 meters. Specifics are the following:

	Measurement Range	**Initial Accuracy**	**Typical Stability**	**Resolution**
Conductivity	0 – 9	± 0.0005	0.0003/month	0.00005 typical
Temperature (°C)	-5 to 35	± 0.005	0.0002 per month	0.0001

Table 6: SBE 16plus V2 parameters.

This instrument has also a **Seapoint Turbidity Meter** able to detect light scattered by particles suspended in water, generating an output voltage proportional to turbidity or suspended solids. Specifics are the following:

- Water depth capability of 6000 m,

- Range of 100 x gain or 0-25 Formazin Turbidity Unit (FTU);
- Sensitivity of 200 mV/FTU;
- Offset voltage is <1 mV of zero;
- Sensing volume < 5 cm from sensor.

Temperature Logger SBE 56: this instrument has a pressure-protected **thermistor** with a 0.5 second time constant, providing initial accuracy of 0.002 °C. Drift is typically less than 0.002°C per year.

Parflux Mark 7G-21 **Sediment Trap** by **McLane** Research Lab was designed to collect a series of settling particle samples in the deep ocean for the purpose of measuring the seasonal or timeseries variability of particle fluxes. Specifics are the following:

- titanium frame and advanced engineering plastics, preventing contamination of samples by corrosion;
- funnel aperture of 0.5 m2 (diameter, 80 cm);
- 21 sampling bottles with individual seals in the rotary mechanism;

Data processing

Time series have been processed after each recovery (June 2015, June 2016); high frequency time series with different sample time (15 min; 30 min) were averaged at an interval of 60 min in order to create a homogenous dataset. Through the use of MATLAB data were cleaned and despiked, following in-situ quality control standards and methodology described in MyOcean (http://catalogue.myocean.eu.org/static/resources/user_manual/myocean/QUID_INSITU_TS_OBSERVATIONS-v1.0.pdf). Current vectors from ADCP and current-meters were decomposed into u (eastward, zonal), v (northward, meridional), and w (vertical) components (*Bensi et al., in preparation*). From harmonic analysis, tidal constituents were obtained, with a signal/noise ratio > 1, and were subtracted to de-tide the time series. Data underwent a low-pass filter (*Flagg et al., 1976*) with cut-off period at 24-33 hours, to remove inertial oscillations, obtaining sub-inertial non-tidal flow. Time series were also compared with data from hydrological stations (CTD / Rosette casts) to check the quality and robustness of time series and to place mooring measurements in a long term variability context.

3 Results

In this chapter, the results obtained from the acquisition, processing and analysis of the geophysical dataset are illustrated. These results are divided into three subsections, presenting the areas with the major concentration of data (see Figure 21): the Isfjorden slope, the Bellsund slope and the INBIS channel system. The first two areas focus on the description of two along-slope features (see subsection 1.1.1), previously identified by *Rebesco et al*. (*2013*). In the third part I will describe a dip-slope feature, a portion of the INBIS Channel System (*Vorren et al*., *1998*). Part of the results (and the relative discussion in section 4) hails from a work in progress paper (*Rui et al*., *submitted*.). Eventually, the oceanographic results produced by *Bensi et al*. (*in prep*.), that I will discuss in section 4, are presented.

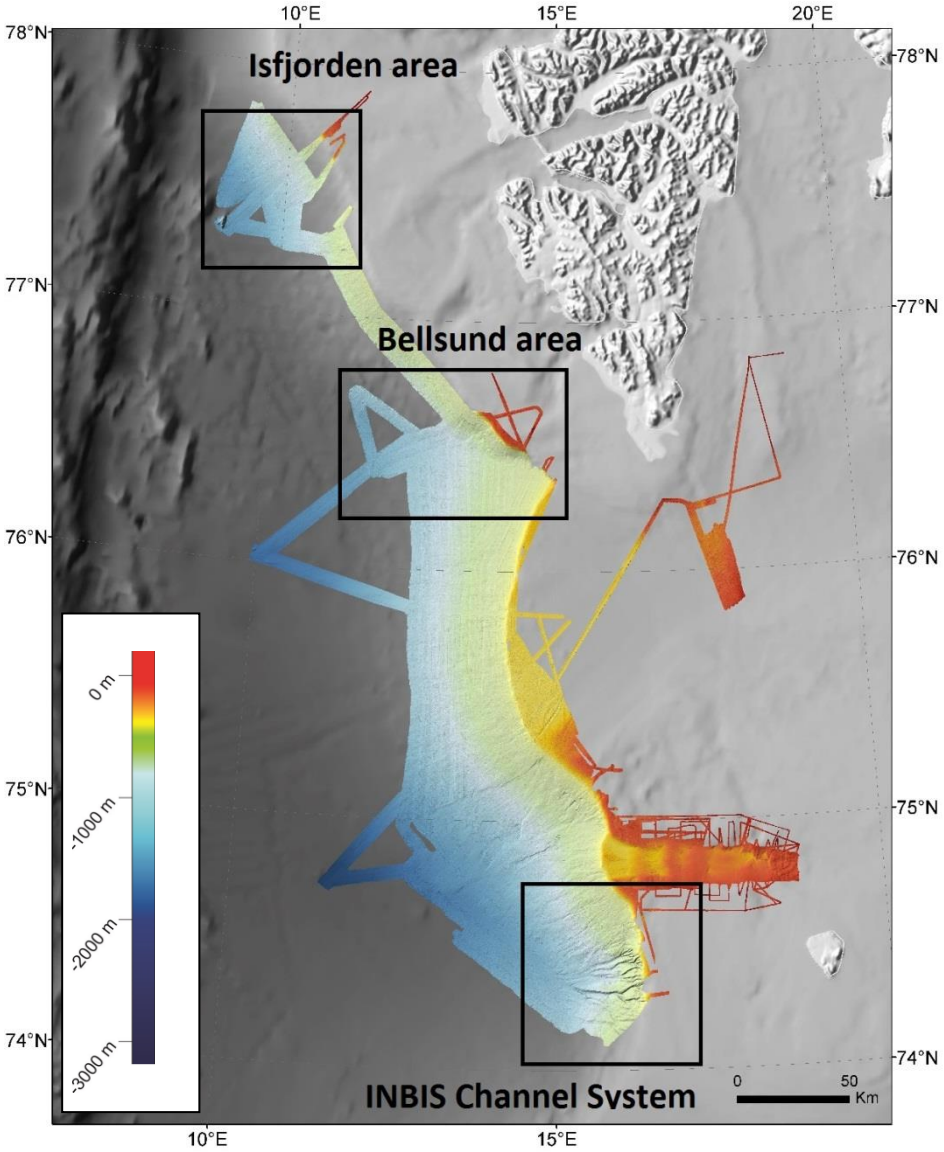

Figure 21: Multibeam data showing the location of the three areas in which I focused the analysis for this Ph.D. project: Isfjorden area, Bellsund area and INBIS Channel System.

3.1 Isfjorden slope

From the analysis of the seismic dataset hailing from EGLACOM cruise (see section 2.2 for details), *Rebesco et al*. (*2013*) noticed seafloor undulations forming a broad upward-convex body (mound) on the continental slope southwest of the Isfjorden TMF. This mound is an along-slope feature (i.e. it is sub-parallel to the shelf edge), centered around 77° 35' N and 9° 39' E, at ~12 km from the shelf edge and at a water depth varying between 1200-2000 meters.

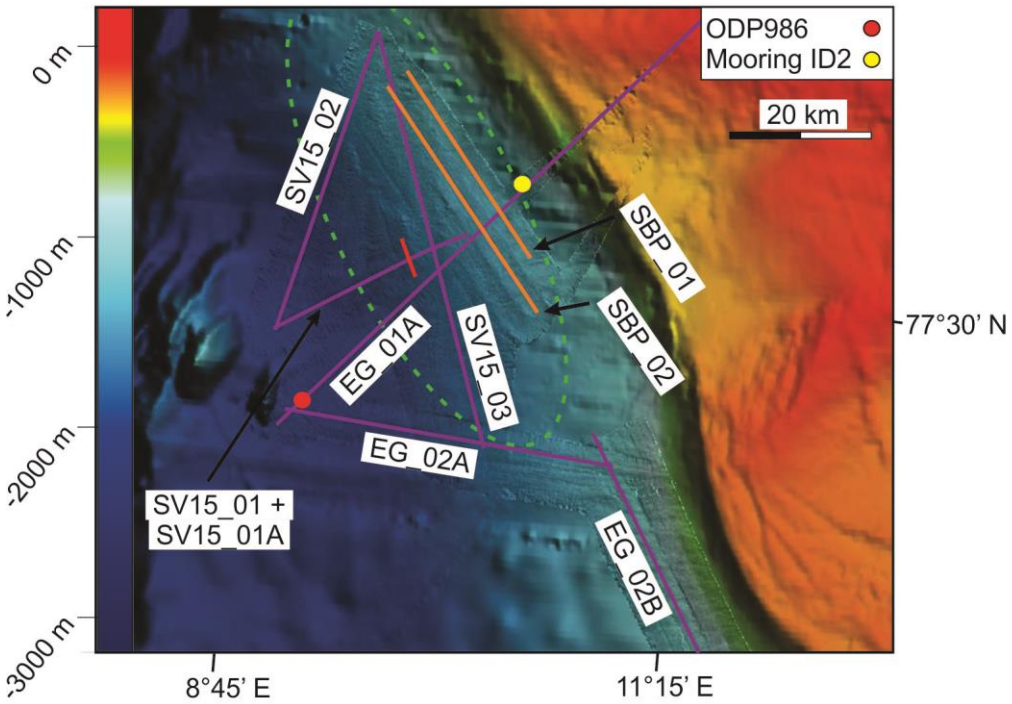

Figure 22: Bathymetric map of the Isfjorden area, with the position of: seismic profiles (purple lines) SV15_01 and SV15_01A (separated by a small red line), SV15_02, SV15_03, EG_02A, EG_02B; sub-bottom profiles (orange lines) SBP_01, SBP_02; mooring ID2 (yellow circle); ODP 986 (red circle). Green dotted line indicates the location of the mound described in section 3.1.

Its width, measured in the dip direction (perpendicular to the shelf edge) is ~40 km, appraisable in both the bathymetric dataset as well as in three seismic profiles hailing from the EDIPO cruise (SV15_01A, SV15_01, SV15_02), while the length of this structure is hard to measure as it probably continues north outside of the available dataset. A profile along the entire length of this mound is missing, but from the swath bathymetry data it is estimated the length of at least 70 km. In particular, from the analysis of seismic profile SV15_02 (see Figure 25), acquired at the northern limit of the bathymetric dataset (see Figure 22), the mound relief and its internal architecture are still visible, hence suggesting that this feature extends further north. The difficulty in estimating the length of the mound is also a consequence its very subdued relief of less than ~100 meters over distances of tens of km,

making it difficult to trace its limits with precision in a bathymetric dataset. The mound is composed of a series of thick sedimentary layers, marked by high to medium amplitude reflectors (see Figure 23 and Figure 24).

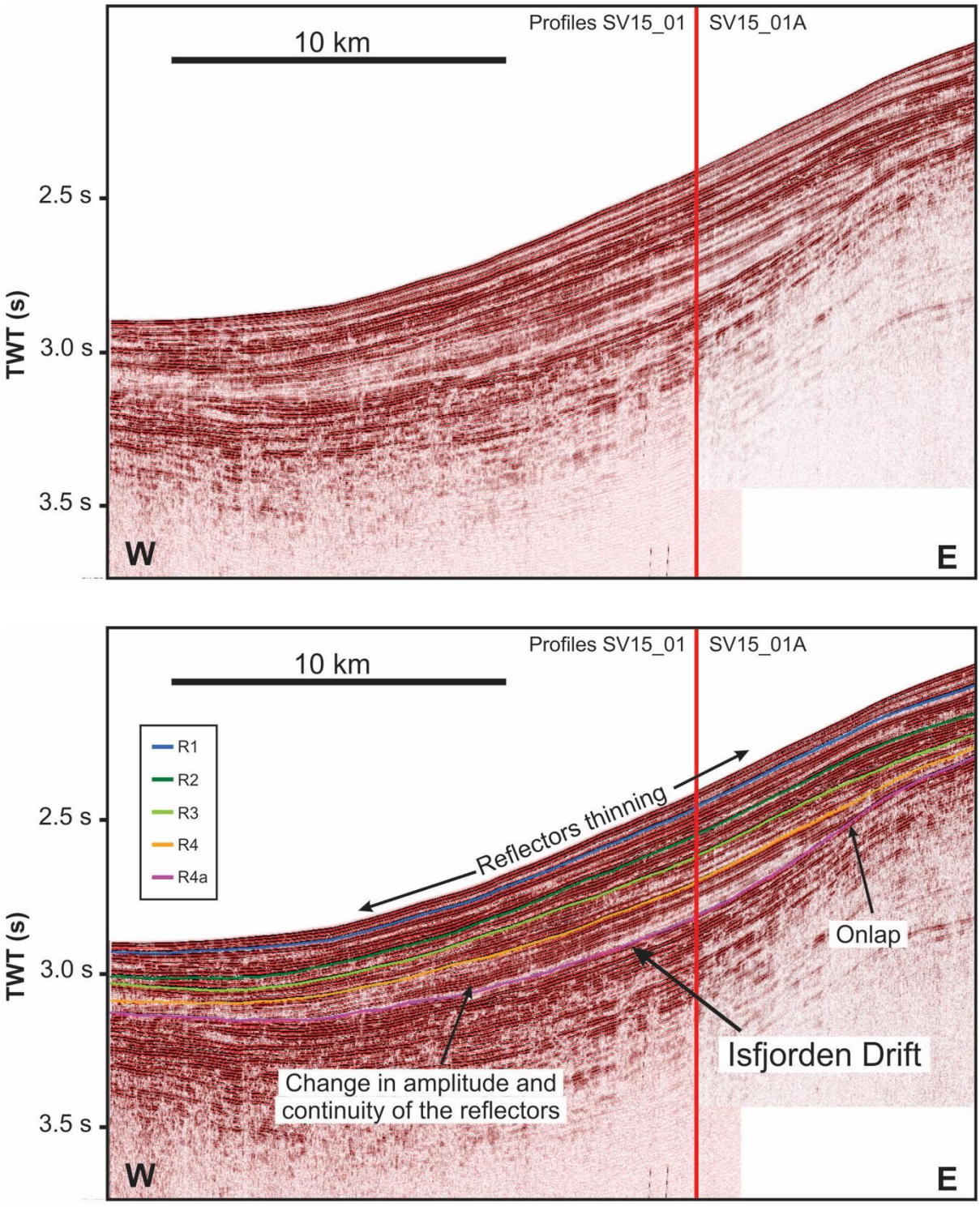

Figure 23: Multichannel seismic profile SV15_01 and SV15_01A, partially crossing the Isfjorden drift. For location see Figure 22.

The amplitude of the reflectors inside the mound decrease with depth: the shallower ones are those with the highest amplitude and the deepest ones (up to reflector R4a) are those with medium amplitude. These reflectors preserve lateral continuity, getting rapidly thinner upslope and terminating in onlap (in the dip direction). Downslope instead, the layers maintain almost the same thickness, reaching the lower portion of the slope (where the dataset ends). Due to this asymmetry, it is easier to mark the upslope limit of the mound compared to the downslope one. The overall shape of the mound is sigmoidal, with reflector concavity varying gradually inside the mound: in the shallower part of the mound, reflectors are slightly convex upward, while deeper reflectors change into a concave upward shape. The upward concavity of the reflectors increases in the upslope direction, augmenting the asymmetry of this feature. Starting from the seismic profiles EG_01A and EG_02A interpreted by *Rebesco et al*. (*2013*), I could trace and extended five (R1, R2, R3, R4, R4a) of the seven reflectors proposed by *Faleide et al*. (*1996*) through four new seismic profiles: SV15_01, SV15_01A, SV15_02 and SV15_03. From the analysis of profile SV15_01 and SV15_01A the sigmoidal shape of the mound is recognizable down to the reflector R4a. Reflectors below R4a are sub-parallel to the shape of the slope, with later continuity upslope and without an onlap termination. Reflector R4a also marks the passage from medium amplitude reflectors (the ones terminating in onlap on R4a) to relative higher amplitude ones, sub parallel to R4a.

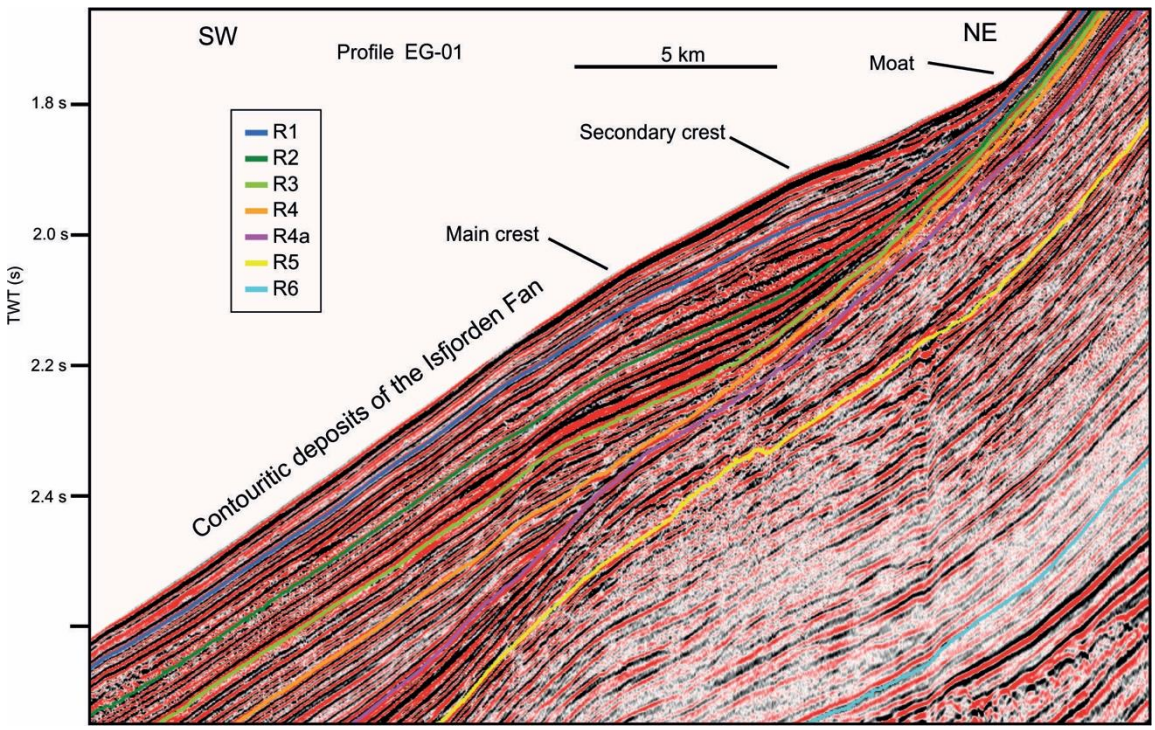

Figure 24: From *Rebesco et al., 2013*: Multichannel seismic profile EG_01, partially crossing the Isfjorden Drift. For location see Figure 22.

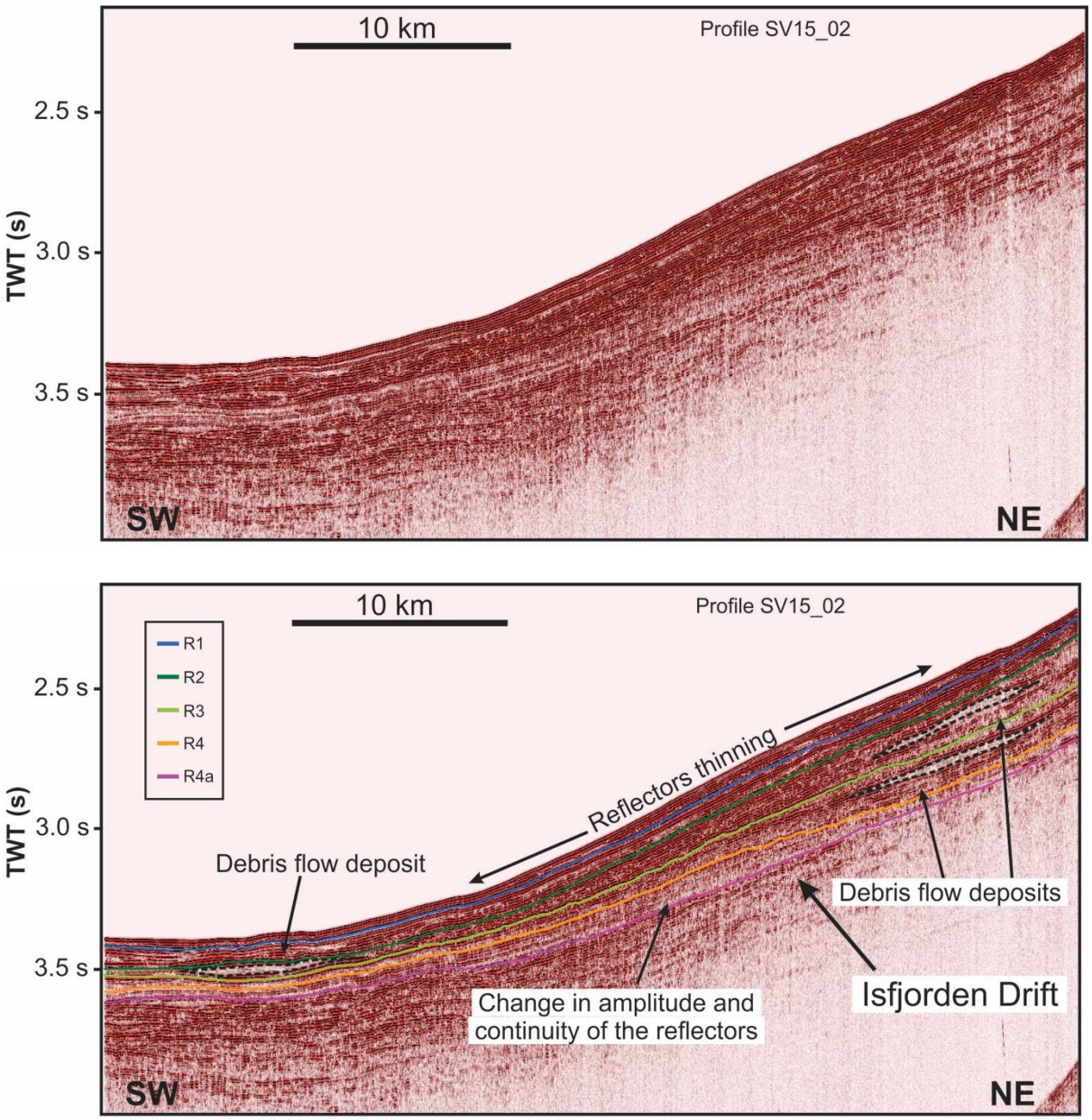

Figure 25: Multichannel seismic profile SV15_02, partially crossing the Isfjorden Drift. For location see Figure 22.

From the analysis of sub-bottom profiles SV15_SBP01 and SV15_SBP02 (see Figure 26 and Figure 27 respectively), located on the upper continental slope at east of the mound, it is possible to observe a series of superficial small lens-shaped deposit. In the first tens of meters below the sea bottom reflectors are subparallel, following the morphology of the bottom, with medium-high amplitude and lateral continuity. This rather constant stratification is interrupted in several spots by lenticular shaped bodies with highly variable dimensions: the thickness of these lenses ranges between less than 10 ms to 50 ms while the length (along the sub-bottom profiles) varies between a hundred meters up to 2 km. All these lenses develop

below a reflector located at 10 ms below the sea bottom, until around 77°30’ N and 10°18’ E where an extensive lens or series of lenses completely mask the deeper reflections.

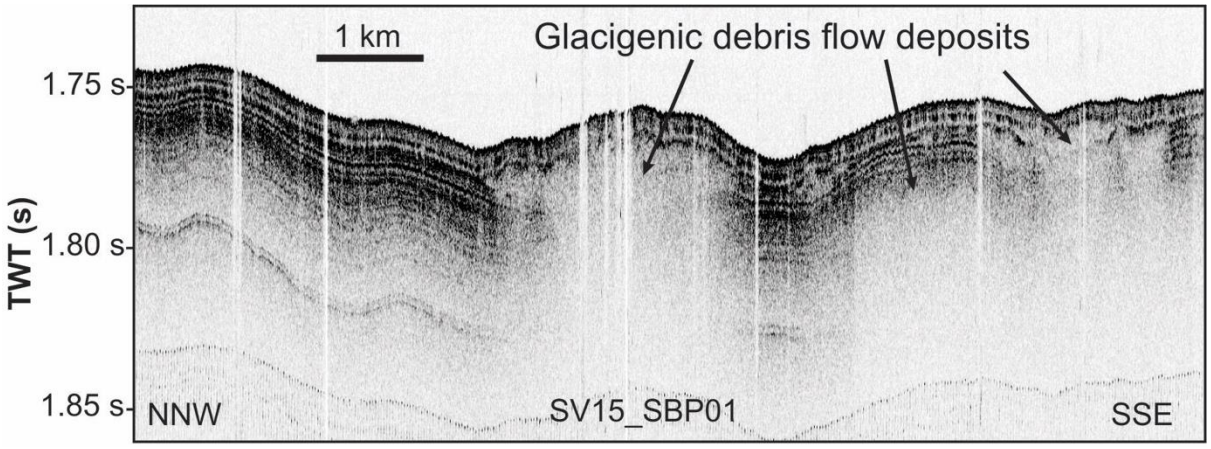

Figure 26: Sub-bottom profile SBP_01, located on the upper part of the slope in the Isfjorden area. For location see Figure 22.

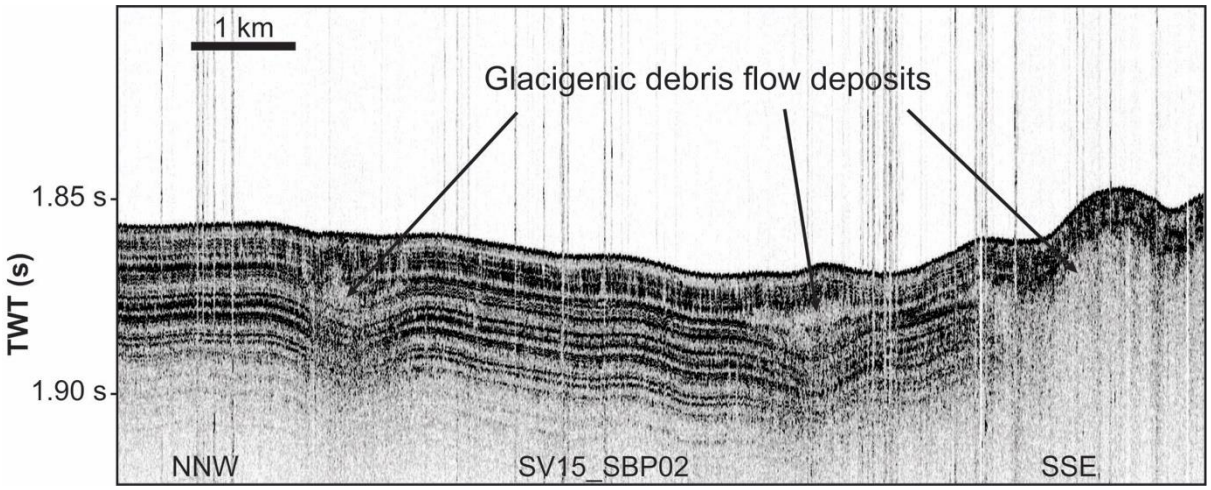

Figure 27: Sub-bottom profile SBP_02, located on the upper part of the slope in the Isfjorden area. For location see Figure 22.

3.2 Bellsund slope

Another mound, identified by *Rebesco et al*. (*2013*) in the EGLACOM dataset (see section 2.2 for details), is located on the continental slope between Storfjorden and Bellsund TMFs. As for the one located on the Isfjorden slope this mound appears to be an along-slope feature, centered possibly around 76° 30' N and 12° 48' E. Compared to the Isfjorden area, this feature is barely visible on the bathymetry dataset, due to the morphology of the area and its ratio between relief and width/length. The Storfjorden TMF partially masks the shape of the mound; the aspect of the mound therefore can be deduced only from the seismic profiles collected in the area.

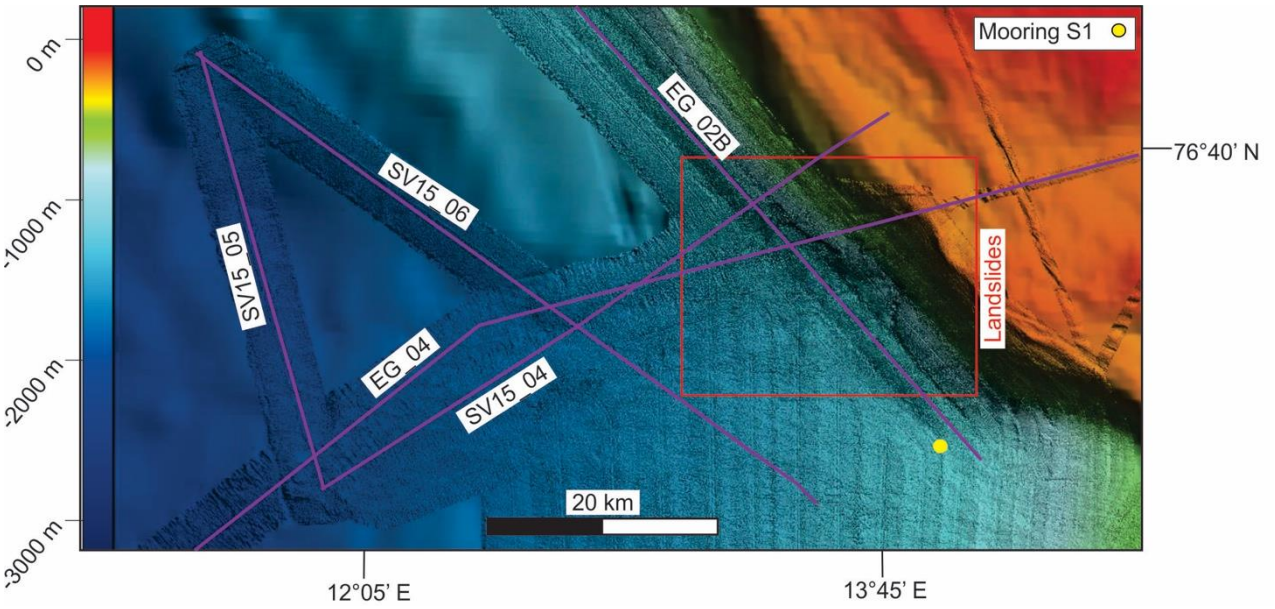

Figure 28: Bathymetric map of the Bellsund area, with the position of: seismic profiles (purple lines) SV15_04, SV15_05, SV15_06, EG_02B, EG_04; mooring S1 (yellow circle). Red rectangle is the location of Figure 30.

From three seismic profiles (EG_04, SV15_04, SV15_06) the relief of the mound is estimated around 100 meters. Starting from the seismic profiles EG_04 interpreted by *Rebesco et al*. (*2013*), it was possible to trace and extended the five reflectors located in the Isfjorden area (R1, R2, R3, R4, R4a) (*Faleide et al., 1996*) through three new seismic profile: SV15_04, SV15_05 and SV15_06. The mound and its shape are hard to identify clearly on the bathymetric dataset. A sigmoidal shape similar to the one of the Isfjorden mound is observable in profile SV15_04, with reflectors between R1 and R4a thickening in the central part of the mound. The concavity of the reflectors changes laterally, from upward concavity in the downslope part to upward convexity in the upslope direction.

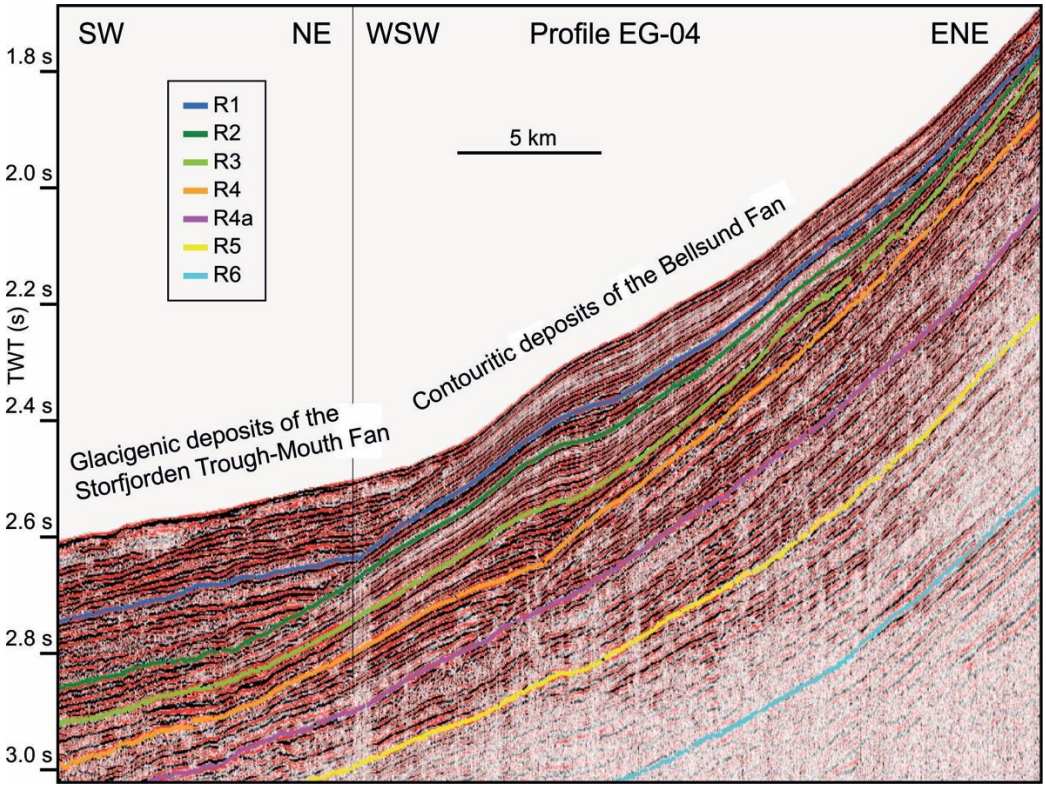

Figure 29: From *Rebesco et al., 2013*: Multichannel seismic profile EG_04, crossing the Bellsund Drift. For location see Figure 28.

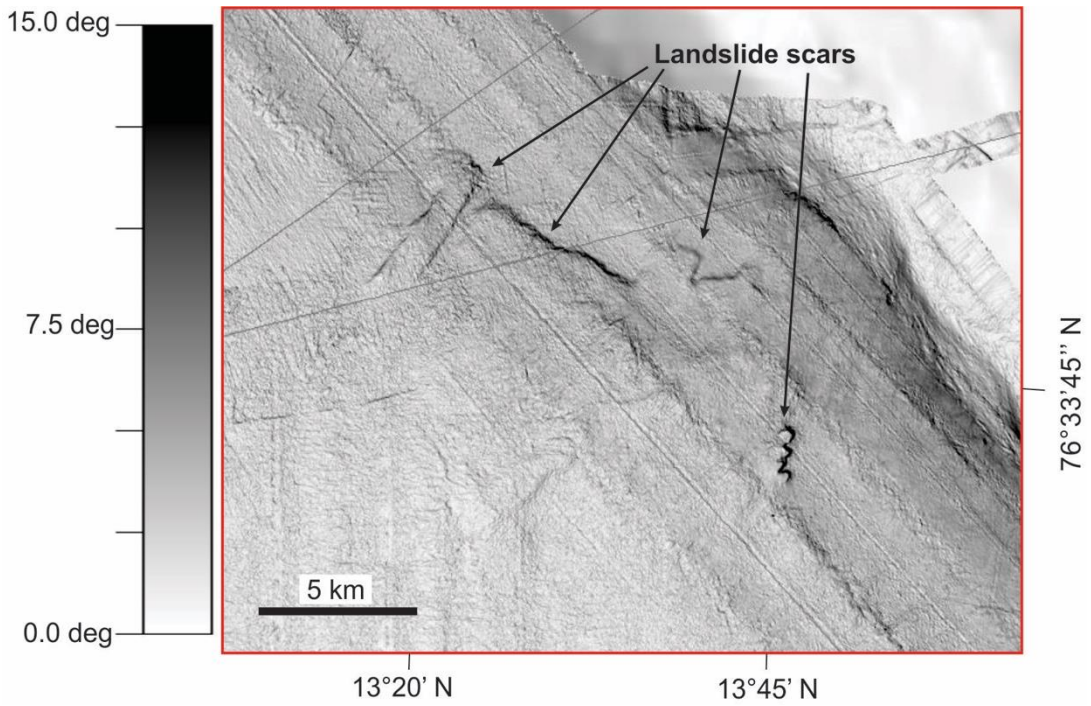

Figure 30: Slope gradient map of the landslide scars in the Bellsund area. For location see Figure 28.

In the upward direction the termination of the reflectors is similar to the one observed in the Isfjorden mound (onlap); downslope it is possible to observe a gentle thinning of the reflectors between R3 and R4. This thinning is in correspondence of 15 km long lenticular thickening in the internal reflectors between R4 and R4a (see Figure 29 and Figure 31).

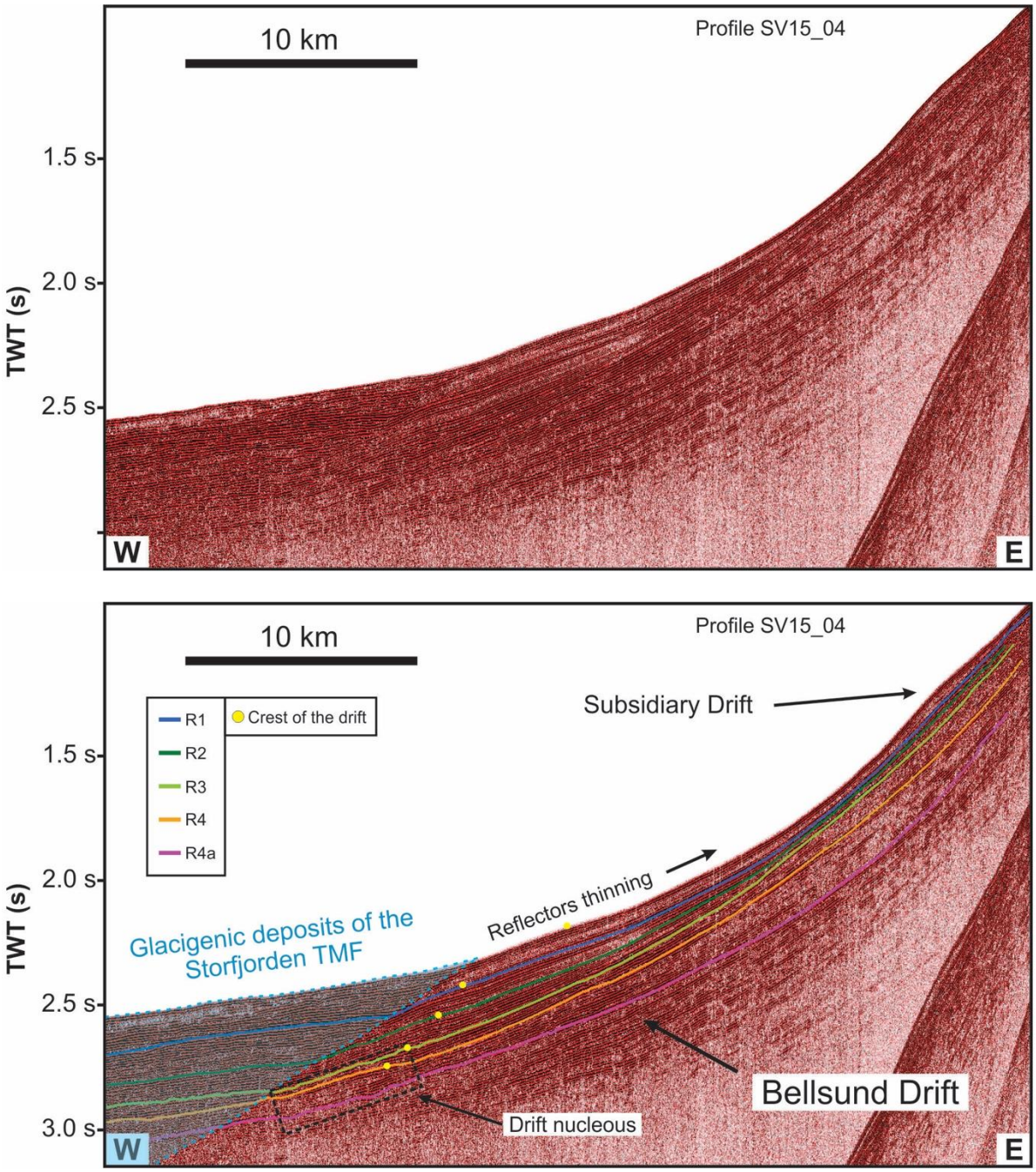

Figure 31: Multichannel seismic profile SV15_04 crossing the Bellsund drift. For location see Figure 28.

On the slope in front of the Bellsund Trough, I observed several landslide scars, located between the shelf edge and the water depths of ~1100 meters (see Figure 30). These landslide scars are located at northeast and upslope of the mound above described. They are characterized by an incision depth of ranging between 10 meters and 25 meters and a variable width ranging between 1 km and 7 km.

3.3 INBIS Channel System

In 2015 during the EGLACOM (*Pedrosa et al., 2011*) and DEGLABAR cruises, a new part of the INBIS Channel System was surveyed, situated west of Bear Island, not buried by debris flow deposits as at first described by *Vorren et al*. (*1998*). This portion, located on the continental slope, develops into a series of gullies and channels previously not analyzed. These features are located within an area from 74°29' N to 74°08' N and from 14°44' E to 16°21' E. Vertically, they extend from the shelf edge (depth of ~420 m) to a depth of around 2150 m (see Figure 33). To provide a detailed description of the INBIS Channel System, I divided the latter has been into an upper, northern and southern part (see Figure 34).

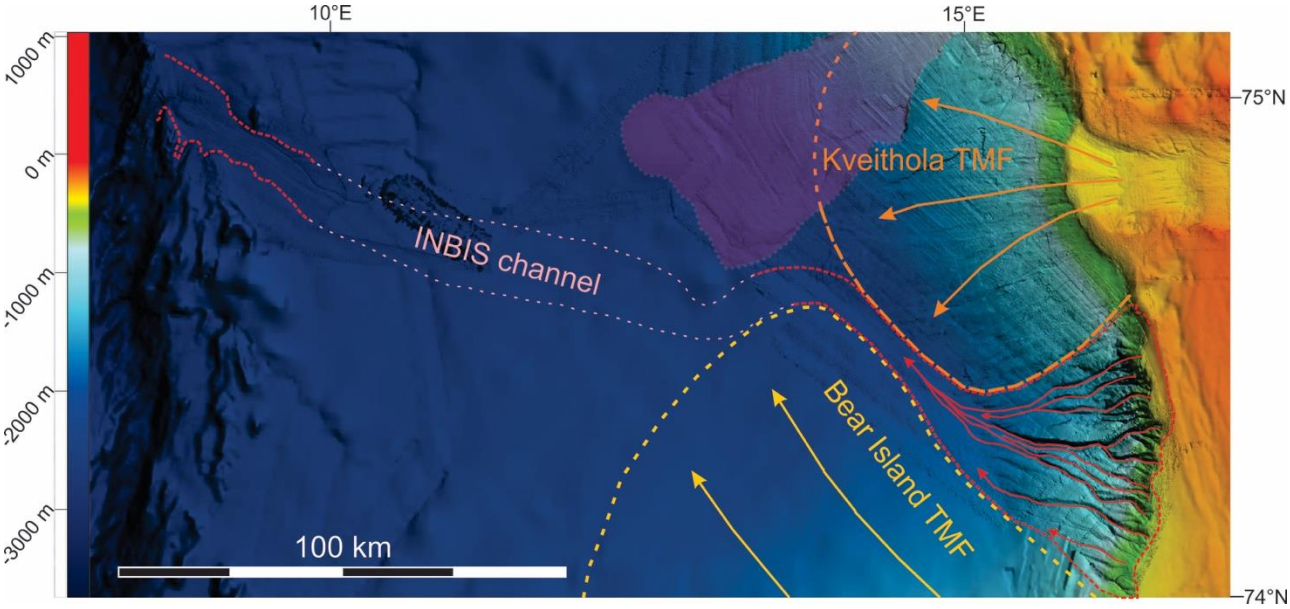

Figure 32: Bathymetric map of the INBIS Channel System. Dotted pink line represents the INBIS Channel identified by *Vorren et al., 1998*. I mapped Kveithola and Bear Island TMFs in orange and yellow respectively. With Red dotted lines I marked the limit of the INBIS Channel System visible on the bathymetric dataset.

3.3.1 The upper part of the channel system

The upper part of the INBIS Channel System develops into an amphitheater shape on the shelf edge west of Bear Island, at ~80 km from the island itself. Laterally, the upper part extends from the Kveithola Trough to the Bear Island TMF (see Figure 32 and Figure 33), forming an arc of ~60 km. In depth the upper part of the INBIS Channel System extends from the shelf edge, which is at a depth of ~420 m, to a depth ranging between 700 m (in the northern part) and 1100 m (in the southern part). The slope in this part has a gradient ranging between 4° and 5°. From the analysis of the bathymetric dataset it is possible to identify 40 gullies crossing slope. The gullies are characterized by an overall V-shaped profile (see Profile H in Figure 34, Profile B in Figure 37, Profile L in Figure 40), with width varying between 150 and 600 m and incision depth varying between 10 and 60 m. The ratio between incision depth and width of the gullies is rather constant around ~ 1/10.

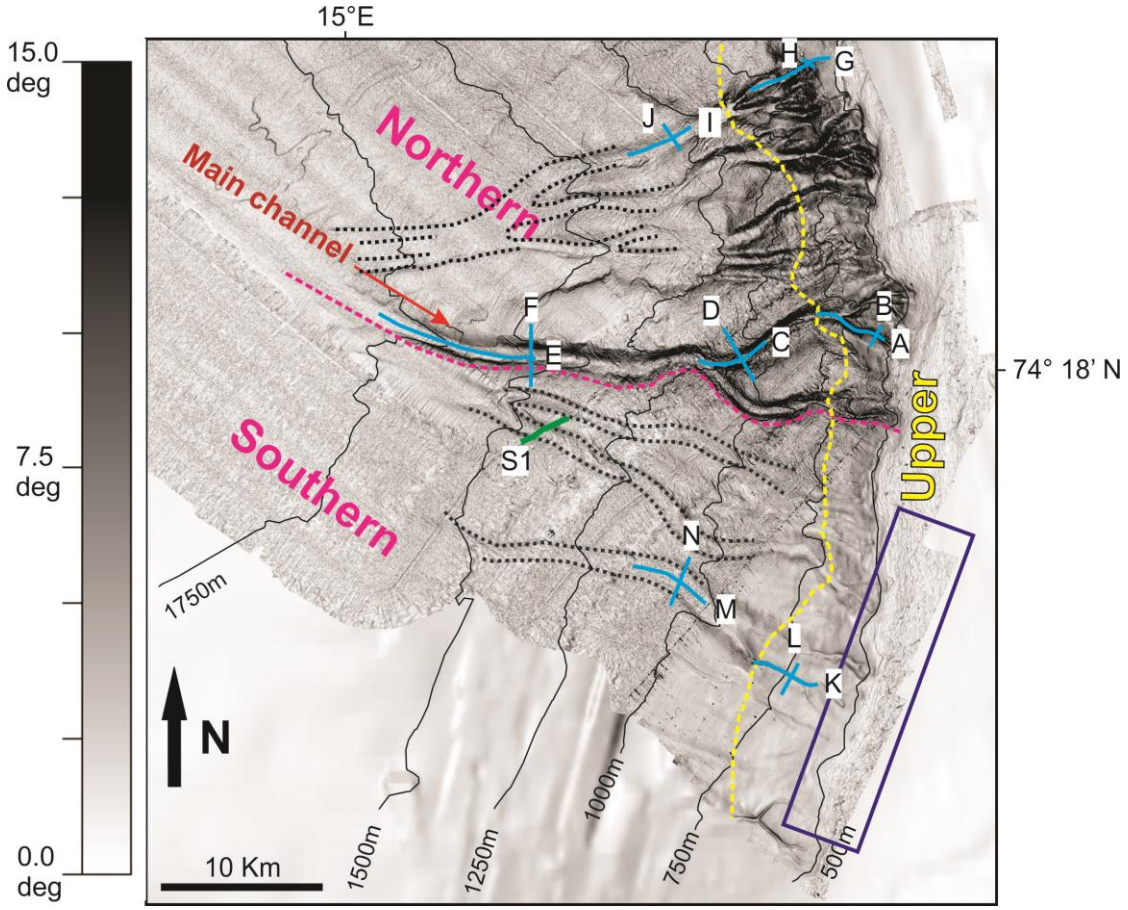

Figure 33: Slope gradient map of the INBIS Channel System. Light blue lines indicate the location of bathymetric profiles. Pink dotted line separates the northern part from the southern one. Yellow line delimits the upper part of the channel. Dotted black lines help in the individuation of deeper channels. Blue rectangle represents the area characterized by the presence of ploughmarks. The green line marks the sub-bottom profile S1 (Figure 42).

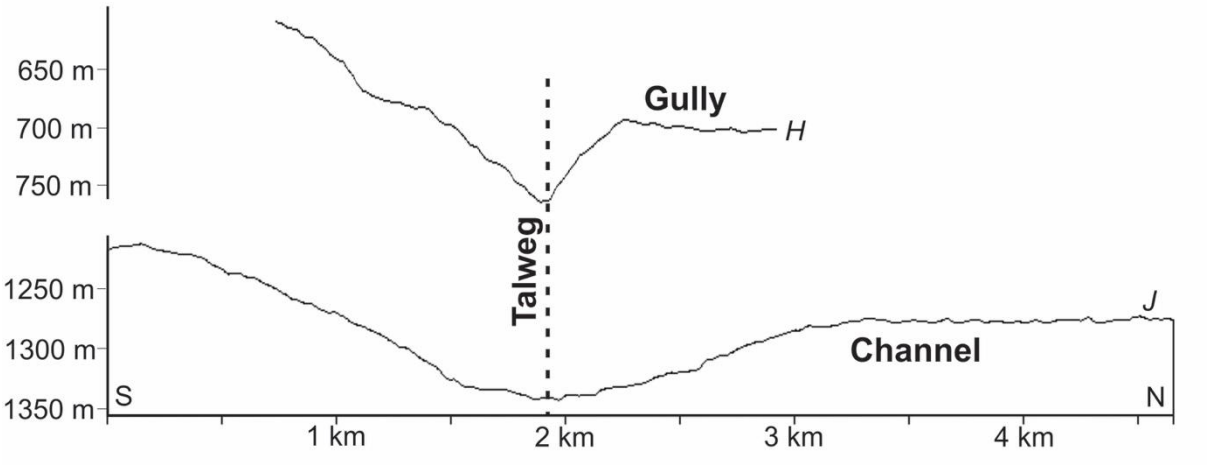

Figure 34: Comparison between a gully in the upper part (Profile H) with its continuation in the northern part of the INBIS Channel System (Profile J). For location see Figure 33.

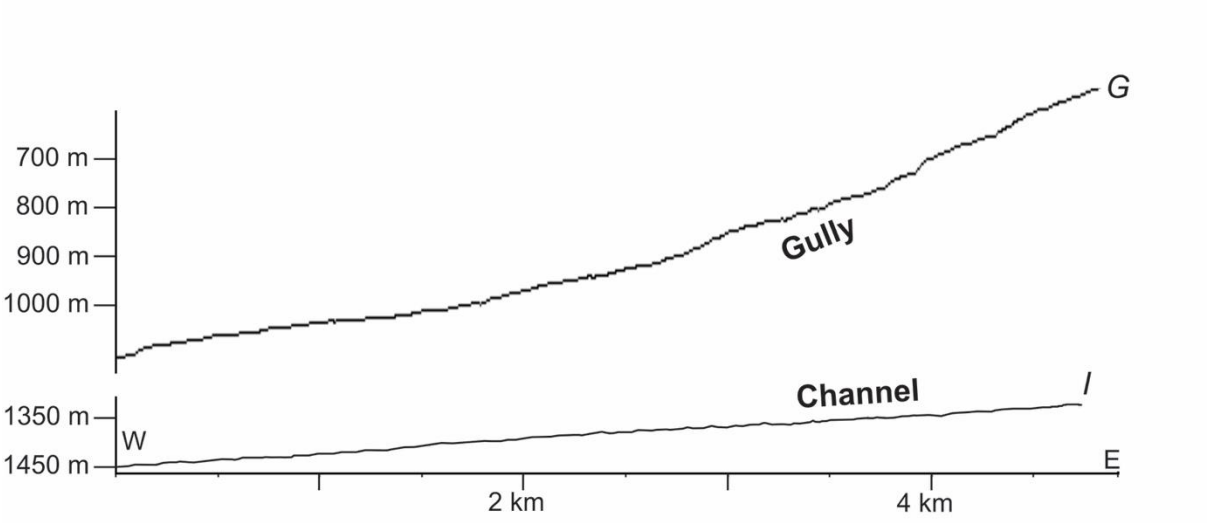

Figure 35: Comparison between a gully in the upper part (Profile G) with its continuation in the northern part of the INBIS Channel System (Profile I). For location see Figure 33.

All the gullies originate at the shelf edge, with a lateral spacing of 450 m to 950 m in the northern part, increasing to approximately 4 km in the southern half (see Figure 33). This difference of lateral spacing results in an uneven distribution of the gullies, with 23 gullies in the northern part and 17 in the southern. The bottom of the gullies is moderately smooth within water depths varying between 420-750 meters. Proceeding below the depth of ~800-900 meters, the bottom of the gullies becomes slightly rougher (see Profile G in Figure 35, Profile A in Figure 36). In the upper portion of the INBIS channel system, over bank deposits (levees) are absent.

The formation of gullies is observed also at the shelf edge also on the Kveithola TMF (*Pedrosa et al., 2011*): these gullies are much smaller than those observed in the INBIS Channel System, with incision depth reaching at most 10 meters and a width of at most 250 meters. These gullies develop from the shelf edge to a depth of ~1000 meters, with a variable lateral spacing ranging between 400 and 700 meters.

In the swath bathymetry data at east of the shelf edge (see Figure 33), it is possible to observe several ploughmarks, with a mean orientation N-S, of variable dimensions, marking the shelf edge. Regarding the intensity of backscatter, values range between -30 dB to -7 dB. Without a proper sediment analysis it is not possible to classify the type of sediment composing the sea bottom, but observing the pattern of the values of the intensity of backscatter, I noticed that lower values are concentrated precisely in correspondence of the gullies, while outside a general stronger intensity is observed. Mean values of intensity of backscatter for the gullies varying between -30 dB and -13 dB; adjacent areas outside of gullies show always higher values, varying between -15 dB and -7 dB. There is always few dB of difference between the intensity of backscatter inside a gully with that of the area adjacent to it.

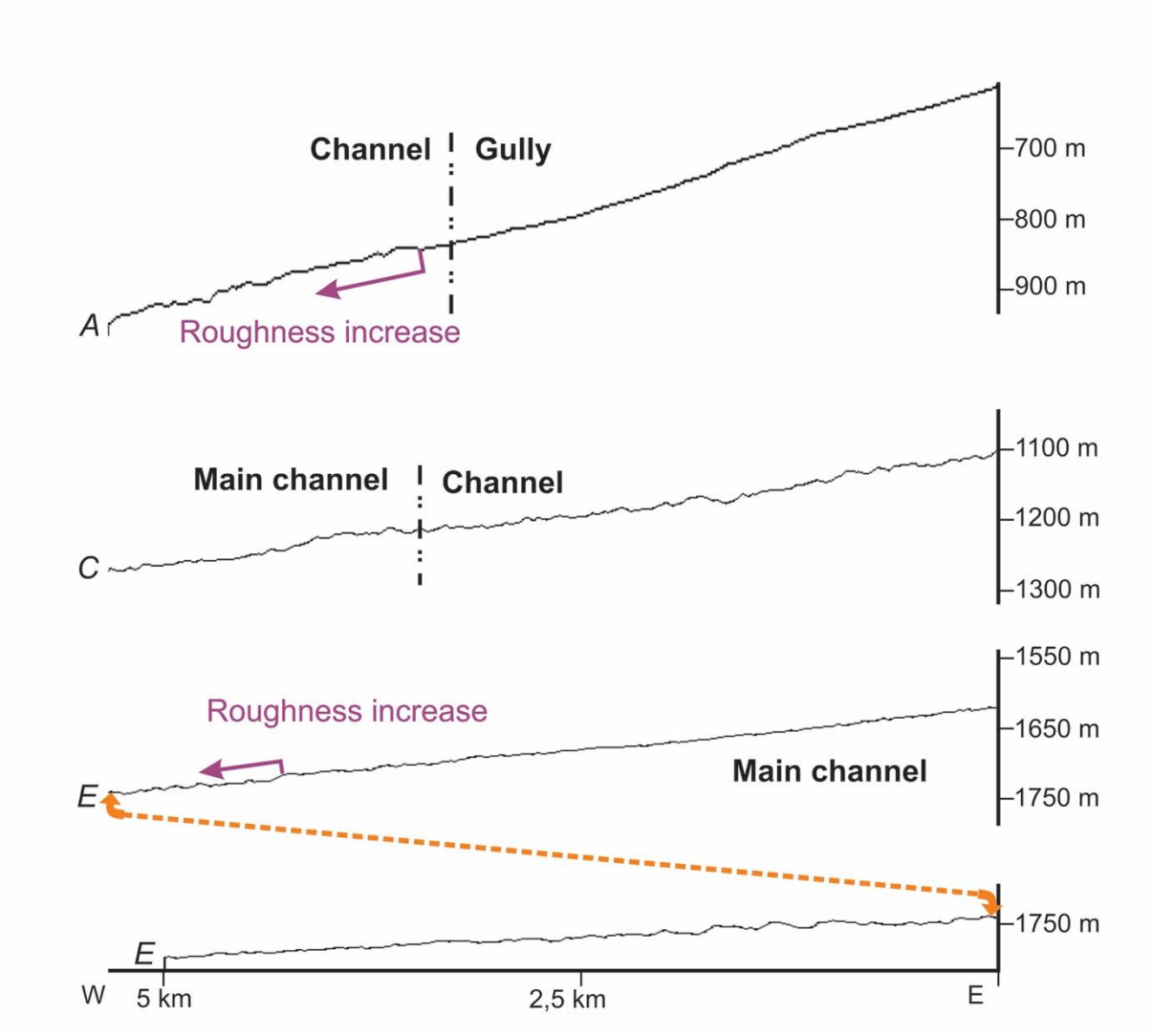

Figure 36: Comparison between a gully in the upper part (Profile A) with its continuation in the northern part of the INBIS Channel System (Profile C) and with the main channel (Profile E). Profile of the main channel is twice as long as the other profiles (10 km instead of 5 km); the profile is divided in two half connected by the orange dotted line. For location see Figure 33.

3.3.2 The northern part of the channel system

The slope gradient in the northern part decreases up to 1°-2°. The gullies present in this part of the channel system, 23 of the total 40, have a symmetrically V-shaped cross section, variable sinuosity and they maintain a ratio of ~ 1/10 between incision depth and width. Northernmost gullies exhibit a slightly less pronounced V-shape, due to a lower incision depth.

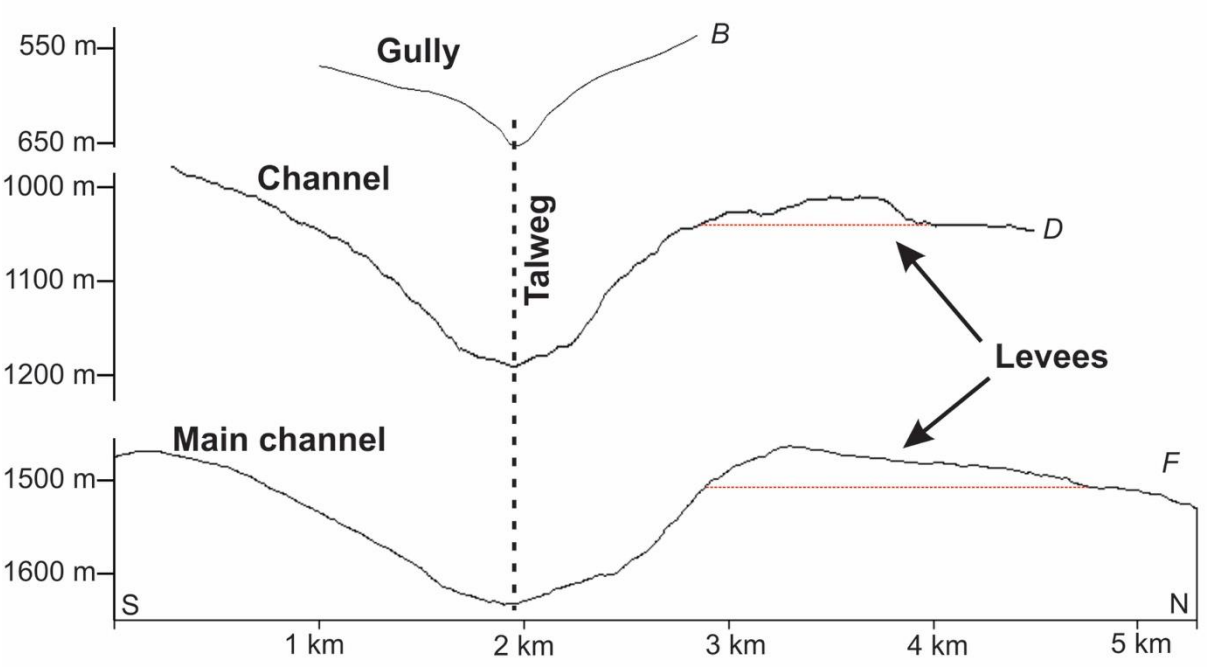

Figure 37: Comparison between a gully in the upper part (Profile B) with its continuation in the northern part of the INBIS Channel System (Profile D) and with the main channel (Profile F). For location see Figure 33.

The gullies grow in dimensions proceeding downslope, converging into 7 larger channels, at variable water depths ranging between 750-1000 meters. These channels are characterized by a U-shaped cross section (see Profile J in Figure 34, Profile D in Figure 37), with widths varying between 600 and 2200 m and incision depths varying between 30 and 150 meters. The ratio between depth and width decreases up to ~1/20. Both incision and width increase downslope, while the bases of the channels become gradually rougher (see Profile A and Profile E in Figure 36). The spacing between the channels is highly variable, ranging from hundreds of meters to a maximum of about 5 km (see Figure 33). Some of the channels present in this part of the INBIS Channel System are characterized by the formation of small levees on the northern flanks. The 7 channels in this part converge and merge at different depths: the 2 southern channels converge around the water depth of 1250 meters; the 3 central channels merge at water depth of 1500 meters, forming a single larger channel and

merging at water depth of 1650 meters with another channel from the north. The northernmost of the 7 channels is the one reaching the lowest incision depth (only few meters) and characterized by a highly asymmetric profile around the water depth of 1200 meters, with lower gradient on the northern flank (see Profile J in Fig 34). This channel marks the northern limit of the INBIS Channel System, as no other gully or channel is visible further north. This channel proceeds isolated downslope until the water depth of 1820-1850 meters. Eventually, all the channels converge into a single one (the main channel) that is about 1000 meters wide initially, at the water depth of 1250 meters, and up to 2500 meters wide further downslope, around the water depth of 1800 meters. The incision depth of the main channel increases downslope, from 30 meters initially up to 150 meters. The bottom surface is relatively flat/even in the shallower portions of this channel, becoming increasingly rougher into the deeper parts (see Profile A, Profile C and Profile E in Figure 36). The margins of the main channel are relatively smooth and symmetric in the upper part, while they become progressively more asymmetric below ~1150 meters water depth, with a steeper gradient to the north and a gentler gradient to the south. At ~ 1450 meters water depth the northern slope of the main channel is characterized by a prominent levee (see Profile D and Profile F in Figure 37).

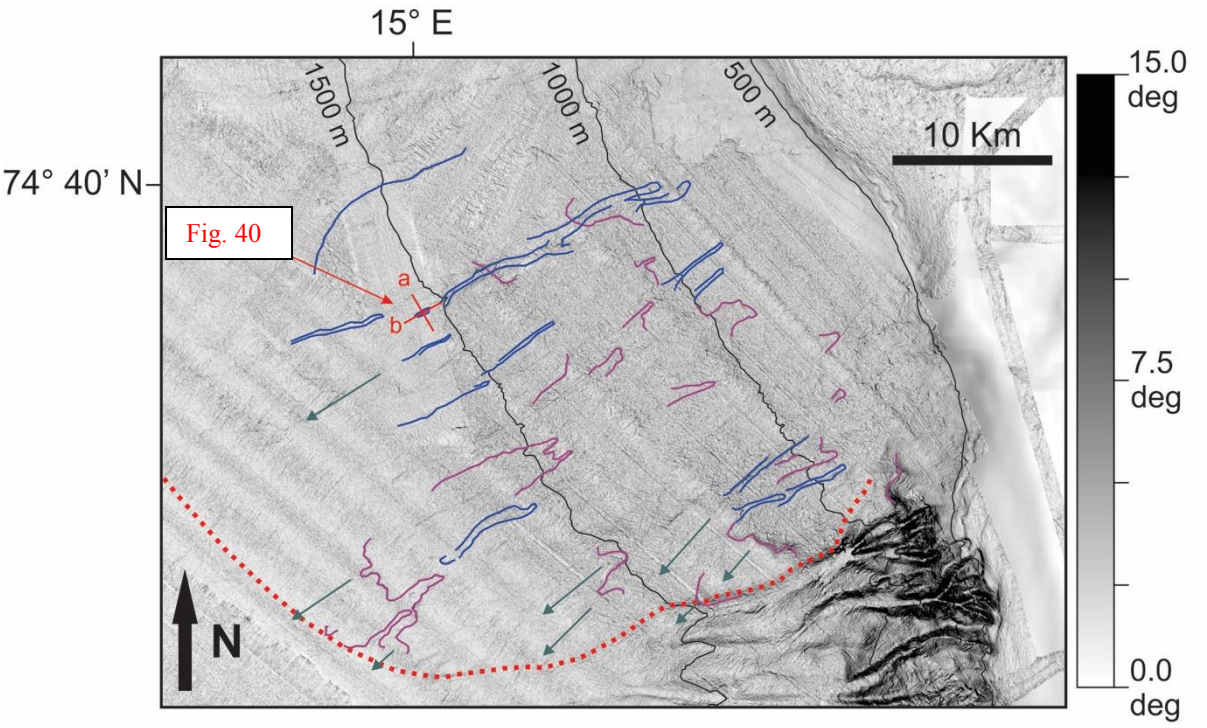

Figure 38: Slope gradient map of the southern portion of the Kveithola TMF. Dotted red line indicates the northern limit of the INBIS Channel System. Purple lines indicate landslide scars, blue lines indicates elongated incisions. In red the position of profiles a and b of Figure 39.

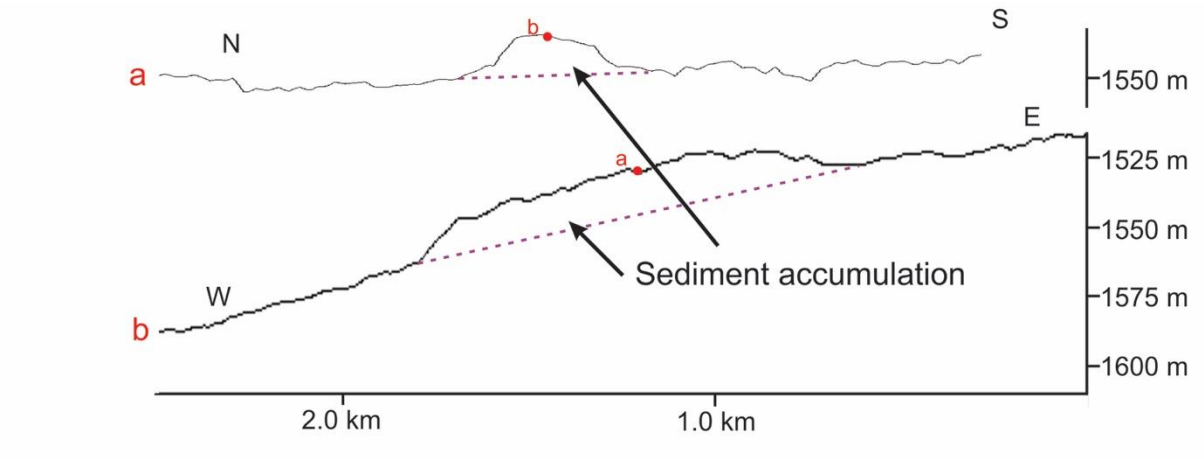

Figure 39: Profiles on the sediment accumulation located on the slope of the Kveithola TMF. For location see Figure 38.

Between the water depth of 1200 and 1450 meters, the main channel is bordered to the north by a slightly upward convex body, with a variable vertical relief of 5-10 meters and a width of about 4 km. The main channel continues westward, progressively growing in both incision depth and width, down to a water depth of 2150 meters.

The Bear Island (see Figure 32) and the Kveithola TMFs affect the orientation of the main channel, as these TMFs extend to this portion of the channel system, forcing the main channel into a NW direction. From the water depth of 2150 meters the main channel proceed towards NW to become the 60 km long and 5-15 km wide, nearly flat bottomed INBIS Channel described by Vorren et al. (1998). The northern part of the channel system is bordered to the north by the Kveithola TMF (see Figure 33 and Figure 38). The southern part of the Kveithola TMF includes several landslide scars that are around 100 m deep and between 1 and 10 km wide (see Figure 38). Superimposed onto these landslide there are several elongated incisions, with a V-shaped cross section. These incisions are between 150 and 400 m wide and between 20 and 50 m deep (see Figure 38). The incisions originate at different water depths along the slope of the TMF and are partially interconnected. The longest one of these incisions extends for 18 km, from a water depth of ~850 meters to a water depth of ~ 1520 meters where it terminates in a small sediment accumulation about 400 meters wide, 1250 meters long, and about 15 meters high (see Figure 39). Some of the incisions seem to merge with the northern, upslope part of the INBIS Channel System (see Figure 33 and 38).

3.3.3 The southern part of the channel system

The southern part of the INBIS Channel System extends from the depth of ~1000 meters to a depth of about 2150 meters (see Figure 33). The gradient of the slope is on average slightly steeper than 1°. Here, the 5 southern gullies proceed outside of the available dataset. The remaining 12 of the 40 gullies identified in the shallower part of the slope merge into three U-shaped channels.

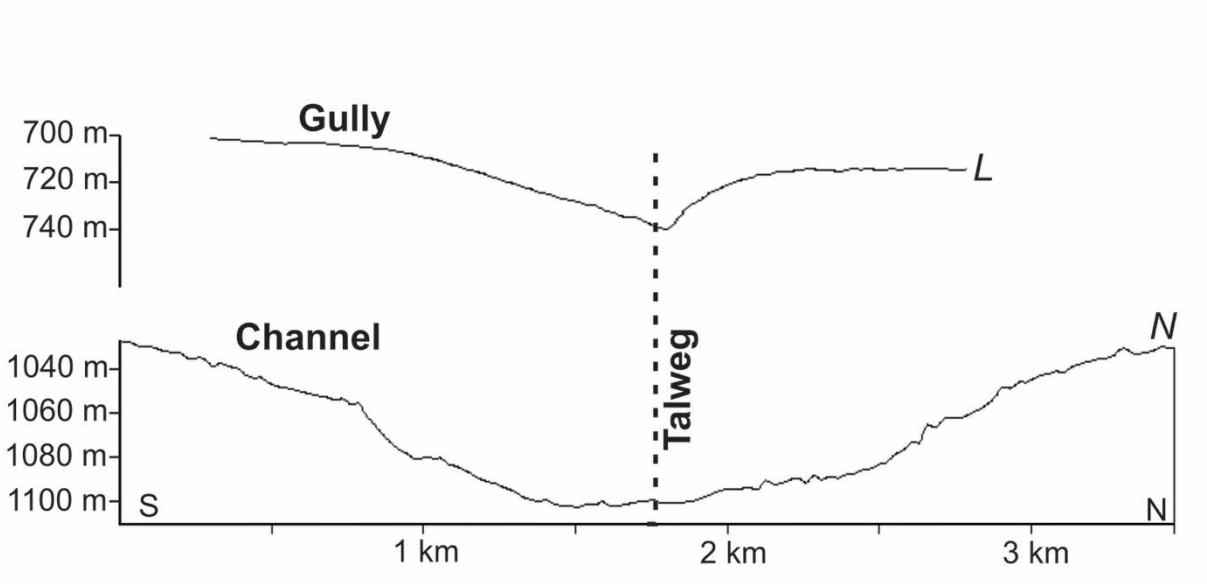

Figure 40: Comparison between a gully in the upper part (Profile L) with its continuation in the southern part of the INBIS Channel System (Profile N). For location see Figure 33.

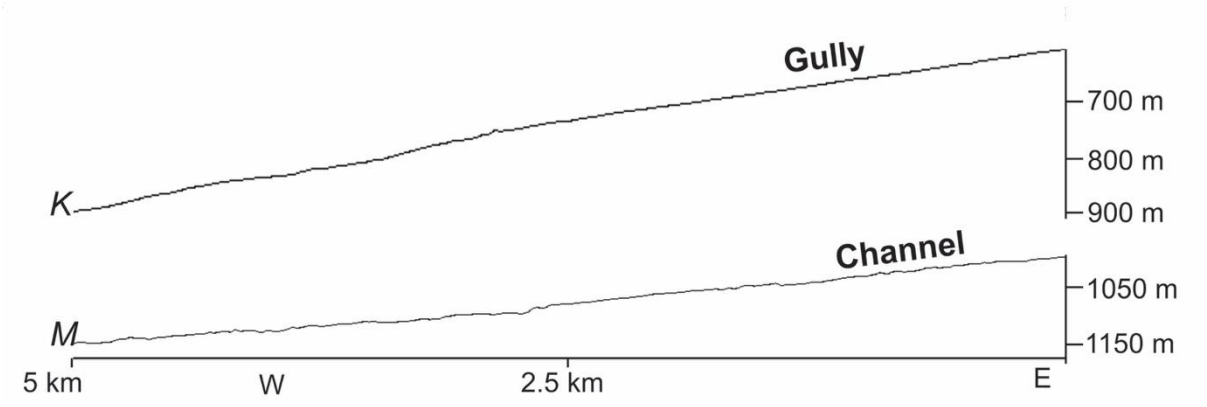

Figure 41: Comparison between a gully in the upper part (Profile K) with its continuation in the southern part of the INBIS Channel System (Profile M). For location see Figure 33.

Among these three channels, the southern one is the largest and the deepest, ranging between 1150 and 2000 meters in width and with an incision depth of 40 and 60 meters (see Profile N in Figure 40). The other two channels are slightly smaller, characterized by variable widths of 900 and 1100 meters and incision depths ranging between 30 and 50 meters. These two channels are partially braided between the water depth of 1350 and 1700 meters (see Figure 33). There are also three smaller incisions, similar in dimensions to the smaller channels observed in the northern part of the INBIS Channel System. These three smaller incisions originate at different depths of 1300 meters, 1350 meters and 1500 meters. The two northern incisions merge into one channel around the water depth of 1550 meters, while the southern seems to proceeds downslope (see Figure 33) though it is not possible to follow it further due to data quality.

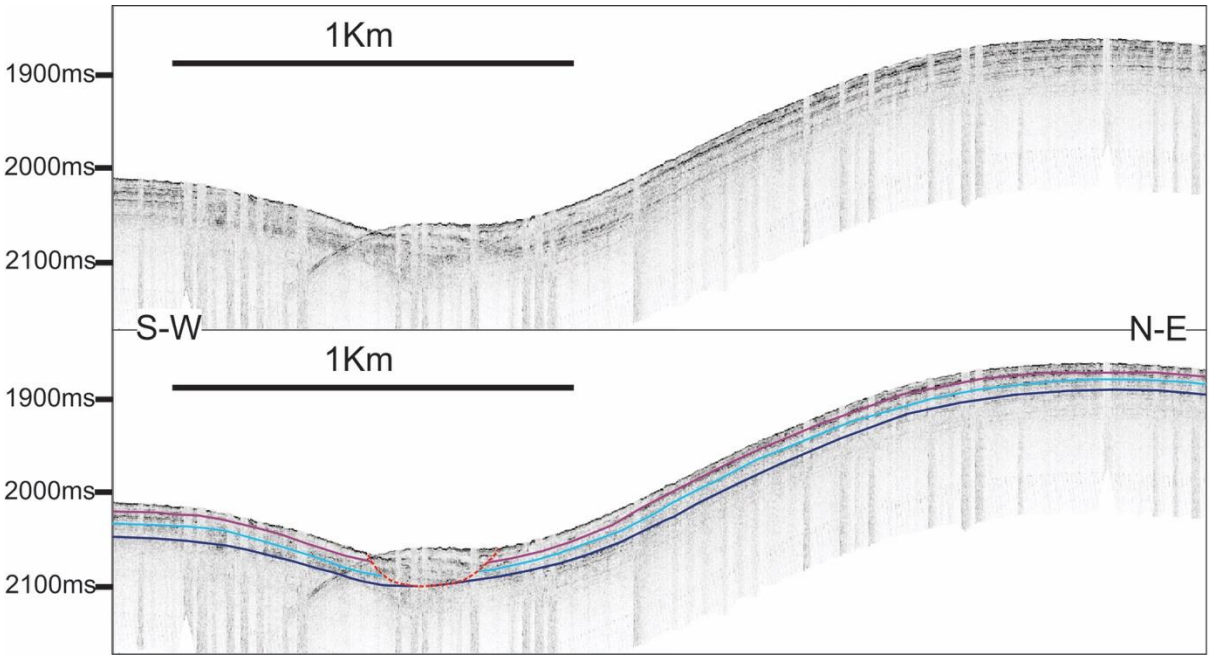

Figure 42: Sub-bottom section S1 on a channel in the southern portion of the INBIS Channel System. Purple, light blue and blue represent respectively reflectors at 10 ms, 25 ms and 40 ms below the bottom. Red dotted line marks the part of the channel thalweg where reflectors are interrupted by reflection hyperbolas. For location see Figure 33.

I identified in the sub-bottom profile data, a high-amplitude reflection, around 10 ms below the bottom (see Figure 42). In the SBP profile S1 it is also possible to observe two other medium amplitude acoustic reflectors, at around 25 ms and 40 ms below the bottom. These three reflectors are characterized by a good lateral continuity among the entire section, interrupted only in correspondence of the center of a channel. This channel is ~1 km large, with the seafloor reflection within the ~400 meters thalweg almost completely masked by reflection hyperbolas (see Figure 42).

3.4 Oceanographic results

I now present the results, hailing from *Bensi et al*. (*in prep*.) that I analyzed in this project and that I will discuss later in section 4.2.

Time series of potential temperature (θ), salinity (S) and density (σ_θ) exhibit a large variability during winter periods (October - April of 2014-2016 for both S1 and ID2). At water depths > 1000 meters, the stable signal of the NSDW, characterized by θ ~ -0.90°C, S ~ 34.90 and σ_θ ~ 28.07 kg m-3, was occasionally altered by fast intrusion of relative warmer, saltier and less dense water, coincident in time at both moorings (the distance between S1 and ID2 is ~170 km).

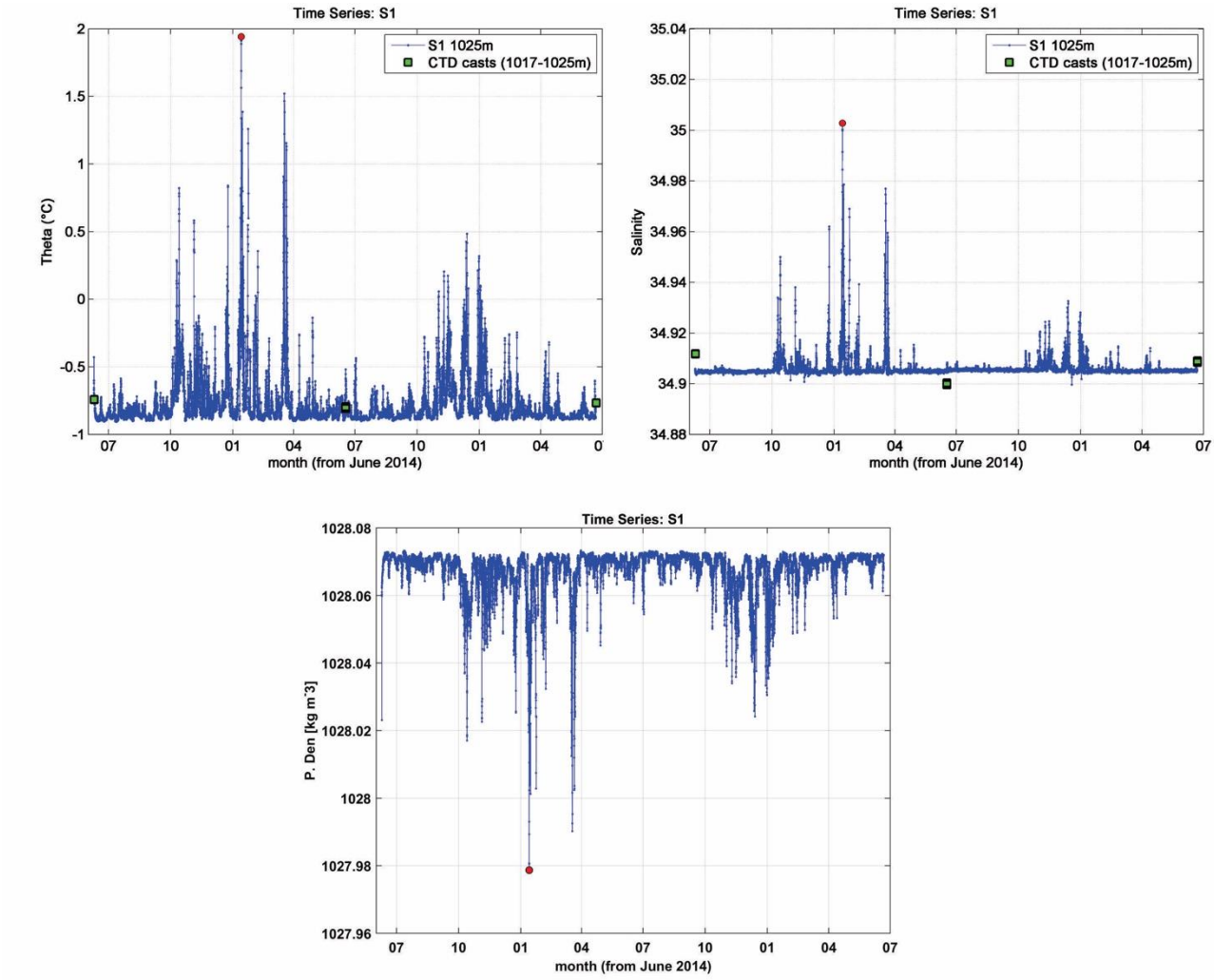

Figure 433: After *Bensi et al., in prep*.: Time Series for mooring S1of θ, S and σ_θ, from June 2014 to June 2016. Green squares represent data collected at mooring depth with CTD casts. Red dots highlight maximum values.

The peak effect of these intrusions is registered during winter period of 2014-2015 (with the apex in January); for mooringS1 peak values are $\theta \sim 1.96°C$, $S \sim 35.00$ and $\sigma_\theta \sim 28.02$ kg m-3 (see Figure 43); for mooring ID2 the peak values are $\theta \sim 1.11°C$, $S \sim 35.31$ and $\sigma_\theta \sim 27.86$ kg m-3 (Figure 44). During the second year at mooring ID2, CT sensors were replaced with temperature (T) loggers; peak values recorded after this switch are ~ 0.34°C, registered in the period of October - February.

In a comparison between the time-series of temperature between S1 and ID2 (Figure 45) it is possible to observe how the input of relatively warm water at the depth > 1000 meters (1025 - 1022 meters exactly) coincides temporally at both stations.

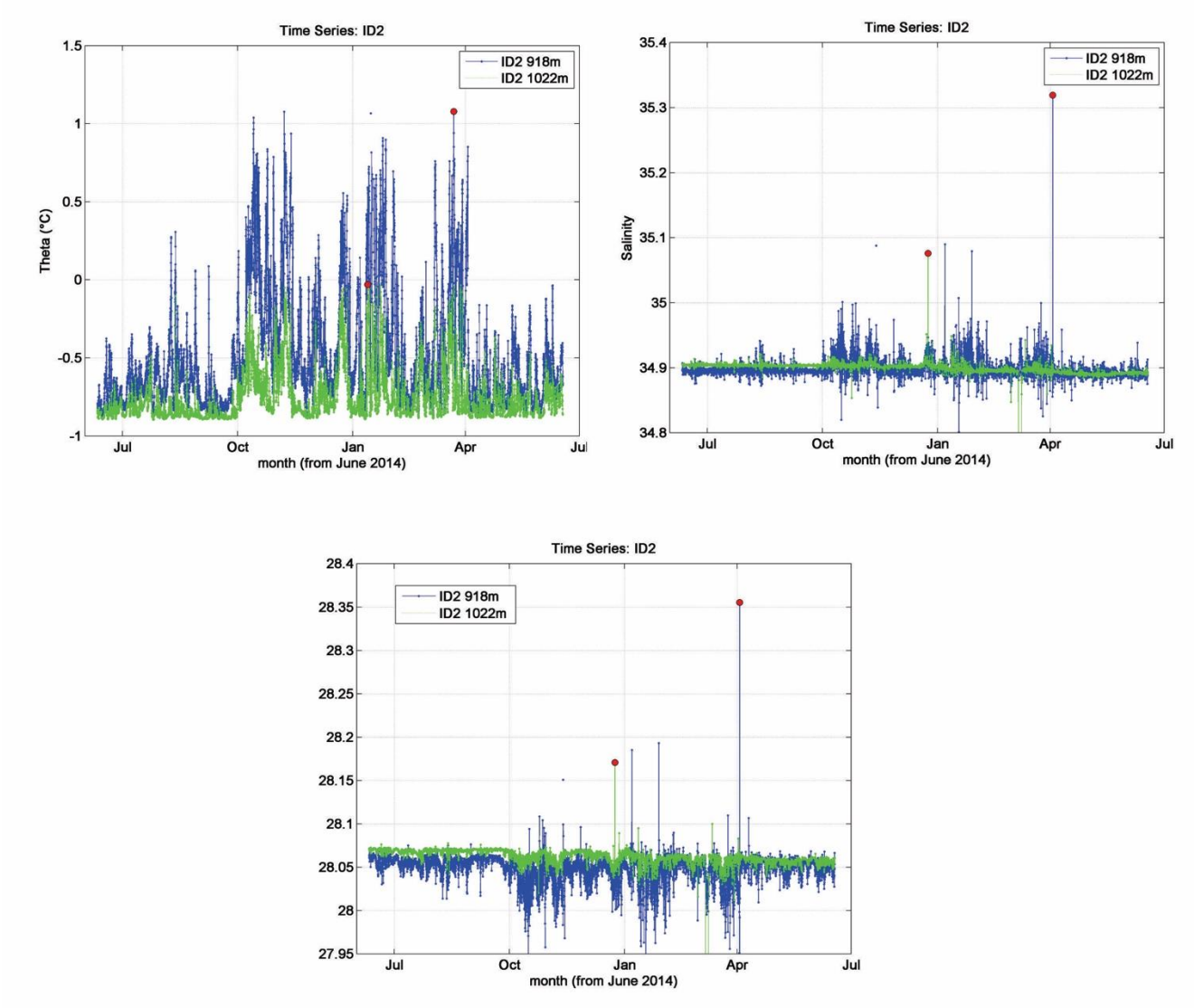

Figure 444: After *Bensi et al., in prep*.: Time Series for mooring ID2 of θ, S and σ_θ, from June 2014 to June 2015. Red dots highlight maximum values.

These time-series were compared with data hailing from CTD casts in the mooring locations, to check the data quality and provide information on spatial distribution of oceanographic properties in the area. In the CTD data, the presence of a nepheloid layer was observed; this phenomenon is quite frequent in areas affected by cascading of dense waters (*Puig et al*., *2013*; *Durrieu de Madron et al*., *2017*).

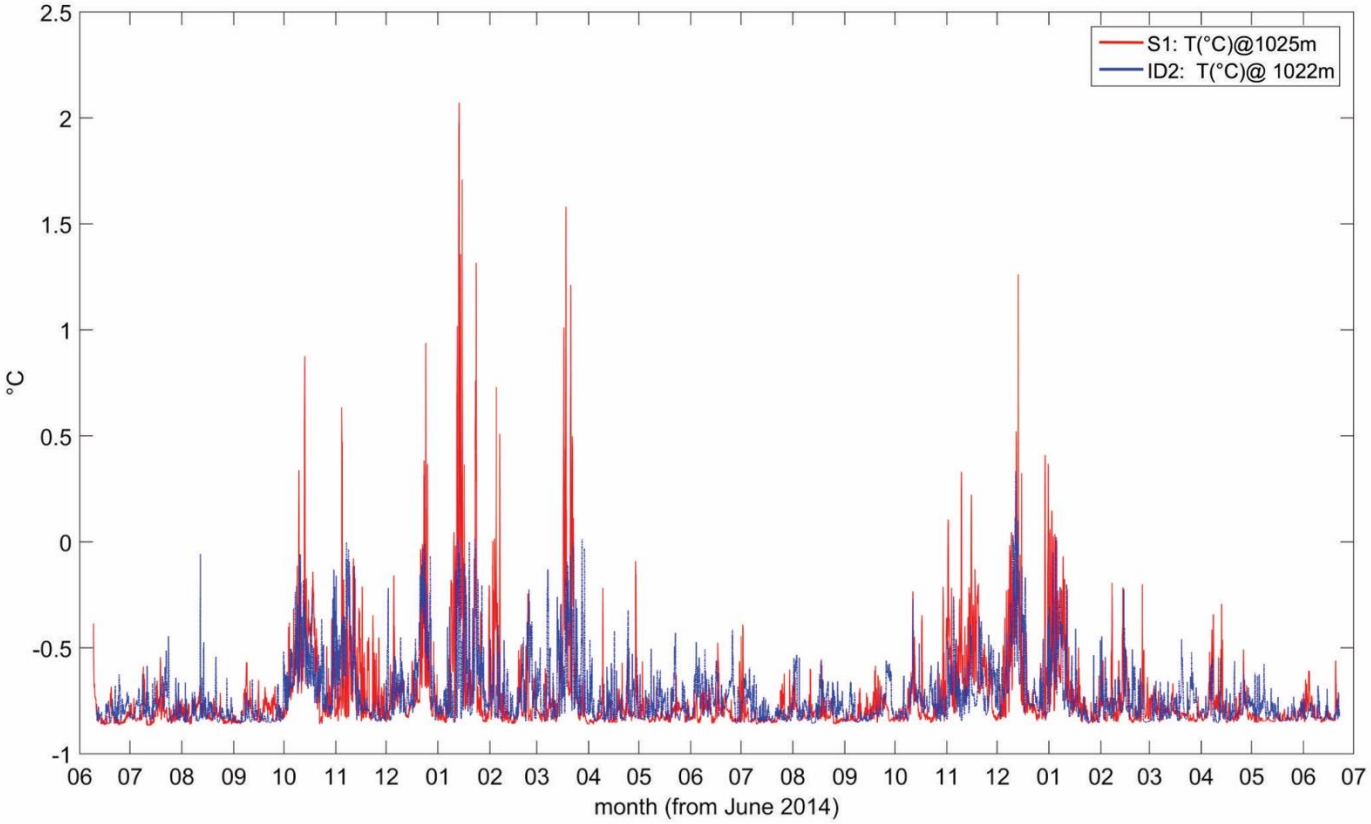

Figure 4545: From *Bensi et al., in prep*.: Comparison of Temperature time-series at mooring S1 (in red) and mooring ID2 (in blue), covering the period from June 2014 to June 2016. Variations of temperature appear to coincide temporally at both stations, suggesting that the process (or processes) responsible for this input of relatively warm water take place simultaneously in the Isfjorden and Bellsund areas.

In this regard, turbidity sensors on mooring S1 registered an increase in turbidity levels, measured in FTU (Formazin Turbidity Unit), between November and April. In a comparison with θ (Figure 46), the increase in turbidity levels reflects only partially the increase in θ, as it appears out-of-phase and separated into two signals: a delayed increase in turbidity, compared to the increase in θ; a short-term current (and θ) increase followed by resuspension of sediment during winters (*Bensi et al*. *in preparation*).

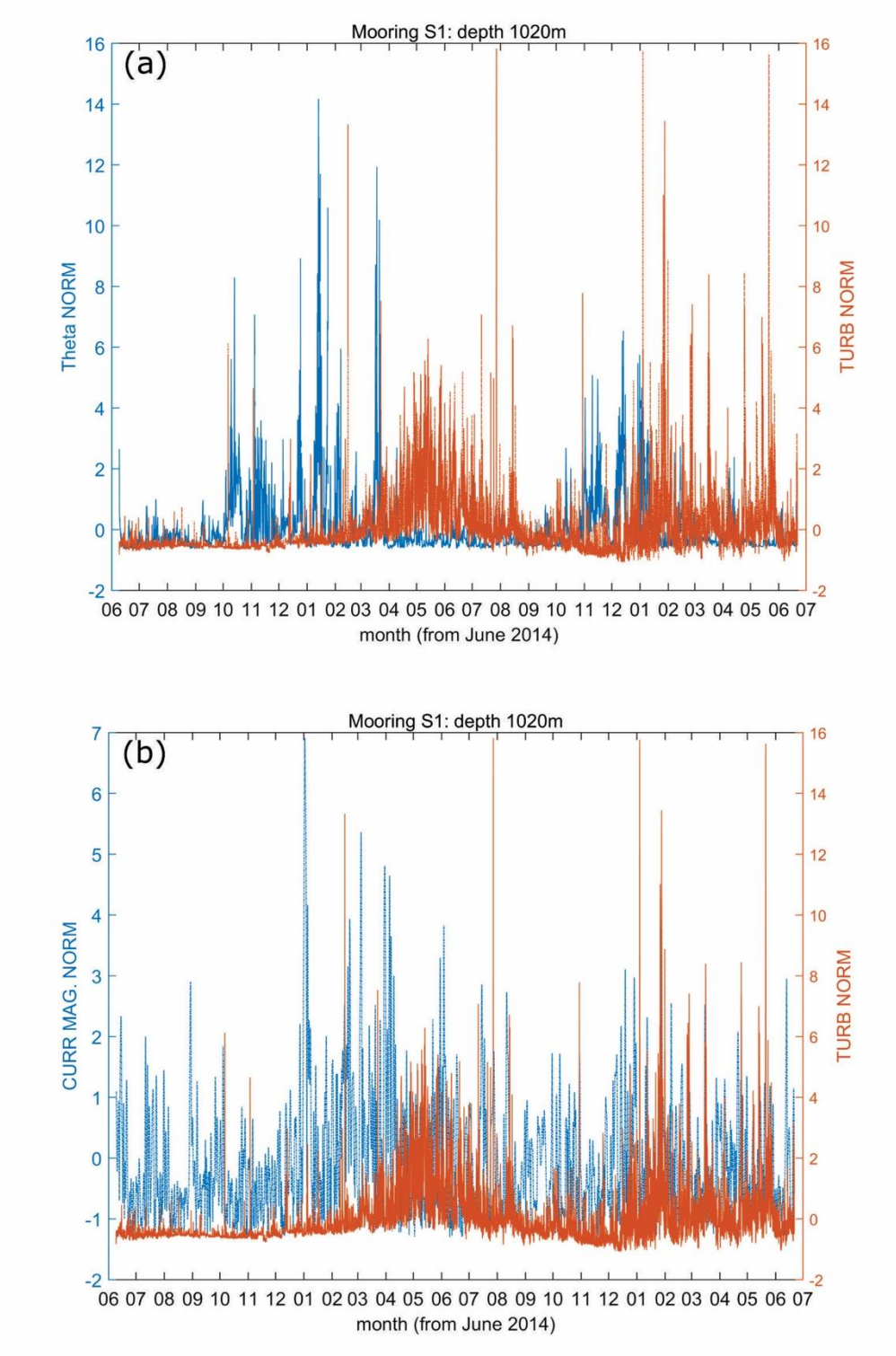

Figure 46: From *Bensi et al., in prep*.: For mooring S1, turbidity vs normalized θ time series in (a), turbidity vs current magnitude in (b), for the period from June 2014 to June 2016.

4 Discussion

In this chapter, the results obtained by the analysis of the geophysical database are discussed and compared with the oceanographic data. The post-LGM dynamics are presented, focusing on the along-slope and dip-slope processes responsible for the formation of the geological features described in chapter 3. In this chapter I will also try to address the relation between LGM and post-LGM glacial dynamics and NW Barents Sea ocean circulation, confronting the geophysical results with the oceanographic ones and discussing their relation.

4.1 The NW Barents Sea post-LGM glacial deposition

Since the expansion of the SBKIS to the shelf edge, around 1.2-1.0 Ma, erosion, transport and deposition of sediment across the western Spitsbergen continental margin have been controlled by the advance and retreat of the ice sheet. As a consequence, the western Spitsbergen continental slope consists in an alteration of glacigenic TMFs and their relative inter-fan areas, formed by Late Pliocene to Quaternary sediment. The former are the product of dip-slope transport and deposition of thick masses of sediment during glacial maxima in the form of glacial debris flow. Inter-fan areas are characterized by a lower amount of deposition, as are not directly fed by an ice stream, resulting in a lower amount of deposition and hence smaller deposits. The INBIS Channel System forms in one of these inter-fan areas.

Along the upper slope of the INBIS Channel System, many predominantly V-shaped gullies of similar size and spacing, with rare levees occur. I interpret these as a result from bypass processes, i.e. erosion of the slope and downslope sediment transport. The less developed levees and their small dimensions suggest that, in this part of the INBIS Channel System, downslope sediment transport was restricted to the gullies without significant over spilling. The gullies grow in dimension down the slope and develop into U-shaped channels with increasingly rough channel bases, which might be related to different degrees of erosion due to a possible increase in the kinetic energy of the fluxes. Another explanation for this increase in the roughness of the bottom might be a small amount of sediment deposition on the downslope part of the systems as a consequence of the increase in dimensions of the gullies/channels combined with the decrease of the slope gradient. In the upper, gully-dominated part, the gradient is up to 5°, and bypass-erosional processes therefore result in V-shaped incisions. Further downslope the gradient decreases (up to 1° – 2°), while gullies evolve into wider channels.

I infer that the bypass processes responsible for gully formation were caused by cascading meltwater from the SBKIS margin during the glacial periods. In fact, similar V-shaped gullies on steep TMF slopes in both the Arctic and Antarctic have also been interpreted to be the products of high-energy gravity-driven erosion processes such as cascading of subglacial

meltwaters (e.g. *Gales et al., 2013*). However, meltwaters are not the only flows that may have contributed to the formation of this upslope part of the INBIS Channel System. These bypass processes might also be the density-driven currents descending the southern flank of the Storfjorden TMF, the northern flank of the Bear Island TMF and the inter-fan area in front of Kveithola TMF, identified by *Vorren et al*. (*1998*) as the primary formation mechanism of the INBIS Channel. Core analysis (GK 23257 in *Vorren et al., 1998*) suggested that these density-driven currents where active mainly during glaciations. The origin of these density-driven currents is attributed to several mechanisms: dense water formed by cooling, sea-ice formation and brine rejection, or turbidity currents generated from small slides on the upper slope. During the build up to glacial maxima, sediments accumulate beyond the shelf edge, transported and deposited by the ice streams. The collapse of these accumulations produces debris and/or turbidity flows (e.g. *Vorren et al., 1998*; *Forwick et al, 2015*). The INBIS Channel in fact (i.e. its deeper part) is partially infilled by glacigenic debris flows, which reached their main activity during glacial maxima (*Laberg & Vorren, 1995*). From about 1000 m water depth and further below, the gullies merge. The flows generating the upper-slope gullies are funneled through the center of the area and, as consequence, 7 larger channels form (see Figure 33). I infer that the merging of a large number of gullies into fewer channels, along with the slope gradient decrease, may cause a change in the balance between erosion/transport and deposition. As a consequence, in the deeper part of these channels the roughness of the bottom increases and levees appear, suggesting that the energy of the fluxes is sufficient to overtop the channels flanks (see Profile D and Profile F in Figure 37). In the area of the INBIS Channel System adjoining Kveithola TMF, the northernmost channel exhibits an increased asymmetry of the flanks; this, together with the absence of gullies further north, might be the result of a consistent infill of sediment. The southern part of the Kveithola TMF has a morphology characterized by slide scars and short incisions, also suggesting the passage of downslope sediment flows. High-latitude glacial margins are in fact prone to gravitational failure as a result of their highly variable sedimentation style and geological processes (*Dowdeswell et al., 1998, 2002, 2004*), both in time and space. It is inferred that these sediment flows crossed the gullies at high angles (see Figure 38) during the glacial maximum or after the beginning of the ice retreat, feeding and partially filling/obliterating the gullies and channels in the shallow northern part of the INBIS. An example of the product of these debris flows could be the sediment accumulation (see Profile a and Profile b in Figure 39) at the downslope part of one of the incisions on the Kveithola TMF (see Figure 38). These flows may have even reached the central part of the inter-TMFs area, feeding both marginal and deeper parts of the INBIS Channel System. Deeper in the channel system, where the channels merge into one (see Figure 33), the channel bottom is in fact irregular, which may be caused by debris flows originating beyond the shelf edge. The accumulation north of the main channel with an upward apex around the water depth of 1200 meters is inferred to be the product of one of such debris flows, descended possibly along one of the visible gully/channel (see Figure 48 and Figure 49).

The channels eventually converge downslope (around variable depths, ranging between 1500 meters and 2100 meters water depth) in the main channel, and several processes probably led to the asymmetry of the flanks here. Firstly, due to the decreasing energy of the flows as a consequence of the lower slope gradient, the finest part of the sediment load is delayed and deflected to the right by the Coriolis force. This produces overbank accumulations (levees) on the right (northern) flank of the channels (*Vorren et al., 1998*). Secondly, the direction of the channel system is constrained by the presence of Kveithola and Bear Island TMFs (see subsection 3.3.2), thus creating asymmetry in channel system. Thirdly, the presence in this area of the northward-flowing West Spitsbergen Current (WSC) may contribute in preventing sediments from settling on the southern side of the channels in this part of the INBIS channel system, supporting deflection of the suspended sediments and deposition on the northern side of the channel.

I envisaged that the INBIS channel system developed through an alternation of phases of ice buildup, glacial maximum and deglaciation, as depicted in Figure 47, 48 and 49.

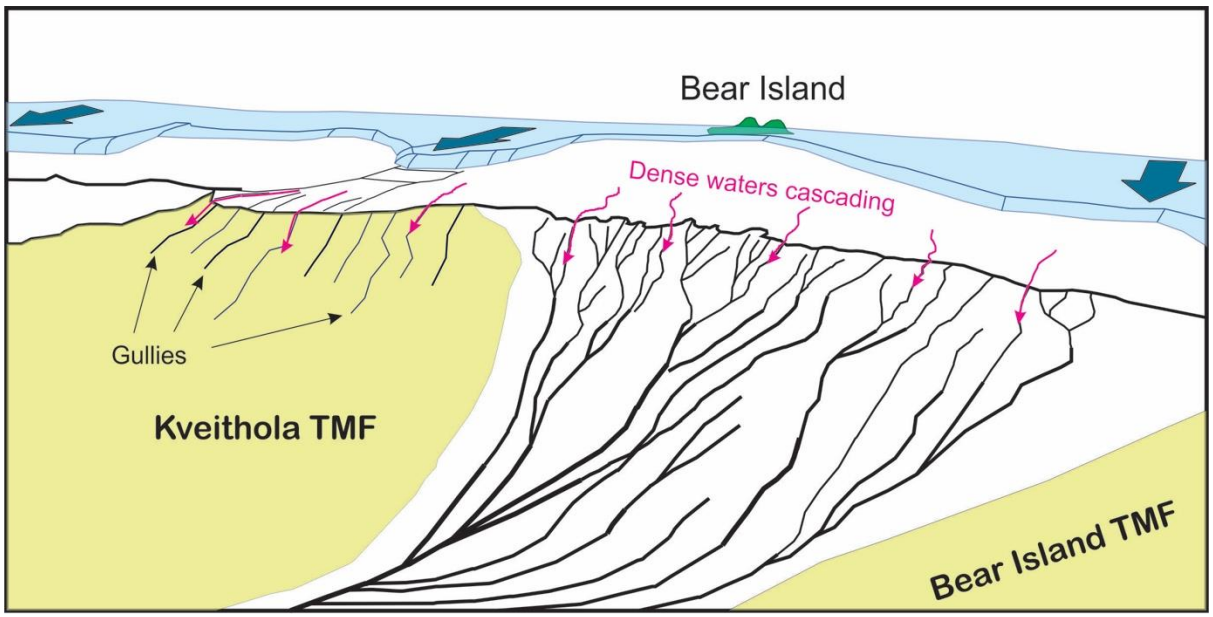

Figure 47: Scheme of the inferred pre-LGM state of the INBIS Channel System. Both the INBIS Channel System and the Kveithola and Bear Island TMFs (in yellow) are crossed by the cascade of dense waters (in pink). These waters flow on the shelf edge and down the slope through bathymetric constrain into previously formed gullies, possibly contributing to their formation. The shelf is characterized by the build-up of the ice sheet (SBKIS). Blue arrows indicate the location and direction of area of fast-moving ice (ice streams). Downslope, the gullies (thin black lines) merge and evolve in channels (thick black lines).

I suggest that gullies and channels may have started their development during the buildup and advance of the ice sheet toward the shelf edge. During this period density driven water currents (related to cooling, sea-ice formation and brine rejection) could carve into the shelf

edge and the uppermost slope. In the case of the LGM, a scheme of the initial pre-LGM situation is presented in Figure 47; I infer that these by-pass processes lasted until at least the first part of the LGM, around 23 ka.

During the second part (i.e. the peak) of the LGM (see Figure 48), between around 23 and 20 ka (*Elverhøi et al., 1995; Rasmussen et al., 2007; Jessen et al., 2010*), the ice sheet and ice streams reached the shelf edge, consistently increasing the amount of sediment transport. In these conditions, massive sediment flows (glacial debris flows) descend down Kveithola and Bear Island TMFs and deposit sediment accumulations contributing to progradation of TMFs.

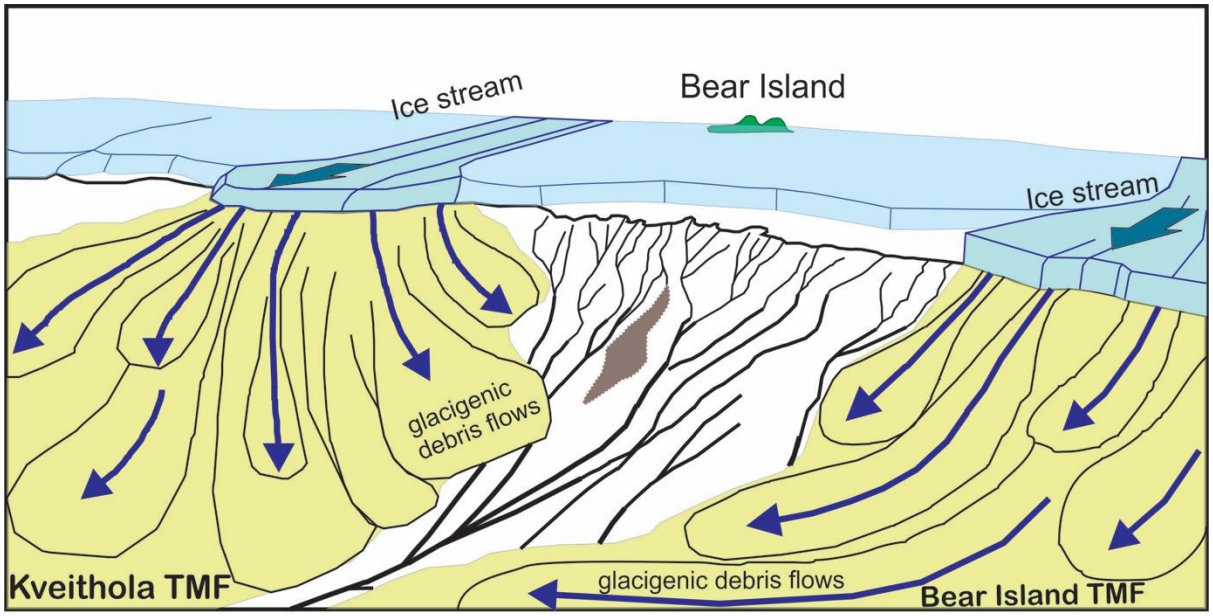

Figure 48: Scheme of the inferred LGM state of the INBIS Channel System. During this phase the ice sheet reached the shelf edge in the area of fast-moving ice (ice streams, slightly darker than the rest of the ice sheet). Blue arrows indicated the flow of glacigenic debris flows, transported by the ice streams, forming depositional lobes on both Kveithola and Bear Island TMF (in yellow). These glacigenic debris flows partially bury the INBIS Channel System (see Figure 51 for a comparison). In this reconstruction, the slow moving part of the ice sheet has not reached the shelf edge directly at east of Bear Island. As consequence, precedent formed structures (gullies) are preserved only the central part of the INBIS Channel System, protected by Bear Island (in green). In grey, a mounded structure, possibly a product of the collapse of a small sediment accumulation on the shelf edge (minor debris flow).

I infer that during this phase the debris flows on the southern part of the Kveithola TMF partially invaded the INBIS Channel System, burying some of the channels, as seen in Figure 48. Smaller gullies and even small channels probably had not developed sufficient dimensions to endure and redirect the flux of sediment of these flows leading to a partial or complete sediment infill and to an obliteration of the smallest features. I also infer that during the LGM the ice sheet reached the shelf edge only in the Kveithola and Bear Island TMFs and not in the area in front of the central part of INBIS Channel System where the gullies are

better preserved (highest incision-depth/width ratio and accentuated V-shape). Moreover, beyond the shelf edge a consistent number of ploughmark is observable; in the dataset I did not find any other morphology supporting the presence of ground ice at the shelf edge in this area. I observed an additional proof supporting this hypothesis (the absence of the ice at the shelf edge during LGM) on the outer shelf in front of Bear Island: the presence of two shelf-edge moraines (see Figure 50 and Figure 49). These are subglacial marine landforms located in areas of slow-moving ice (e.g. by *Batchelor et al., 2017* on the seafloor of Røstbanken, west of the Lofoten Islands, Norway), indicating areas of still-stands or minor re-advances during general ice-sheet retreats (*Batchelor & Dowdeswell 2015*). I suggest that the presence of two shelf-edge moraines on the shelf in front of Bear Island, distant between 2 km and 5 km from the shelf edge, represent the outer shelf limit of grounded ice during the LGM.

I interpret the upward-convex body, observed to north of the main channel (see subsection 3.3.2 and Figure 33, Figure 48 and Figure 49), as a collapse of a small sediment accumulation beyond the shelf edge.

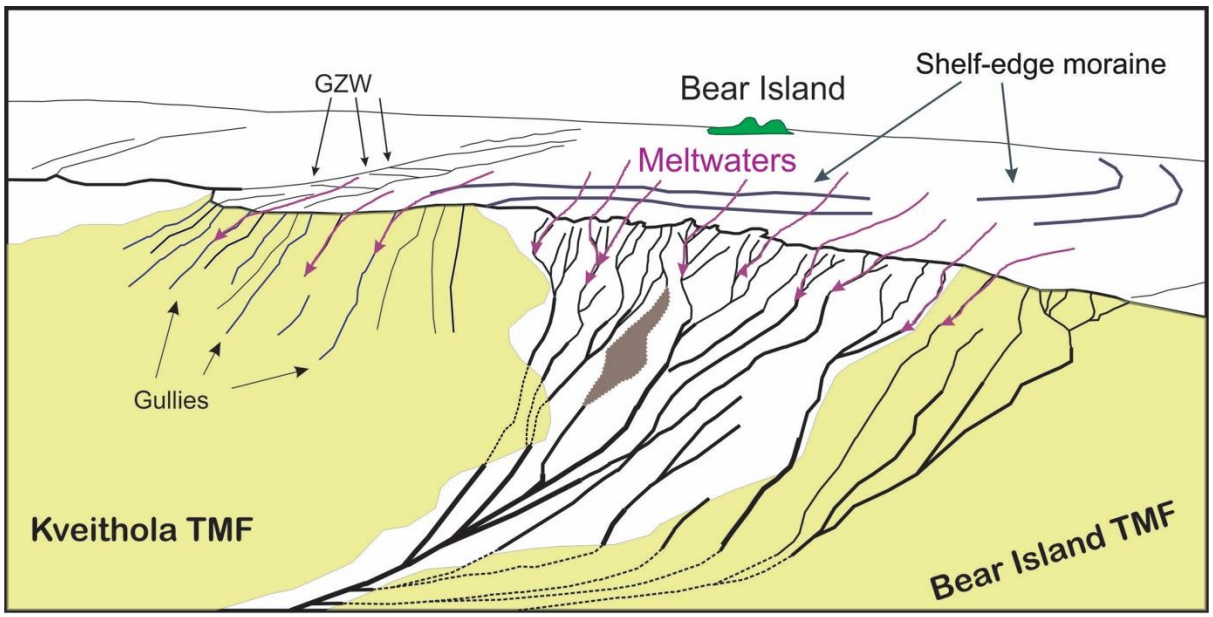

Figure 49: Scheme of the inferred post-LGM state of the INBIS Channel System. During the ice sheet retreat, glacigenic debris flows cease to descend downslope. Meltwaters (in purple), produced during the ice retreat, flows past the shelf edge and downslope, both in the INBIS Channel System and the in Kveithola and Bear Island TMFs (in yellow). Meltwaters carve new gullies on the glacigenic debris flow deposits on the TMFs (see Figure 45 for comparison). In the INBIS Channel System, the precedent formed gullies are crossed by these meltwaters (bathymetric constrain), undergoing erosion and consequently increasing in dimensions. Shelf-edge morains (labeled in grey) marks the maximum extension and/or still-stand period of the ice sheet (see Figure 48), in the shelf area between the edge and Bear Island (see Figure 50).

The resulting debris flow, smaller compared to those responsible for the progradation of TMFs, flew through the upper part of the channel system, inside a gully and deposited where the slope gradient diminish. In another interpretation, I infer that this body is a mass wasting generated from one of the flanks of the gullies in the upper part of the slope. Anyhow, I was not able to find any morphology in the dataset supporting this hypothesis.

Eventually, with the start of the deglaciation and retreat of the ice sheet, around 20-19 ka (*Hughes et al., 2016*), glacial debris flows characteristic of peak glaciations ceased. I inferred that the production of meltwaters has been the dominant process during this phase (see Figure 49): meltwaters kept flowing through the gullies and channels that survived the sediment flows – dominated phase, partially contributing to the growth of gullies and channel observable in the present day. However I infer that sediment flows have continued to descend down the TMFs as mass transports. The last are the product of the many landslides observable in Figure 38 and flew in short term incisions similar to gullies in dimensions, but shorter and less developed. *Lucchi et al.* (*2012, 2013*) suggests that the distribution and triggering of submarine landslide on the slope of TMFs is linked to meltwaters.

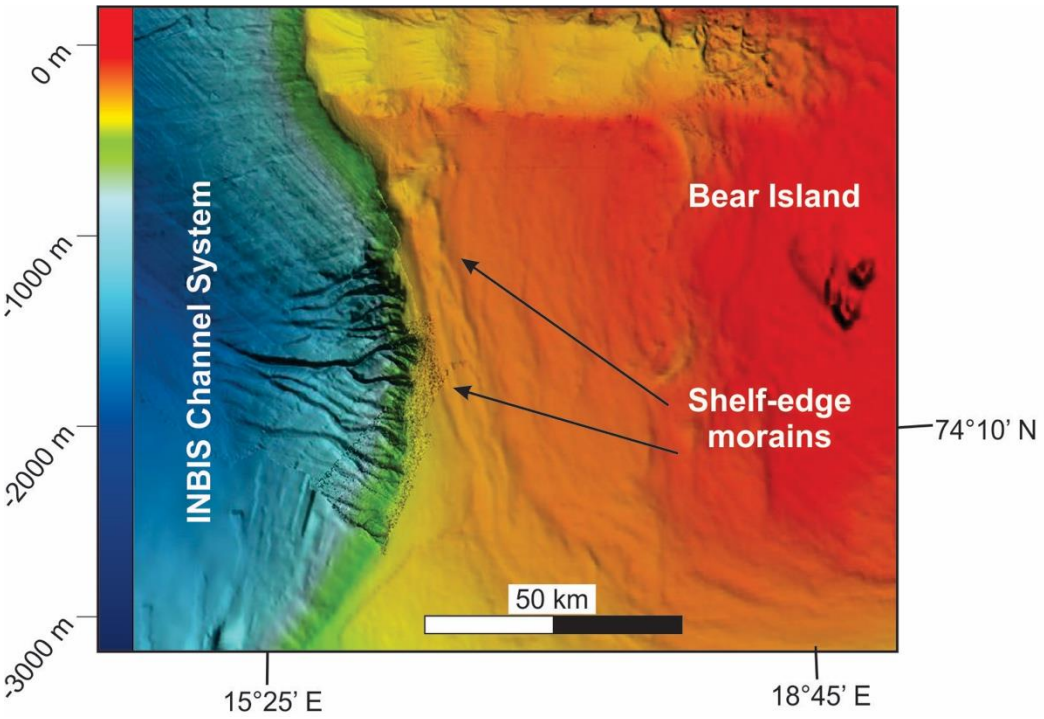

Figure 460: Bathymetric map of the shelf area comprise between the INBIS Channel System and Bear Island. Shelf-edge morains, distant between 2 km and 5 km from the shelf edge, represent the outer shelf limit of grounded ice during the LGM, presented in Figure 48.

The advance and retreat of ice streams produce an interbedding between glacial debris flow deposits and meltwaters plumite deposits. The latter are characterized by high water content

that generates slope instability when rapidly loaded by sediment (i.e. glacial debris flow) during glacial maxima (*Rebesco et al., 2013*).

The presence of meltwaters in this third phase is supported also by the formation of gullies at the shelf edge of Kveithola TMF. These gullies are smaller compared to those individuated on the shelf edge of the INBIS Channel System, with dimensions similar to those observed on the other TMFs along the west Spitsbergen margin (e.g. *Pedrosa et al., 2011*). I infer that the gullies individuated on the Kveithola TMF are those formed only after the debris flow - dominated phase, as during the last debris flows buried precedent formed gullies (if present). On the contrary the absence of direct influx of glacial debris flows in the INBIS Channel System allowed the preservation of gullies at shelf edge. Meltwaters produced during deglaciation could flow along preexisting gullies, increasing their dimensions. Finally I suggest that the formation of the INBIS Channel System is not to be attributed only to the LGM, but that the alteration of phases described above is a cycle repeated several time. The first gullies at shelf edge may have appeared when the SBKIS reached the shelf edge for the first time, around 1.2-1.0 Ma. From that moment, repeated cycles of advance and retreat of the ice sheet led to the expansion of Kveithola and Bear Island TMFs. The INBIS Channel System was protected from the effects of fast moving ice thanks to presence to the East of the Bear Island, which acted as an obstacle for the advances (and retreats) of the ice sheet. As a consequence I infer that the formation of the gullies and their development into a channel system is to be attributed to cyclic production and flow of meltwaters during deglaciation phases together with the absence of direct massive sediment flow (glacial debris flow) during glacial maxima.

From the analysis of the bathymetric dataset in the area of Isfjorden and Bellsund, I identified geological structures associated with dip-slope glacial dynamics analogous to those observed in the INBIS area. The landslide scars described in section 3.2 (see Figure 30) on the slope of the Bellsund area appear very similar to those described on the Kveithola TMF, with comparable dimensions and distribution pattern. Formation of elongated along-slope landslides is observed in several areas along the west Spitsbergen continental margin (e.g. *Rise et al., 2006; Hjelstuen et al., 2007; Pedrosa et al., 2011; Lucchi et al., 2012*). I suggest that these landslides have a genesis similar to that of those individuated on the Kveithola TMF, i.e. they were produced by the collapse of plumite/contourite deposits rapidly loaded by glacigenic debris flows during LGM, descending either down the Storfjorden TMF or from the shelf edge between the Storfjorden and the Bellsund TMFs (Hornsund). In the Isfjorden area, the analysis of sub bottom profiles SV15_SBP01 (see Figure 26) and SV15_SBP02 (see Figure 27) revealed a series of superficial transparent lens shaped bodies with variable dimensions around the water depth of 700 meters. I infer that these bodies may be buried debris flow deposits, similar to those observed further downslope by *Rebesco et al.* (*2013*) on the sub-bottom profiles on the Isfjorden drift. I suggest that these buried debris flow deposits were produced by glacial debris flows descending from the southern part of the

Isfjorden TMF or originated at the shelf edge between Isfjorden and Bellsund TMFs, during LGM.

4.2 Depicting the relationship between glacial deposition and ocean circulation

In the Isfjorden and Bellsund areas, two along-slope mounded features are identified from the analysis of the seismic dataset and interpreted as contourites (*Rebesco et al., 2013*). Bottom currents have generated contourite deposits along the western (and northern) margin of Svalbard for at least 3 million years (*Eiken and Hinz, 1993*). The interpretation by *Rebesco et al.* (*2013*) classifies the two contourites located in the Isfjorden and Bellsund areas as plastered drifts, i.e. mounded and possibly elongated drifts located along gentle slopes (see Figure 10) (*Faugères and Stow, 2008; Rebesco et al., 2014*). In particular these two drifts are controlled by the persistent flow of the WSC described in subsection 1.1.2. Due to the high velocities (>20cm/s) close to WSC axis, sediment deposition is hindered above 1000 meters water depth, and erosion takes place in the uppermost part of the continental slope (*Beszczyńska-Möller et al., 2012*).

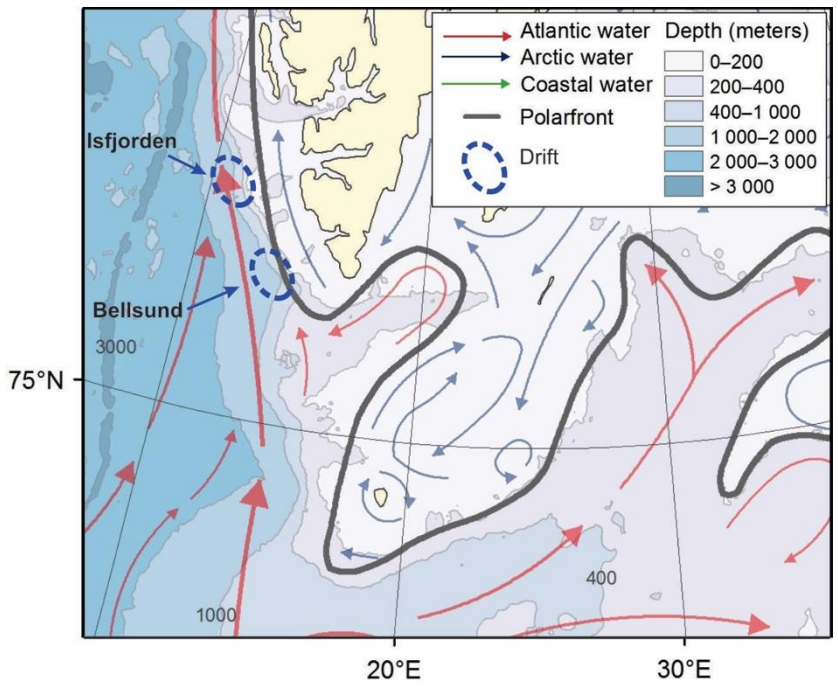

Figure 51: Modified after *Stiansen and Filin, 2007*: Map of the ocean circulation on the west Spitsbergen margin in the NW Barents Sea, with the location (blue dotted lines) of the Isfjorden and Bellsund drifts.

Within the WSC, at a water depth of about 1400 meters, NSDW is flowing with a velocity of around 9 cm/s (*Beszczyńska-Möller et al., 2012*). This flow (still relatively fast compared to that of the adjacent water masses) favors the deposition of sediments and its buildup in a mounded shape. On the new seismic profiles acquired on both Isfjorden and Bellsund drifts (see section 3.1 and 3.2 for details), I was able to identify and trace five of the seven

reflectors proposed by *Faleide et al*. (*1996*). In these seismic profiles, the sigmoidal shape of the drifts is distinguishable up to reflector R4a, while below the last, reflectors are conformable to the seafloor. Reflector R4a also marks the passage from medium amplitude reflections, between reflectors R4 and R4a, to relative high amplitude reflection, below R4a. In agreement to what already stated by *Rebesco et al*. (*2013*), I infer that reflector R4a marks the onset of drift formation, suggesting that it began around 1.3 Ma, possibly coinciding with the ice expansion of Early Pleistocene (see subsection 1.1.1) and the development of TMFs (*Forsberg et al*., *1999; Butt et al*., *2000*). With regards to the formation of the Bellsund drift, I envisage that the 15 km long lensoidal feature identified between reflector R4 and R4a on profile SV15_04 (see Figure 31) corresponds to the origin nucleous of the drift. The progressive upslope migration of the crest of the drift was already inferred by *Rebesco et al*. (*2013*) from the analysis of seismic profile EG_04 (see Figure 29); moreover, in this last profile, a similar nucleous to the one described above, can be observed.

For the formation of sediment drifts such as those observed in the Isfjorden and Bellsund area, the presence of a current that reaches the bottom such as the WSC is an essential, but not sufficient condition. The second essential condition for the formation of a drift is in fact a significant supply of suspended sediment, which can occur through diverse sedimentary processes (*Stow et al*., *2008*), discussed further below.

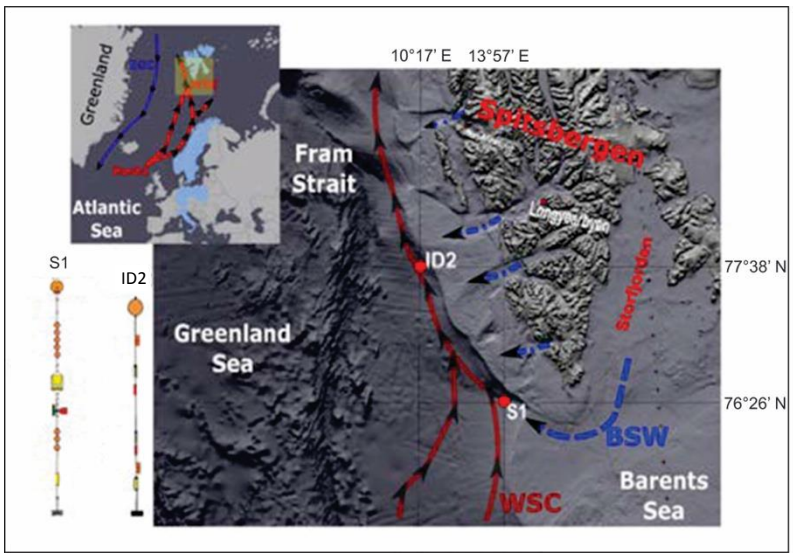

Figure 52: From *Bensi et al., in prep*.: Map of the location of moorings ID2 and S1. In Red the flow of the WSC, in blue the inferred flows of BSW and shelf convection.

The formation of the two plastered drifts of Isfjorden and Bellsund is attributed to the action of the WSC. It transports sediment hailing from beyond the shelf edge through gravity mass processes during glacial conditions, turbid meltwaters during the deglaciation phase and

episodic cascade down the slope of dense shelf water plumes (*Rebesco et al., 2013*). This is similar to what inferred for other drifts on glaciated margin (e.g. Lofoten Drift in Norwegian Sea, by *Laberg et al., 1999, 2002*; NW Weddell Sea (Antarctica), by *Smith et al., 2010*).

I found proof of the presence of gravity mass transport and turbid meltwaters (respectively during glaciation and deglaciation) in the bathymetric and sub-bottom dataset, as previously discussed (see section 4.1). The third process, episodic cascades of dense shelf water plumes, was hypothesized for this area (*Rebesco et al., 2013*) in analogy to what stated by several studies on dense water cascading in the Storfjorden (*Quadfasel et al., 1988*; *Akimova et al., 2011*) or in general in the Arctic Ocean and Greenland Sea (*Rudels, 1995*).

The data hailing from the two moorings ID2 and S1, located respectively in the Isfjorden and Bellsund areas (see Figure 51 and Figure 52), showed results that suggest the possible influence of dense shelf water plumes (*Bensi et al., in preparation*). The T-S anomalies observed at moorings S1 and ID2 are synchronous, suggesting that the triggering processes happened at the same moment along the west Svalbard margin. These T-S anomalies could be related to local mesoscale features (e.g. eddies or lateral advection) acting at the same time in both locations (*Bensi et al., in prep.*); however, this phenomenon is excluded as in this polar region the mesoscale is in the order of tenth of kilometers (10-20 km) (*Zhao et al., 2015*), while the distance between the mooring is ~170 km. Possibly, these inflows of relative warm and salty water occurring mainly during the winter season could be either BSW strongly modified during its descent along slope due to the entrainment with Atlantic waters (see subsection 1.1.2), or the response of the deep ocean to strong wind bursts, which are able to trigger dense water formation on the shelf (similarly to what is reported for the Greenland margin, e.g. *Magaldi et al. 2011*). Initially these waters are cold and salty due to the mechanisms responsible for their formation, in particular brine rejection and dry wind-induced cooling and evaporation, resulting in a higher density than the surrounding waters. These cold and salty plumes (TS plumes) start descending along slope as density-driven bottom-arrested currents, possibly collecting a large quantity of sediments. During their descent, these density-driven currents modify their original temperature and salinity properties, mixing with the surrounding water through entrainment (see subsection 1.1.2). However, their kinetic energy increases thanks to large amount of sediments collected, which partially compensate the thermohaline density loss. As a result of this process, these sediment-enriched plumes reach larger depths (> 1000 m) than their equilibrium point in the water column (*Fohrmann et al., 1998*) based on their thermohaline properties. A scheme of this phenomenon is presented in Figure 53.

The arrival of similar sediments-enriched fluxes is registered by the turbidity sensor at mooring S1, as seen in Figure 46. The variability registered by the turbidity sensor could include two signals: a short-term delayed (hours-days) turbidity increase, following peak of T-S; a highly delayed (months) turbidity increase, reaching the mooring during late winter

and early spring. I infer that the first signal is associated with sea-ice formation and/or meteorological events; the delay may be attributed to the turbidity current structure, with the arrival of a density (T-S) part of the flux at first, followed briefly by the sediment enriched part, registered by the increase in turbidity. As proved by *Azipiroz-Zabala et al*. (*2017*), turbidity currents may develop into a fast-flowing head and a slower body. The sediment load of the head is limited: it is in fact a small and erosive frontal-cell that outpaces and feeds with sediments the rest of the turbidite. The body is the larger part of the turbidity current, enriched in sediment and slower.

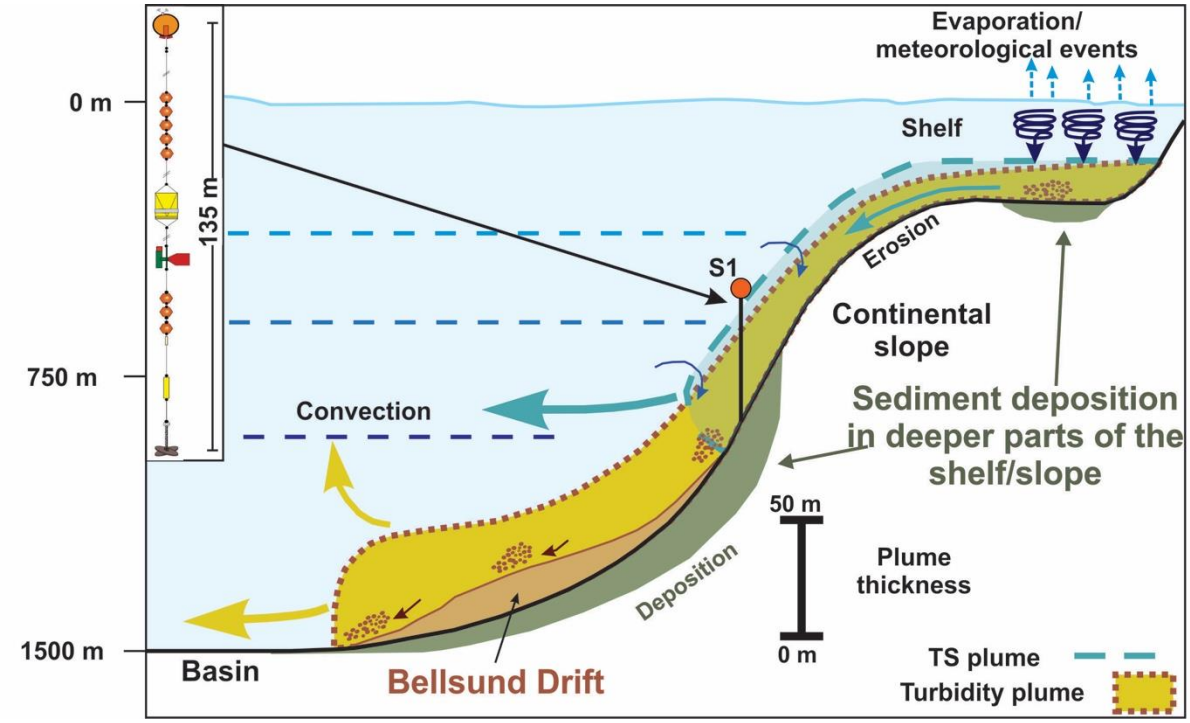

Figure 53: Modified after *Fohramnn et al., 1998*: Cartoon of shelf-slope convection, adapted for the area of the Bellsund drift (mooring S1). Meteorological events (light blue arrow in top right corner) cause the formation of dense shelf water. Cascading down the slope of these dense water forms either a TS (temperature-salinity driven) plume (in light blue) or a turbidity plume (yellow) if a certain amount of sediment is collected. Turbidity plume, due to its sediment-increased density, reaches lower part of the slope, compared to the TS plume, where the sediment is deposited forming the drift.

I suggest that the density driven currents turn into turbidity currents descending down the slope through bathymetric constrain. The presence of suspended sediment in a turbidity current increase noticeably the density, exceeding the value expected by the water θ and S properties, providing an augmentation of its driving force (*Kämpf & Backhaus, 1998*; *Kneller & Buckee, 2000*). I suggest that turbidity currents proceed through the water column, undergoing a strong entrainment process (see subsection 1.1.2) with the WSC and becoming warmer and slightly less salty. Thanks to the presence of sediment, turbidity currents can effectively reach and surpass the water depth of 1000 meters, were surrounding water is

colder and with a higher σ_θ, resulting in a warm signature below the Atlantic layer (*Quadfasel et al., 1988*). A scheme of the entire process is presented in Figure 53.

4.3 Evolution of the west Spitsbergen margin through glacial cycles

The geological features analyzed and discussed in this Ph.D project exhibits strong similarity with the features described in other studies related to glacial depositional processes and on ocean circulation along the west Spitsbergen margin (e.g. *Jungclaus et al., 1995; Gawarkiewicz et al., 1997; Vorren et al., 1998; Laberg et al., 1999; Anderson et al., 2002; Dowdeswell et al, 2002; Knies et al., 2009; Akimova et al., 2011; Rebesco et al., 2011, 2013; Lucchi et al., 2012, 2013; Gales et al., 2013; Skogseth et al., 2003, 2013; Batchelor et al., 2017; Madrussani et al., 2017*). Relying on this, I suggest that the evolution from the LGM of the west Spitsbergen margin, intended as the result of the glacigenic and oceanographic processes of erosion, transport and deposition of sediments, is composed by three phases, each one associated to a specific dominant process. I infer that during glacial maxima along the west Spitsbergen continental margin the dominant process is the downslope descent of glacigenic debris flows (see debris flow deposits in Isfjorden and Bellsund areas, subsections 3.1 and 3.2) sediments deposited at the shelf break / upper slope by the ice are remobilized and transported downslope in the areas where the ice reached the shelf edge, with a remarked intensity in the areas characterized by the presence of an ice stream. These glacial debris flows are able to effectively obliterate and/or bury any precedent formed structures (see INBIS Channel System, subsection 3.3.2). As a result, the margin is a lateral juxtaposition of TMFs and inter-TMFs areas (see Figure 8). During deglaciation periods, ice melting and retreat produce meltwaters along the entirety of the ice sheet. Meltwaters flows through the shelf edge and down the slope of both TMFs and inter-TMFs areas, carving erosional features or depositing meltwater plumite sediments (see Figure 49). The last, when interbedded with debris flow deposits, generate slope instability, causing the collapse of part of the slope (i.e. landslides) (see Figure 38 and Figure 39). I suggest that on a large scale the formation of gullies is homogeneous along the margin, with small scale variability in dimensions due to the formation on a TMF or in an Inter-TMFs area. In both cases, gullies develop only for a limited downslope distance, without forming interconnected systems. On the contrary, the INBIS Channel System represents a unique exception in the NW Barent Sea, due to fact that the shelf is “protected” by the presence of Bear Island (see Figure 48 and 49). Finally, I suggest that during periods characterized by the build-up of the ice sheet (i.e. glacial period, before the glacial maximum), the sediment input is related to the flow of density driven current. Glacial debris flows are likely not present in these periods, as the ice sheet (and ice streams) has not yet reached the shelf edge. Similarly, meltwaters are likely not abundant, as the ice front is relatively inshore during this phase. Conversely, it is inferred that the formation of BSW and/or violent meteorological events on the shelf produce, during winters, plumes of cold and salty waters. These plumes are able to travel through the shelf edge collecting sediments and developing into turbidity currents (see Figure 53). I hence think that these turbidity current flows effectively transport large amount of suspended sediment into deeper parts of the slope during their downslope movement through bathymetric constraints. I

infer that deposition of the suspended sediment on the continental slope is controlled by the presence of the bottom currents, i.e. the lower part of the WSC, generating contourite structures in the inter-TMFs area of the margin (see Figure 51). I suggest that only relatively fine-grained, suspended part of the turbidite flows are involved in the formation of contourites along the margin, whereas the coarse-grained, bedload part continue its flow towards the Knipovich Ridge (see Figure 31).

5 Conclusions

In this study, the evolution of the NW Barents Sea margin has been reconstructed from the LGM to present. Through the analysis of geophysical and oceanographic datasets, I studied the processes of erosion, transport and deposition affecting the west Spitsbergen margin related to paleo-ice sheet dynamics.

New data were acquired during several research cruises in the area, to increase the available dataset.

The analysis focused in three selected area of the west Spitsbergen margin. These areas are characterized by specific processes and/or by a high concentration of data types.

Through the analysis of bathymetric and sub-bottom data, I described a hitherto unsurveyed part of the INBIS Channel System (*Vorren et al., 1998*), unique example of channel system in the Barents Sea. This gully/channel dominated part of the channel system is located at the shelf edge and upper slope to east of Bear Island, between the Kveithola and Bear Island TMF. I infer that from there, all channels merge into the INBIS Channel, a 60 km long channel extending down to the Knipovich Ridge. From the analysis of the observed morphology, I proposed an evolution model related to the processes responsible for the formation of the specific features of the upper part of the channel system. I infer that the formation of the well-developed gullies forming the INBIS Channel System is the product of repeated meltwaters flowing down the slope. Preservation of these erosive forms was possible mainly thanks to the presence of Bear Island. The last acted as an obstacle for the dynamics of the ice sheet and hence imposed slow-moving ice conditions. The island as a result protected the shelf from massive sediment transport (i.e. glacigenic debris flows). As a consequence, the ice sheet did not reached the shelf edge in this area during the LGM, as suggested by the presence of the moraines inshore from the shelf-edge.

On the slope near Bellsund and Isfjorden, through the analysis of bathymetric, sub-bottom and seismic data, the description of two contourite plastered drifts was improved. Recent data collected directly on top of these contourites confirm previous interpretations (*Rebesco et al., 2013*) and provide some new insights on the structure of the drifts and on their genesis. These contourites drifts are shaped by the persistent flow of the WSC, which controls sediment erosion, transport and deposition along the slope. The onset of these drifts coincides with the development of TMFs on the west Spitsbergen margin in the Early Pleistocene.

Oceanographic data (time-series of potential and in-situ temperature, salinity, density, turbidity and current velocity), collected from to two moorings located on Bellsund and Isfjorden drifts (*Bensi et al., in prep*.), were analyzed. From these data, it was possible to study the supply of suspended sediment, essential for the formation of drifts. I infer that during winter, dense shelf waters (i.e. BSW) form due to vigorous meteorological events,

formation of sea ice and wind-induced cooling and evaporation. These dense waters travel along the shelf within density driven currents, and collect consistent amounts of sediments that transform them into turbidity currents. The incorporation of sediments in fact increases the density of these waters to a level that is higher than that of a TS plume (*Fohramnn et al., 1998*). I infer that these turbidity currents flow downslope following the bathymetric constraints. These turbidity currents reach deeper depth in the water column compared to TS plumes, surpassing the thermohaline equilibrium point. I infer that these turbidity flows are the main supply of relatively fine-grained suspended sediment to the continental slope in present days. Moorings registered the passage of these fluxes, as inflows of water with relatively higher temperature, salinity and density values. Variations of these values are temporally simultaneous in the time-series from the two different contourite drifts. This seems to suggest that the processes responsible for the formation of these flows act simultaneously in both Bellsund and Isfjorden areas, pointing to meteorological processes affecting the shelf.

Lastly, I propose a model for the evolution of the west Spitsbergen margin, which considers the cyclic effect of glacial processes and ocean circulation. I infer that during glacial maxima and deglaciations the margin is dominated by the presence of the ice sheet. During glacial maxima, massive glacigenic debris flows focused at the mouth of ice streams generate TMFs (separated by inter-TMF areas). During deglaciations, the processes responsible for the erosion of gullies along the upper part of the continental slope are mainly represented by meltwaters flows. Instead, during periods of ice-sheet build-up, erosion, transport and deposition along the margin are controlled by the ocean circulation (i.e. the WSC). Glacigenic debris flows are absent and meltwaters are not abundant on the continental slope, due to the inshore location of the ice sheet. The sediment input is related to the flow of density driven currents. These currents effectively feed the lower part of the continental slope with suspended sediment, allowing bottom currents to shape the morphology of the bottom. I hence infer that all the features observed on the west Spitsbergen margin are the results of an alternation of these three cyclic phases.

References

Aagaard K., Carmack E.C., 1989, *The role of sea ice and other freshwater in the Arctic circulation*, J. Geohys. Res. 94, pp. 14,485-14,498.

Aagaard K., Greisman P., 1975, *Towards new mass and heat budgets in the Arctic Ocean*, J. Geophys. Res. 80, pp. 3821-3827.

Aagaard K., Swift J.H., Carmack E.C., 1985, *Thermohaline circulation in the arctic Mediterranean seas*, J. Geophys. Res. 90, pp. 4833-4846.

Aagaard K., Foldvik A., Hillman S.R., 1987, *The west spitsbergen current: disposition and water mass transformation*, J. Geophys. Res. 92, pp. 3778-3784.

Anderson, J.B., Shipp, S.S., Low, A.L., Wellner, J.S., Mosola, A.B., 2002, *The Antarctic Ice Sheet during the Last Glacial Maximum and its subsequent retreat history: a review*, Quaternary Science Reviews 21, pp. 49–70.

Akimova A., Schauer U., Danilov S., Núñez-Riboni I., 2011, *The role of the deep mixing in the Storfjorden shelf water plume*, Deep Sea Res. Part I 58, pp. 403-414.

Azpiroz-Zabala M., Cartigny M.J.B., Talling P., Parsons D., Sumner E.J., Clare M.A., Simmons S.M., Cooper C., Pope E.L., 2017, *Newly recognized turbidity current structure can explain prolonged flushing of submarine canyons*, Science Advances, pp. 1-12.

Baringer M.O., Price J.F., 1997, *Mixing and Spreading of the Mediterranean Outflow*, Journal of Physical Oceanography 27, pp. 1654-1677.

Batchelor C.L., Dowdeswell J.A., 2015, *Ice-sheet grounding-zone wedges (GZWs) on high-latitude continental margins*, Marine Geology 363, pp. 65-92.

Batchelor C.L., Dowdeswell J.A., Ottensen D., 2017, *Submarine Glacial Landforms*, in: Micallef A., Krastel S., Savini A., 2017, Submarine Geomorphology, pp. 207 – 234.

Bensi M., Cardin V., Rubino A., Notarstefano G. Poulain P., 2013, *Effects of winter convection on the deep layer of the Southern Adriatic Sea in 2012*, Journal of Geophysical Research. 118.

Bensi M., Kovacevic V., Langone L., De Vittor C., Relitti F., Bazzaro M., Laterza R., Lucchi R.G., Rebesco M., Ursella L., Aliani S., Miserocchi S., and with the collaboration of the EUROFLEETS-2 BURSTER Team, 2016, *DEFROST (DEep Flow Regime Off SpiTsbergen) Cruise Report*, Istituto Nazionale di Oceanografia e di Geofisica Sperimentale – OGS.

Bensi M., Langone L., Kovacevic V., Ursella L., Goszczko I., Aliani S., Rebesco M., Rui L., De Vittor C., Deponte D., Lucchi R.G., Wåhlin A., Soltwedel T., Skogseth R., Nilsen F., Beszczynska-Möller A., et al., *Shelf and slope dynamics offshore the west Svalbard continental margin*, Paper in preparation.

Beszczynska-Möller A., Fahrbach E., Schauer U., Hansen E., 2012, *Variability in Atlantic water temperature and transport at the entrance to the Arctic Ocean, 1997–2010,* ICES J. Mar. Sci. 69, pp. 852–863.

Breidenthal R.E., Baker M.B., 1985, *On entrainment at stratified interfaces*, Symposium on Turbulence and Diffusion 7h, pp. 43-46.

Butt F.A., Elverhøi A., Solheim A., Forsberg C.F., 2000, *Deciphering late Cenozoic development of the western Svalbard Margin from ODP Site 986 results*, Mar. Geol. 169, pp. 373–390.

Canals M., Casamor J.L., Lastras G., Monaco A., Acosta Yepes, J., Berne S. Loubrieu B., Weaver P., Greham A., Dennielou B., 2004, *The Role of Canyons in Strata Formation*, Oceanography (Washington D.C.) 17, pp. 80-91.

Charles C.D., Rind D., Jouzel J., Koster R.D., Fairbanks R.G., 1994, *Glacial-interglacial changes in moisture sources for Greenland: Influence on the ice core record of climate*, Science 263, pp. 508-511

Clark C.D., 1993, *Mega-scale glacial lineations and cross-cutting ice-flow landforms*, Earth surface processes and landforms 18, pp. 1–29.

Cox G.F.N., Weeks W.F., 1974, *Salinity variations in sea ice*, Journal of Glaciology, Vol. 13, pp. 109-120.

Crane K., Vogt P.R., Solheim A., 1995, *Seafloor atlas of the northern Norwegian-Greenland Basin*, Norsk Polarinstitutt Meddelelser 137, pp. 172.

Dowdeswell J.A., Cofaigh C. Ó, 2002, *Glacier-Influenced Sedimentation on High-Latitude Continental Margins*, The Geological Society of London.

Dowdeswell J.A., Cofaigh C. Ó, Pudsey C.J., 2004, *Continental slope morphology and sedimentary processes at the mouth of an Antarctic paleo-ice stream*, Marine Geology 204, pp. 203-214.

Dowdeswell J.A., Elverhøi A., Spielhagen R., 1998, *Glacimarine sedimentary processes and facies on the Polar North Atlantic Margins*, Quaternary Science Reviews, vol. 17, pp. 243-272.

Dowdeswell J.A., Ottesen D., 2013, *Buried iceberg ploughmarks in the early Quaternary sediments of the central North Sea: a two-million year record of glacial influence from 3D seismic data*, Marine Geology 344, pp. 1–9.

Durrieu de Madron X., Houpert L., Puig P., Sanchez-Vidal A., Testor P., Bosse A., Estournel C., Somot S., Bourrin F., Bouin M.N., Beauverger M., Beguery L., Calafat A., Canals M., Cassou C., Coppola L., Dausse D., D'Ortenzio F., Font J., Heussner S., Kunesch S., Lefevre D., Le Goff H., Martìn J., Mortier L., Palanques A., Raimbault P., 2012, *Interaction of dense shelf water cascading and open-sea convection in the northwestern Mediterranean during winter 2012*, Geophysical Res. Let. 40, pp. 1379-1385.

Durrieu de Madron X., Ramondenc S., Berline L., Houpert L., Bosse A., Martini S., Guidi L., Conan P., Curtil C., Delsaut N., Kunesch S., Ghiglione J.F., Marsaleix P., Pujo-Pay M., Séverin T., Testor P., Tamburini C., 2017, *Deep sediment resuspension and thick nepheloid layer generation by open-ocean convection*, J. Geophys. Res. Oceans 122, pp. 2291-2318.

Eiken O., Hinz K., 1993, *Contourites in the Fram Strait*, Sedimentary Geology 82, pp. 15-32.

Elverhoi, A., Andersen, E.S., Dokken, T., Hebbeln, D., Spielhagen, R., Svendsen, J.I., Sorflaten, M., Rornes, A., Hald, M., Forsberg, C.F., 1995, *The growth and decay of the late Weichselian ice sheet in western Svalbard and adjacent areas based on provenance studies of marine sediments*, Quat. Res. 44, 303e316.

Engen Ø., Faleide J.I., Dyreng T.K., 2008, *Opening of the Fram Strait gateway: A review of plate tectonic constraints*, Tectonophysics 450, pp. 51-69.

Evans J., Dowdeswell J.A., Grobe H., Niessen F., Stein R., Hubberten H.W. and Whittington R.J., 2002, *Late Quaternary sedimentation in Kejser Franz Joseph Fjord and the continental margin of East Greenland*, Geological Society, London, Special Publications, 203, 149-179.

Facchin L., Caburlotto A., Casamor J.L., Zgur F., Accettella D., Deponte D., Kovacevic V., Monti M., Visnovic P., Pelos C., Cotterle D., Rui L., 2017, *EDIPO/DEGLABAR Cruise Report, OGS Explora, 2015*, Istituto Nazionale di Oceanografia e di Geofisica Sperimentale – OGS.

Faleide J.I., Solheim A., Fiedler A., Hjelstuen B.O., Andersen E.S., Vanneste K., 1996, *Late Cenozoic evolution of the western Barents Sea–Svalbard continental margin*, Global Planet. Change 12, pp. 53-74.

Faugères J.-C., Stow D.A.V., 2008, *Contourite drifts: nature, evolution and controls*, In: Rebesco, M., Camerlenghi, A. (Eds.), *Contourites*, Developments in Sedimentology 60, Elsevier, Amsterdam, pp. 257-288.

Fohrmann H., Backhaus J.O., Blaume F., Rumohr J., 1998, *Sediments in bottom-arrested gravity plumes: Numerical case studies*, J. Phys. Oceanogr. 28, pp. 2250-2274.

Forsberg C.F., Solheim A., Elverhoi A., Jansen E., Channell J.E.T., Andersen E.S., 1999, *The depositional environment of the western Svalbard margin during the late Pliocene and the Pleistocene: Sedimentary facies changes at Site 986*, In: Raymo M., Jansen E., Blum P., Herbert T.D. (Eds.), Proceeding Ocean Drilling Program. Scientific Results, vol. 162, pp. 233–246. Ocean Drilling Program, College Station, TX.

Forwick M., Laberg J.S., Hass H.C., Osti G., 2015, *The Kongsfjorden Channel System offshore NW Svalbard: downslope sedimentary processes in a contour-current-dominated setting*, Arktos, 1 (1).

Gačić M., Lascaratos A., Manca B.B., Mantziafou A., 2001, *Adriatic Deep Water and Interaction with the Eastern Mediterranean Sea*, In: Cushman-Roisin B., Gačić M., Poulain PM., Artegiani A. (eds) Physical Oceanography of the Adriatic Sea. Springer, Dordrecht

Gales J.A., Forwick M., Laberg J.S., Vorren T.O., Larter R.D., Graham A.G.C., Baeten N.J., Amundsen H.B., 2013, *Arctic and Antarctic submarine gullies – A comparison of high latitude continental margins*, Geomorphology 201, pp. 449-461.

García M., Batchelor C.L., Dowdeswell J.A., Hogan K.A., Cofaigh C.Ó., 2016, *A glacier-influenced turbidite system and associated landform assemblage in the Greenland Basin and adjacent continental slope*, Geological Society, London, Memoirs, 46, pp. 461-468.

García M., Dowdeswell J.A., Ercilla G., Jakobsson M., 2012, *Recent glacially influenced sedimentary processes on the East Greenland continental slope and deep Greenland Basin*, Quaternary Science Reviews 49, pp. 64-81.

Gascard J.-C., Richez C., Rouault C., 1995, *New insights on largescale oceanography in Fram Strait: The West Spitsbergen Current*, in Arctic Oceanography: Marginal Ice Zones and Continental Shelves, Coastal Estuarine Stud., vol. 49, pp. 131–182.

Gawarkiewicz G., Weingartner T., Chapman D.C., 1997, *Sea ice processes and water mass modification and transport over Arctic shelves*, in The Sea, vol. 10, The Global Coastal Ocean, edited by K. H. Brink and A. R. Robinson, pp. 171–190.

Gawarkiewicz G., Chapman D.C., 1995, *A numerical study of dense water formation and transport on a shallow, sloping continental shelf*, Journal of Geophysical Research 100.

Gusev E., 2001, *New Insight on the Knipovich Ridge tectonic positions*, Geology and Geophysics of the Knipovich Ridge, pp.13-14.

Hald M., Ebbesen H., Forwick M., Godtliebsen F., Khomenko L., Korsun S., Olsen L.R., Vorren T.O., 2004, *Holocene paleoceanography and glacial history of the West Spitsbergen area, Euro-Arctic margin*, Quaternary Science Reviews 23, pp. 2075-2088.

Hanebuth T.J.J., Rebesco M., Urgeles R., Lucchi R.G., Freudenthal T., 2014, *Drilling glacial deposits in offshore polar regions*, Eos, vol. 95, Issue 31, pp. 277-278.

Harris C.L., Pluddeman A.J., Gawarkiewicz G., 1998, *Water mass distribution and polar front structure in the western Barents Sea*, Journal of Geophysical Research Atmospheres 103, pp. 2905-2917.

Harris P.T., Whiteway T., 2011, *Global distribution of large submarine canyons: geomorphic differences between active and passive continental margins*, Marine Geology 285, 69–86.

Heezen B.C., Hollister C.D., 1964, *Deep sea current evidence from abyssal sediments*, Marine Geology 1, 141–174.

Hjelstuen B.O., Eldholm O., Faleide J.I., 2007, *Recurrent Pleistocene mega-failures on the SW Barents Sea margin*, Earth Planet Sci. Lett. 258, pp. 605-618.

Hollister C.D., Heezen B.C., 1972, *Geological effects of ocean bottom currents: Western North Atlantic*, In: Gordon A.L. (Ed.), *Studies in Physical Oceanography 2*. Gordon and Breach, New York, pp. 37-66.

Hughes A.L.C., Gyllencreutz R., Lohne Ø. S., Mangerud J., Svendsen J. I., 2016, *The last Eurasian ice sheets – a chronological database and time-slice reconstruction, DATED-1*, Boreas, Vol. 45, pp. 1–45.

Hughes-Clarke J.E., Mayer L.A., Wells D.E., 1996, *Shallow-water imaging multibeam sonars: A new tool for investigating sea floor processes in the coastal zone and on the continental shelf*, Marine Geophysical Researches 18, pp. 607-629.

Hyvärinen H. 1968, *Late-Quaternary sediment cores from lakes on Bjørnøya*, Geografiska Annaler 50, p. 235–245.

Jakobsson M., Backman J., Rudels B., Nycander J., Frank M., Mayer L., Jokat W., Sangiorgi F., O'Regan M., Brinkhuis H., King J., Moran K., 2007, *The early Miocene onset of a ventilated circulation regime in the Arctic Ocean*, Nature 447, 986–990.

Jakobsson M., Mayer L.A., Coakley B., Dowdeswell J.A., Forbes S., Fridman B., Hodnesdal H., Noormets R., Pedersen R., Rebesco M., Schenke H.-W-, Zarayskaya Y.A., Accettella D., Armstrong A., Anderson R.M., Bienhoff P., Camerlenghi A., Church I., Edwards M.,

Gardner J. V., Hall J.K., Hell B., Hestvik O.B., Kristoffersen Y., Marcussen C., Mohammad R., Mosher D., Nghiem S.V., Pedrosa M.T., Travaglini P.G., Weatherall P., *The International Bathymetric Chart of the Arctic Ocean (IBCAO) Version 3.0*, Geophysical Research Letters.

Jessen S.P., Rasmussen T.L., Nielsen T., Solheim A., 2010, *A new Late Weichselian and Holocene marine chronology for the western Svalbard slope 30,000-0 cal years BP*, Quaternary Science Reviews 29, pp. 1301-1312.

Jones G.A., Keigwin, L.D., 1988, *Age determinations on sediment core PS1295-4*, Supplement to: Jones G.A., Keigwin L.D., 1988, *Evidence from Fram Strait (78°N) for early deglaciation*, Nature, 336(6194), p. 56-59.

Jonsson S., Foldvik A., Aagaard K., 1992, *The structure and atmospheric forcing of the mesoscale velocity field in Fram Strait*, J. Geophys. Res. 97, pp. 12,585–12,600.

Jungclaus H.J., Backhaus J.O., Fohrmann H., 1995, *Outflow of dense water from the Storfjord in Svalbard: A numerical model study*, Journ. Of Geoph. Res. 100, pp. 24719-24728.

Kämpf J.O., Backhaus J.O., 1998, *Shallow, brine-driven free convection in polar oceans: nonhydrostatic numerical process studies*, Journal of Geophysical Research 103, pp. 5557-5593.

Kearey P., Brooks M., Hill I., 2013, *An introduction to Geophysical Exploration*, John Wiley & Sons, pp. 1-272.

Kneller B., Buckee C., 2000, *The structure and fluid mechanics of turbidity currents: a review of some recent studies and their geological implications*, Sedimentology 47, pp. 62-94.

Knies J., Vogt C., Stein R., 1999, *Late Quaternary growth and decay of the Svalbard/Barents Sea ice sheet and paleoceanographic evolution in the adjacent Arctic Ocean*, Geo-Marine Letters, 18:195-202.

Knies J., Matthiessen J., Vogt C., Laberg J. S., Hjelstuen B. O., Smelror M., Larsen E., Andreassen K., Eidvin T., & Vorren T. O., 2009, *The Plio-Pleistocene glaciation of the Barents Sea–Svalbard region: a new model based on revised chronostratigraphy*, Quaternary Science Reviews, 28(9), pp. 812–829.

Laberg J.S., Dahlgren T., Vorren T.O., Haflidason H., Bryn P., 2002, *Seismic analyses of cenozoic contourite drift development in the Northern Norwegian Sea*, Mar. Geophys. Res. 22, pp. 401–416.

Laberg J.S., Guidard S.J., Mienert J., Vorren T.O., Haflidason H., Nygård A., 2007, *Morphology and morphogenesis of a high-latitude canyon; the Andøya Canyon, Norwegian Sea*, Marine Geology 246, pp. 68-85.

Laberg J.S., Vorren T.O., Knutsen S.-M., 1999, *The Lofoten contourite drift off Norway*, Mar. Geol. 159, pp. 1–6.

LabSea Group, 1998, *The Labrador Sea Deep Convection Experiment*, Bull. Am. Meteorol. Soc. 79, pp. 2033–2058.

Landvik J.Y., Bondevik S., Elverhøi A., Fjeldskaar W., Mangerud J., Salvigsen O., Siegert M.J., Svendsen J.I., Vorren T.O., 1998, *The last glacial maximum of Svalbard and the Barents Sea area: ice sheet extent and configuration*, Quat. Sci. Rev. 17, p. 43–75.

Langehaug, H.R. and Falck E., 2012, *Changes in the properties and distribution of the intermediate and deep waters in the Fram Strait*, Progr. in Oceanogr. 96, pp. 57–76.

Lawver L.A., Müller R.D., Srivastava S.P., Roest W., 1990, *The opening of the Arctic Ocean*, In: Bleil U., Thiede J. (Eds.), *Geological History of the Polar Oceans: Arctic versus Antarctic*, NATO ASI Series C, vol. 308, pp. 29–62.

Lockhart D., Saade E., Wilson J., 2001, *New Developments in Multi-beam Backscatter Data Collection and Processing*, Marine Technology Society Journal 35, pp. 46-50.

Lucchi R.G., Pedrosa M.T., Camerlenghi A., Urgeles R., De Mol B., Rebesco M., 2012, *Recent submarine landslides on the continental slope of Storfjorden and Kveithola Trough-Mouth Fans (north west Barents Sea)*, In: Yamada Y., Kawamura K., Ikehara K., Ogawa Y., Urgeles R., Mosher D., Chaytor J., Strasser M. (Eds.), *Submarine Mass Movements and Their Consequences*. *Advances in Natural and Technological Hazards Research*, Springer Science book series, 31, pp. 735–745.

Lucchi R.G., Camerlenghi A., Rebesco M., Urgeles R., Sagnotti L., Macri P., Colmenero-Hildago E., Sierro F.J., Melis R., Morigi C., Barcena M.A., Giorgetti G., Villa G., Persico D., Flores J.A., Pedrosa M.T., Caburlotto A., 2013, *Postglacial sedimentary processes on the Storfjorden and Kveithola trough-mouth fans: impact of extreme glacimarine sedimentation*, Glob. Planet. Change 111, pp. 309-326.

Lucchi R.G., Kovacevic V., Aliani S., Caburlotto A., Celussi M., Corgnati L., Cosoli S., Deponte D., Ersdal E.A., Fredriksson S., Goszczko I., Husum K., Ingrosso G., Laberg J.S., Lacka M., Langone L., Mansutti P., Mezgec K., Morigi C., Ponomarenko E., Realdon G., Relitti F., Robijn A., Skogseth R., Tirelli V., 2014, *EUROFLEETS-2 Cruise Summary Report - PREPARED: Present and past flow regime on contourite drifts west of Spitsbergen*, R/V G.O. Sars, Cruise No. 191, 05/06/2014 – 15/06/2014, Tromsø – Tromsø (Norway), OGS

Madrussani G., Rossi G., Rebesco M., Picotti S., Urgeles R., Llopart J., 2017, *Sediment properties in submarine mass-transport deposits using seismic and rock-physics off NW Barents Sea*, Marine Geology, in press.

Magaldi M.G., Haine T.W.N., Pickart R.S., 2011, *On the nature and variability of the East Greenland Spill Jet: a case study in summer 2003*, J. Phys. Oceanogr.

Manca B.B., Ibello V. Pacciaroni M., Scarazzato P., Giorgetti A., 2006, *Ventilation of deep waters in the Adriatic and Ionian Seas following changes in thermohaline circulation of the Eastern Mediterranean*, Climate Research - CLIMATE RES 31, pp. 239-256.

Manley T. O., 1995, *Branching of Atlantic Water within the Greenland-Spitsbergen passage: An estimate of recirculation*, J. Geophys. Res. 100, 20,627– 20,634.

Margold M., Stokes C R., Clark C.D., 2015, *Ice streams in the Laurentide Ice Sheet: Identification, characteristics and comparison to modern ice sheets*, Earth Science Reviews 143, pp. 117–146.

Mienert J., Thiede J., Kenyon N.H., Hollender F.-J., 1993, *Polar continental margins: Studies off East Greenland*, EOS 74, pp. 225-236.

Marshall J., Schott F., 1999, *Open-ocean convection: Observations, theory and models*. *Reviews of Geophysics*, Vol. 37, pp. 1-64.

Nittis K., Lascaratos A., Theocharis A., 2003, *Dense water formation in the Aegean Sea: Numerical simulations during the Eastern Mediterranean Transient*, Journal of Geoph. Res. 108, pp. 21-1 – 21-15.

Normark W.R., Posamentier H., Mutti E., 1993, *Turbidite systems: State of the art and future directions*, Reviews of Geophysics, v. 31, p. 91–116.

Normark W.R., Carlson P.R., 2003, *Giant submarine canyons: Is size any clue to their importance in the rock record?*, in: Extreme depositional environments: mega end members in geologic time, Geological Society of America, Vol. 370.

O' Cofaigh C., Andrews J.T., Jennings A.E.,Dowdeswell J.A., Hogan K.A., Kilfeather A.A., Sheldon C., 2012, *Glacimarine lithofacies, provenance and depositional processes on a West Greenland trough-mouth fan*, Journal of Quaternary Science, pp. 13-26.

Ó Cofaigh C., Davies B.J., Livingstone S.J., Smith J.A., Johnson J.S., Hocking E.P., Hodgson D.A., Anderson J.B., Bentley M.J., Canals M., Domack E., Dowdeswell J.A., Evans J., Glasser N.F., Hillenbrand C.D., Larter R.D., Roberts S.J. & Simms A.R., 2014, *Reconstruction of ice-sheet changes in the Antarctic Peninsula since the Last Glacial Maximum*, Quaternary Science Reviews 100, pp. 87-110.

Peakall J., Kane A.I., Masson D.G., Keevil G., McCaffrey W., Corney R., 2012, *Global (latitudinal) variation in submarine channel sinuosity*, Geology, 40, pp. 11-14.

Pedrosa M.T., Camerlenghi A., De Mol B., Urgeles R., Rebesco M., Lucchi R.G., 2011, *Seabed morphology and shallow sedimentary structure of the Storfjorden and Kveithola trough-mouth fans (North West Barents Sea)*, Marine Geology, 286, 65-81.

Pfirman S. L., Bauch D., and Gammelsrød T., 1994, *The Northern Barents Sea: Water mass distribution and modification, in The Polar Oceans and Their Role in Shaping the Global Environment*, Geophys. Monogr. Ser. 85, pp. 77 – 94.

Polyakov I.V., Alekseev G.V., Timokhov L.A., Bhatt U., Colony R.L., Simmons H.L., Walsh D., Walsh J.E., Zakharov V.F., 2004, *Variability of the intermediate Atlantic Water of the Arctic Ocean over the last 100 years*, Journal of Climate 17(23), pp. 4485-4497.

Polyakov I.V., Bhatt U.S., Walsh J.E., Abrahamsen E.P., Pnyushkov A.V., Wassmann P.F., 2013, *Recent oceanic changes in the Arctic in the context of long-term observations*, Ecological Applications 23(8), 2013, pp. 1745-1764.

Puig P., Durrieu de Madron X., Salat J., Schroeder K., Martín J., Karageorgis A.P., Palanques A., Roullier F., Lopez-Jurado J.L., Emelianov M., Moutin T., Houpert L., 2013, *Thick bottom*

nepheloid layers in the western Mediterranean generated by deep dense shelf water cascading, In Progress in Oceanography, Volume 111, pp. 1-23.

Pusceddu A., Mea M., Gambi C., Bianchelli S., Canals M., Sanchez-Vidal A., Calafat A., Heussner S., Durrieu de Madron X., Avril J., Thomsen L., García R., Danovaro R., 2010, *Ecosystem effects of dense water formation on deep Mediterranean Sea ecosystems: an overview*, Advances in Oceanography and Limnology 1, pp. 67-83.

Quadfasel D., Rudels B., Kurz K., 1988, *Outflow of dense water from a Svalbard fjord into the Fram Strait*, Deep-Sea Res. 35, Part A, pp. 1143-1150.

Raymo M.E., Jansen E., Blum P., Herbert T.D. (Eds.), 1999, *Proc*. *ODP*, Sci. Results, 162: College Station, TX (Ocean Drilling Program).

Rasmussen T., Thomsen E., Ślubowska A.M., Jessen S., Solheim A., Koc N., 2007, *Paleoceanographic evolution of the SW Svalbard margin (76°N) since 20,000 14C yr BP*, Quaternary Research - QUATERNARY RES. 67, pp. 100-114.

Rebesco M., 2005, *Contourites*, In: Selley R.C., Cocks L.R.M., Plimer I.R. (Eds.), *Encyclopedia of Geology*, Elsevier, Oxford, pp. 513-527.

Rebesco M., Camerlenghi A., 2008, *Late Pliocene margin development and mega debris flow deposits on the Antarctic continental margins: Evidence of the onset of the modern Antarctic Ice Sheet*, Palaeogeography, Palaeoclimatology, Palaeoecology, Volume 260, Issues 1–2, pp. 149-167.

Rebesco M., Özmaral A., Urgeles R., Accettella D., Lucchi R.G., Rüther D., Winsborrow M., Llopart J., Caburlotto A., Lantzsch H., Hanebuth T.J.J., *Evolution of a high-latitude sediment drift inside a glacially-carved trough based on high-resolution seismic stratigraphy (Kveithola, NW Barents Sea)*, Quaternary Science Reviews, Volume 147, pp. 178-193.

Rebesco M., Liu Y., Camerlenghi A., Winsborrow M., Laberg J. S., Caburlotto A., Diviacco P., Accettella D., Sauli C., Wardell N., Tomini I., 2011, *Deglaciation of the western margin of the Barents Sea Ice Sheet — A swath bathymetric and sub-bottom seismic study from the Kveithola Trough*, Marine Geology, 279, 141-147.

Rebesco M., Hernández-Molina F.J., Rooij D.V., Wåhlin A., 2014, *Contourites and associated sediments controlled by deep-water circulation processes: State-of-the-art and future considerations*, Marine Geology 352, pp. 111-154.

Rebesco M., Laberg J. S., Pedrosa M. T., Camerlenghi A., Lucchi R. G., Zgur F., Wardell N., 2013a, *Onset and growth of Trough-Mouth Fans on the North-Western Barents Sea margin — implications for the evolution of the Barents Sea/Svalbard Ice Sheet*, Quaternary Science Reviews xxx, 1-8.

Rebesco M., Stow D.A.V., 2001, *Seismic expression of contourites and related deposits: a preface*, Marine Geophysical Research 22, pp. 303-308.

Rebesco M., Wahlin A., Laberg J.S., Schauer U., Beszczynska-Möller A., Lucchi R.G., Noormets R., Accettella D., Zarayskaya Y., Diviacco P., 2013b, *Quaternary contourite drifts of the Western Spitsbergen margin*, Deep-Sea Research I 79, pp. 156-168.

Rise L., Ottesen D., Longva O., Solheim A., Andersen E.S., Ayers S., 2006, *The Sklinnadjupet slide and its relation to the Elsterian glaciation on the mid-Norwegian margin*, Mar. Petrol. Geol. 23, pp. 569-583.

Rudels B., 1987, *On the mass balance of the Polar Ocean, with the emphasis on the Fram Strait*, Skr. Nor. Polarinst. 188, pp. 53.

Rudels, B., 1995, *The thermohaline circulation of the Arctic Ocean and the Greenland Sea*, Philos. Trans. R. Soc. London, Ser. A 352, pp. 287-299.

Rudels B., Meyer R., Fahrbach E., Ivanov V.V., Østerhus S., Quadfasel D., Schauer U., Tverberg V., Woodgate R.A., 2000, *Water mass distribution in Fram Strait and over the Yermak Plateau in summer 1997*, Ann. Geophys. 18, pp. 687–705.

Rui L., Rebesco M., Casamor J.L., Laberg J.S., Rydningen T.A., Caburlotto A., Forwick M., Urgeles R., Accettella D., Madrussani G., Demarte M., Ivaldi R., in prep., *Depicting a high-latitude channel system: the INBIS Channel (NW Barents Sea)*, submitted.

Rüther D. C., Mattingsdal R., Andreassen K., Forwick M., Husum K., 2011, *Seismic architecture and sedimentology of a major grounding zone system deposited by the Bjørnøyrenna Ice Stream during Late Weichselian deglaciation*, Quaternary Science Reviews 30, 2776–2792.

Rüther D. C., Bjarnadóttir L.R., Junttila J., Husum K., Rasmussen T.L., Lucchi R.G., Andreassen K., 2012, *Pattern and timing of the northwestern Barents Sea Ice Sheet deglaciation and indications of episodic Holocene deposition*, Boreas, pp. 1-19.

Rydningen T.A., Laberg J.S., Kolstad V., 2015, *Seabed morphology and sedimentary processes on high-gradient trough mouth fans offshore Troms, northern Norway*, Geomorphology, 205-219.

Rubino A., Romanenkov D., Zanchettin D., Cardin V., Hainbucher D., Bensi M., Boldrin A., Langone L., Miserocchi S., Turchetto M., 2012, *On the descent of dense water on a complex canyon system in the southern Adriatic basin*, In Continental Shelf Research, Volume 44, pp. 20-29.

Sanchez-Vidal A., Veres O., Langone L., Ferré B., Calafat A., Canals M., Durrieu de Madron X., Heussner S., Mienert J., Grimalt J.O, Pusceddu A., Danovaro R., 2015, *Particle sources and downward fluxes in the eastern Fram strait under the influence of the west Spitsbergen current*, Deep Sea Research Part I: Oceanographic Research Papers 103, pp. 49-63.

Saloranta T.M., Haugan P.M., 2001, *Northward cooling and freshening of the warm core of the West Spitsbergen Current*, Polar Research 23, 79-88.

Salvigsen O. and Slettemark ø., 1995, *Past glaciation and sea levels on Bjørnøya, Svalbard*, Polar Research, 14, pp. 245-251.

Scase M., Caulfield C., Dalziel S., Hunt J., 2006, *Time-dependent plumes and jets with decreasing source strengths*, Journal of Fluid Mechanics 563, pp. 443-461.

Schott F., Visbeck M., Fischer J., 1993, *Observations of vertical currents and convection in the central Greenland Sea during the winter of 1988/89*, J. Geophys. Res. 98(C8), pp. 14,401-14,421.

Schott F., Visbeck M., Send U., Fischer J., Stramma L., Desaubies Y., 1996, *Observations of deep convection in the Gulf of Lions, northern Mediterranean, during the winter of 1991/ 92*, J. Phys. Oceanogr. 26, pp. 505–524.

Schauer U., Fahrbach E., Østerhus S., Rohardt G., 2004, *Arctic warming through the Fram Strait: Oceanic heat transport from 3 years of measurements*, J. Geophys. Res. 109.

Shcherbina A.Y., Talley L.D., Rudnick D.L., 2004, *Dense water formation on the northwestern shelf of the Okhotsk sea: 1. direct observations of brine rejection*, Journal of Geophysical Research: Oceans, 109.

Shepard F.P., Emery K.O., 1941, *Submarine Topography off the California Coast: Canyons and Tectonic Interpretations*, Geological Society of America Special Paper 31, 171 p.

Shepard G.E., Müller R.D., Seton M., 2013, *The tectonic evolution of the Arctic since Pangea breakup: Integrating constraints from surface geology and geophysics with mantel structure*, Earth-Science Reviews 124, pp. 148-183.

Skogseth R., 2003, *Dense water production processes in Storfjorden*, Reports in Meteorology and Oceanography 2, pp. 194.

Skogseth R., Fer I., Haugan P.M., 2005, *Water-mass transformations in Storfjorden*, Continental Shelf Research 25, pp. 667– 695.

Skogseth R., Fer I., Haugan P.M., 2013, *Dense-Water Production and Overflow From an Arctic Coastal Polynya in Storfjorden*, Geophysical Monograph Series, pp. 1-17.

Ślubowska M.A., Koç N., Rasmussen T.L., Klitgaard-Kristensen D., 2005, *Changes in the flow of Atlantic water into the Arctic Ocean since the last deglaciation: Evidence from the northern Svalbard continental margin*, 80°N, Paleoceanography 20, pp. 4014, 1-15.

Smith J.A., Hillenbrand C.-D., Pudsey C.J., Allen C.S., Graham A.G.C., 2010, *The presence of polynyas in the Weddell Sea during the Last Glacial Period with implications for the reconstruction of sea-ice limits and ice sheet history*, Earth Planet. Sci. Lett. 296 (3–4), pp. 287–298.

Spielhagen R.F., Werner K., Sørensen A.S., Zamelczyk K., Kandiano E., Budeus G., Husum K., MarchittoT.M., Hald M., 2011, *Enhanced Modern Heat Transfer to the Arctic by Warm Atlantic Water*, Science, pp.450-453.

Sternberg R.W., Aagaard K., Cacchione D., Wheatcroft R.A., Beach R.A., Roach A.T., Marsden M.A.H., 2001, *Long-term nearbed observations of velocity and hydrographic properties in the northeast Barents Sea with implications for sediment transport*, Cont. Shelf Res. 21, pp. 509-529.

Stiansen J.E., Filin A.A., 2007, *Joint PINRO/IMR report on the state of the Barents Sea ecosystem 2006, with expected situation and considerations for management*, IMR/PINRO Joint Report Series, 209.

Stokes C.R., Clark C.D., 2001, *Paleo-ice streams*, Quaternary Science Reviews, Vol. 20, Issue 13, pp. 1437-1457.

Stow D.A.V., Kahler G., Reeder M., 2002, *Fossil contourites: type example from an Oligocene palaeoslope system, Cyprus*, In: Stow D.A.V., Pudsey C.J., Howe J.A., Faugères J.-C., Viana A.R. (Eds.), *Deep-water Contourite Systems: Modern Drifts and Ancient Series, Seismic and Sedimentary Characteristics*, Geological Society, London, Memoir 22, pp. 443-455.

Stow D.A.V., Hunter S., Wilkinson D., Hernández-Molina F.J., 2008, *The Nature of Contourite Deposition*, In: Rebesco M., Camerlenghi A. (Eds.), Contourites, Developments in Sedimentology 60, pp. 143–156.

Svendsen J. I., Alexanderson H., Astakhov V. I., Demidov I., Dowdeswell J. A., Funder S., Gataullin V., Henriksen M., Hjort C., Houmark-Nielsen M., 2004, *Late Quaternary ice sheet history of northern Eurasia*, Quaternary Science Reviews 23, pp. 1229-1271.

Taylor J., Dowdeswell J.A., Kenyon N.H., 2003, *Canyon and Channel Systems in the Lofoten Basin, Norwegian Margin*, European Margin Sediment Dynamics, Springer, pp. 94.

Talwani M., Eldholm O., 1977, *Evolution of the Norwegian-Greenland Sea*, Geological Society of America 88, pp. 969-999.

Teigen S.H., Nilsen F., Gjevik B., 2010, *Barotropic instability in the West Spitsbergen Current*, J. Geophys. Res. 115, pp. 1-18.

Teigen S.H., Nilsen F., Skogseth R., Gjevik B., Beszczynska-Möller A., 2011, *Baroclinic instability in the West Spitsbergen Current*, J. Geophys. Res. Oceans 116, C07012.

Theocharis A., Georgopoulos D., 1993, *Dense water formation over the Samothraki and Limnos Plateaux in the north Aegean Sea (eastern Mediterranean)*, Cont. Shelf Res. 13, pp. 919 – 993.

Theocharis A., Nittis K., Kontoyannis H., Kioroglou S., Drakopoulos P., 1998, *Intermediate and deep water formation in the central and south Aegean Sea*, 3rd MTP-II Workshop: On the Variability of the Mediterranean Sea.

Thiede J., Myhre A.M., 1996, *Introduction to the North Atlantic-Arctic gateways: plate tectonic-paleoceanographic history and significance*, Proceedings of the Ocean Drilling Program, Scientific Results, Vol. 151, pp. 1-21.

Thiede J., Winkler A., Wolf-Welling T.C.W., Eldholm O., Myhre A.M., Baumann K.H., Henrich R., Stein R., 1998, *Late Cenozoic history of the Polar North Atlantic: results from ocean drilling*, Quaternary Science Reviews 17, pp. 185–208.

Vilibić I., Grbec B., Supić N., 2004, *Dense water generation in the north Adriatic in 1999 and its recirculation along the Jabuka Pit*, Deep Sea Research Part I: Oceanographic Research Papers 51, pp. 1457-1474.

Vilibić I., Mihanović H., 2003, *A study of resonant oscillations in the Split harbour (Adriatic Sea)*, Estuarine Coastal Shelf Sci. 56, pp. 861-867.

Visbeck M., Marshall J., Jones H., 1996, *Dynamics of isolated convective regions in the ocean*, J. Phys. Oceanogr. 26, pp. 1721–1734.

Vogt P.R., Taylor P.T., Kovacs L.C., Johnson G.L., 1979, *Detailed aeromagnetic investigation of the Arctic Basin*, Journal of Geophysical Research 84, pp. 1071–1089.

Vorren T.O., Laberg J.S., 1996, *Late glacial air temperature, oceanographic and ice sheet interactions in the southern Barents Sea region*, in: Andrews J.T., Austin W.E.N., Bergsten

H., Jennings A.E. (Eds.), *Late Quaternary Palaeoceanography of the North Atlantic Margins*, Special Publication No. 111, Geological Society, London, pp. 303-321.

Vorren T.O., Laberg J.S., Blaume F., Dowdeswell J. A., Kenyoh N.H., Mienert J., Rumohr J., Werner F., 1998, *The Norwegian-Greenland sea continental margins: morphology and late quaternary sedimentary processes and environment*, Quaternary Science Reviews, Vol. 17, pp. 273-302.

Vorren T.O., Laberg J.S., 2001, *Late Quaternary sedimentary processes and environment on the Norwegian-Greenland Sea continental margins*, Sedimentary Environments Offshore Norway – Palaeozoic to Recent, Norwegian Petroleum Society Special Publications, Elsevier, Vol. 10, pp 451-456.

Vorren T.O., Sejrup H.P., Dowdeswell J.A., 2003, *The Norwegian Margin*, European Margin Sediment Dynamics, Springer, pp. 25-26.

Vrbka L., Jungwirth P., 2005, *Brine rejection from freezing salt solutions: A molecular dynamics study*, Physical Review Letters 95, pp. 148501.

Vrbka L., Jungwirth P., 2007, *Molecular dynamics simulations of freezing of water and salt solutions*, Journal of Molecular Liquids 134, pp. 64-70.

Weertman J., 1974, *Stability of the junction of an ice sheet and an ice shelf*. *Journal of Glaciology* 13 (67), pp. 3–11.

Wettlaufer J.S., Worster M.G., Huppert H.E., 1997, *Natural convection during solidification of an alloy from above with application to evolution of sea ice*, J. Fluid. Mech. 344, pp. 291-316.

Wilken M. and Mienert J., 2006, *Submarine glacigenic debris flows, deep-sea channels and past ice-stream behaviour of the East Greenland continental margin*, Quat. Science Rev., pp. 784-810.

Winsborrow M.C.M., Andreassen K., Corner G.D., Laberg J.S., 2010, *Deglaciation of a marine-based ice sheet: Late Weichselian palaeo-ice dynamics and retreat in the southern Barents Sea reconstructed from onshore and offshore glacial geomorphology*, Quat. Sci. Rev. 29, pp. 424-442.

Wohlfarth B., Björck S., Possnert G., 1995, *The Swedish Time Scale — A potential calibration tool for the radio-carbon time scale during the Late Weichselian*, Radio-carbon 37(2), 347–60.

Yilmaz Ö., 2001, *Seismic Data Analysis: Processing, Inversion, and Interpretation of Seismic Data*, Society of Exploration Geophysicists.

Zhao M., Timmermans M-.L., 2015, *Vertical scales and dynamics of eddies in the Arctic Ocean's Canada Basin*, Journal of Geophysical Research 120, pp. 8195-8209.